THE CARBON-OXYGEN DISTRIBUTION IN NEW YORK BIGHT

PHASE I - STEADY STATE

Donald J. O'Connor

John L. Mancini

Manhattan College
Environmental Engineering & Science
Bronx, New York 10471

August, 1979

MESA New York Bight Project
National Oceanic and Atmospheric Administration
Marine Eco-System Analysis

ACKNOWLEDGEMENT:

The assistance and cooperation of the following individuals is gratefully acknowledged:

Mr. Lawrence Swanson
Dr. Joel O'Connor
Dr. Gary Meyer
Dr. Gregory Han
Dr. Donald Hensen
Dr. John Walsh

Members of Manhattan College who made significant contributions to the Study included Dr. Dominic M. Di Toro, who developed the minimum energy analysis and Messrs. Andrew Anderson and Richard Pope, whose efforts and attention to details provided an important input to the Study.

TABLE OF CONTENTS

LIST OF TABLES

LIST OF FIGURES

INTRODUCTION AND PURPOSE

Water quality in New York Bight is affected by a variety of inputs from both anthropogenic activities and natural phenomena. The temporal and spatial distributions of the various water quality constituents are determined by the magnitude of these inputs, in conjunction with the hydrodynamic transport of the system. For non-conservative substances, the distributions are also affected by the relevant kinetic factors. The transport within the region is due to a complex interaction of tidal forces, wind effects and density gradients, associated with temperature and salinity gradients. In the region, known as the apex, the transport is also affected by the Hudson River discharge. Although the Bight receives the wastewater inputs from a number of municipalities in both New Jersey and Long Island, the most significant influx is from the Hudson and Raritan Rivers, which carry the partially treated wastewaters and urban runoff from the New York metropolitan area.

The overall purpose of this research is to develop an analytical framework to assess the impact of these inputs on the water quality of the New York Bight, taking into account the effect of the additional sources such as atmospheric inputs, sludge disposal and natural phenomena. It is planned to interact this analysis with those presently being conducted in the various regions, by the EPA 208 program. It should provide a basis for the coordination of waste treatment programs between the various counties and states, and thus the ultimate effect of water pollution abatement programs may be put into broader perspective. The purpose of this report is to present a preliminary framework as an initial step in the overall analysis of water quality management in the New York Bight.

SUMMARY AND CONCLUSIONS:

The steady-state analysis presented in this report provides a basis for assessment of dissolved oxygen in the New York Bight, particularly in the apex area. The analysis indicates that the discharge of carbonaceous and nitrogenous wastes does not materially affect the dissolved oxygen levels through bacterial oxidation. Furthermore, the discharge of solids (sludge disposal, dredge spoils and construction debris) do not influence these concentrations on a bight-wide scale. The localized sludge disposal area is evidently affected in this regard, but this area is restricted to a relatively limited extent. On the other hand, the depression of dissolved oxygen, particularly in the hypolimnetic waters, is affected by phytoplankton respiration and decay and the vertical transport structure. It is probable that the discharge of wastewater from the treatment plants and urban runoff has some effect on the growth of phytoplankton and the subsequent decay through the inorganic nutrient route. The degree to which water quality conditions are affected by these inputs may be quantified by the development and validation of a model defining these kinetic interactions. The analysis, developed in this second phase, will be extended to incorporate the kinetic routes, relating the growth and decay of the phytoplankton to the nutrient concentrations resulting from these wastewater inputs. Thus, the effect of the discharges will be defined, providing a basis for areawide water quality planning, particularly with respect to the relative influence of the point sources from treatment plants and the distributed sources from urban runoff by contrast to the effects of other inputs such as the disposal practices and atmospheric inputs.

The present analysis is directed to the definition of a transport structure, in accordance with the original contract to provide the Brookhaven investigators with a reasonable transport field for summer conditions. The transport equations included advective and dispersive terms in a multi-segmented horizontal system with two vertical layers. The advective terms were developed by a minimum energy principle, which yielded the general observed flow patterns in the Bight. The overall transport field also included consistent values of the various dispersion coefficients. It is recognized that advective-dispersive models of this nature do not necessarily result in a unique solution for the transport. However, its validity to represent average summer conditions is demonstrated by its ability to reproduce the salinity distribution for the two years.

The analysis further indicates that the dissolved oxygen concentration in the hypolimnetic waters is particularly sensitive to the respiration and decay rates of the phytoplankton and the vertical dispersion coefficients. Relatively small changes of these parameters, within the range of measured values, causes significant changes in the dissolved oxygen levels.

Thus, from both a transport and kinetic viewpoint, the present analysis reasonably reproduces observed water quality conditions and permits assussment of the effect of wastewater inputs. In view of the potential significance of these discharges on dissolved oxygen and other water quality parameters this analysis had indicated the analytic direction on which to proceed and provided a valid basis for the more definitive time variable analysis.

I. BASIC EQUATIONS

The distribution of a conservative constituent in a coastal region such as New York Bight may be described by the following equation:

$$\frac{\partial s}{\partial t} = \frac{\partial}{\partial x}(E_x \frac{\partial s}{\partial x}) + \frac{\partial}{\partial y}(E_y \frac{\partial s}{\partial y}) + \frac{\partial}{\partial z}(E_z \frac{\partial s}{\partial z}) - U \frac{\partial s}{\partial x} - V \frac{\partial s}{\partial y} - W \frac{\partial s}{\partial z} \qquad (I\text{-}1)$$

in which

s = concentration of a conservative substance

x,y,z = longitudinal, lateral and vertical axes

E_x,E_y,E_z = dispersion coefficient

U,V,W = advective coefficient

In applying this equation to the steady-state distribution of salinity, the appropriate horizontal boundary conditions are the flow and a specified concentration at the origin of the apex, a zero flux at the land-sea boundaries elsewhere in the horizontal plane and the oceanic value of the salinity at the outer limits of the system. The vertical boundary condition is a zero flux at the air-water and water-bed boundaries.

Equation (I-1) is used to establish a transport field, which is required for the analysis of water quality constituents of a non-conservative nature. The equation defining the distribution of such substances include, in addition to the transport factors, the sources and sinks of the material;

$$\frac{\partial c}{\partial t} = j + \Sigma S_o - \Sigma S_i \qquad (I\text{-}2)$$

in which

c = concentration of a non-conservative constituent

j = flux, as defined in equation (I-1)

ΣS_o = sum of the sources

ΣS_i = sum of the sinks

The latter terms refer to the various physical, chemical and biological mechanisms which affect the particular substance and to the various inputs to the system associated with river runoff, waste inputs, the atmosphere and the bed.

Application of equation (I-2) to the steady-state distribution of dissolved oxygen leads to

$$0 = j + P - R_p - R_b \qquad \text{(I-3)}$$

in which

P = Photosynthetic production

R_p = phytoplankton respiration

R_b = bacterial respiration

Oxygen transfer at the air-water interface and the bed are accounted for by the boundary conditions at the respective interfaces. The rates of oxygen production, P, and of uptake, R_a and R_b, are functions of the phytoplankton and bacterial concentrations, in conjunction with the inorganic nutrients and organic food. The carbon, nitrogen and phosphorus in the latter emanate from the various inputs to the Bight, among which is the Hudson River inflow, containing the residues of these substances from the metropolitan area. It is in this fashion that the analysis, described in this report, may be sequentially correlated to the wastewater inputs, providing a basis for water quality management.

Application of equations (I-1) and (I-2) require knowledge of the various transport and kinetic coefficients. The advective transport coefficients are evaluated by a method based on the principles of continuity and minimum energy. The procedure consists in the solution of a set of linear equations, corresponding to the number of segments into which the system is divided. Knowledge of the velocity at a limited number of locations permits determination of the velocity at the remaining locations such that continuity is maintained. A more complete description and application is presented in a subsequent section.

The dispersive transport and kinetic coefficients may be evaluated in an approximate fashion by decoupling the horizontal and vertical components of these equations (I-1) and (I-2). Thus, in regions where the vertical gradients and concentrations are greater than the horizontal by an order of magnitude, an analysis may be developed including only those components which make up the vertical flux without considering the horizontal. Conversely, in those regions where the horizontal terms predominate, the vertical components may be neglected as a reasonable approximation. These approximations lead to simplified forms of the differential equations, which are readily integrated and by which the various coefficients may be relatively easily evaluated. In addition, they provide a means to test the sensitivity of the various components.

The vertical analysis is appropriate outside the zone of influence of the Hudson River plume. In such regions the analysis of vertical distribution of dissolved oxygen is particularly suitable since the horizontal gradients are much less than the vertical gradiants and also the flux associated with the horizontal gradient much less than the kinetic sources and sinks of oxygen, due to photosynthetic activity and respiration. The analysis may therefore apply to regions outside of the Hudson River plume where these conditions are, in general, fulfilled. Furthermore, a steady-state condition may be realized during the middle to later summer, when the temperature and density stratification are reasonably constant at their maximum values. Specification of the boundary conditions of oxygen transfer at the air-water interface and the bed permit evaluation of the vertical dispersion, as well as the photosynthetic production and respiration. It is recognized that a given measured distribution of dissolved oxygen does not yield a unique set of transport and kinetic coefficients. However, the additional data of chlorophyll, which may be correlated to primary production, and dissolved organic carbon, which may be related to respiration, provide a further degree of confirmation. The analysis thus provides relatively narrow ranges within which the numerical values of the coefficients may vary.

The horizontal analysis may be applied within the Hudson River plume. Since the plume is most evident during periods of high runoff, time variable conditions probably prevail. This fact, in addition to the presence of vertical gradients makes this analysis more approximate by contrast to the vertical. However, it does permit reasonable estimates to be made of the transport coefficients in the horizontal plane - the lateral and longitudinal dispersion coefficients. The analyses presented in the following sections provide simplified procedures for the assignment of the range of transport and kinetic coefficient for the three-dimensional segmented model described in subsequent sections.

II. VERTICAL ANALYSIS

One of the most significant factors responsible for the vertical gradients in water quality is the density stratification due to temperature and salinity differences. This condition is most pronounced during the summer and generally produces a relatively well-mixed surface layer and a poorly-mixed lower layer. Differences in concentration of many water quality parameters exist between the two layers during this period and are particularly evident in the case of dissolved oxygen. Its concentration is effected not only by the vertical stratification and the associated dispersion, but also by the various sources and sinks in each zone - photosynthetic production and exchange with the atmosphere in the upper layer and biological respiration and benthal demand in the lower. The following analysis includes these reactions with vertical dispersive transport under a steady-state condition.

Basic Equations and Boundary Conditions

The basic differential equation which defines the vertical distribution of dissolved oxygen under the steady-state conditions:

$$0 = \frac{d}{dz}\left(E(z)\frac{dc}{dz}\right) + \Sigma S_o - \Sigma S_i \qquad \text{(II-1)}$$

in which

c = concentration of dissolved oxygen

E = vertical dispersion coefficient

ΣS_o = kinetic sources

ΣS_i = kinetic sinks

The concentration, c, may be expressed in terms of the deficit, $D = c_s - c$, in which c_s = equilibrium saturation value of dissolved oxygen for a given surface temperature and salinity. The primary kinetic source is the photosynthetic production of oxygen by phytoplankton and the sink is algal and bacterial respiration. Equation (II-1) may then be expressed as follows:

$$0 = \frac{d}{dz}\left(E(z)\frac{dD}{dz}\right) + R(z) - P(z) \qquad \text{(II-2)}$$

in which R(z) and P(z) are respectively the volumetric oxygen utilization and production rates. The former includes both the phytoplankton and bacteria contributions. Since production and respiration are operative in the surface layer, while only the latter is effective in the lower layer, the water column may be divided into two regions, delineated by the pycnocline. Equation (II-2) directly applies to the upper layer, while the lower layer is described by this equation without the production term.

Since there are two second-order differential equations, one for each layer, four boundary conditions are required to evaluate the constants of integration. The upper layer is identified by the subscript, T, and the lower by the subscript, B. The boundary conditions are provided by flux balances at the air-sea interface, the pycnocline and the bed and by the concentration equality at the pycnocline:

$$z = 0 \qquad E_T \frac{dD_T}{dz} = K_L D_o \tag{II-3}$$

$$z = p \qquad D_{Tp} = D_{Sp} \tag{II-4}$$

$$E_T \frac{dD_T}{dz} = E_B \frac{dD_B}{dz} \tag{II-5}$$

$$z = H \qquad E_B \frac{dD_B}{dz} = S \tag{II-6}$$

in which

D_o, D_p = deficits at the interface and at the pycnocline (M/L^3)

K_L = oxygen transfer coefficient (L/T)

S = areal oxygen utilization rate at the bed M/L^2T.

Solution of Equations

The first integration of equation (II-2) for the upper layer yields

$$E_T \frac{dD_T}{dz} = \int_o^P P(z)dz - \int_o^P R(z)dz + C_1 \tag{II-7}$$

and the second

$$D_T = \int \frac{dz}{E(z)} [\int_o^P P(z)dz - \int_o^P R(z)dz + C_1 z] + C_2 \tag{II-8}$$

Applying the first boundary condition (equation (II-3)) to equation (II-7) yields

$$C_1 = K_L D_o$$

and $C_2 = D_o$

By averaging the dispersive and kinetic terms in the upper layer, equation (II-8) becomes after substituting the values of C_1 and C_2:

$$D_T = [\frac{P_T - R_T}{E}]Z^2 + \frac{K_L D_o Z}{E} + C_o \qquad \text{(II-9)}$$

In the lower layer, the photosynthetic contribution is zero and the first integration of equation (II-2) yields

$$E_B \frac{dD_B}{dZ} = -R_B Z + C_3 \qquad \text{(II-10)}$$

Applying the fourth boundary condition (equation (II-6)) to equation (II-10) provides the evaluation of C_3:

$$C_3 = S + R_B H$$

Substitution of this result into equation (II-10) and integration leads to:

$$D_B = -\frac{R_B Z^2}{2E_B} + \frac{Z(S + R_B H)}{E_B} + C_4 \qquad \text{(II-11)}$$

The remaining constants D_o and C_4 are determined by the second and third boundary conditions (equations (II-4) and (II-5)). Equating (II-7) and (II-10) at Z = p and solving for D_o yields:

$$D_o = -\frac{(P_T - R_T)}{K_L} p + K_L [R_B(H - P) + S] \qquad \text{(II-12)}$$

Equating (II-9) and (II-11) at z = p permits evaluation of C_4:

$$C_4 = -\frac{(P_T - R_T)}{2E_T} p^2 + \frac{p}{E_b} [\frac{R_b(H - p)}{2} + S] + D_o [1 + \frac{K_L p}{E_T}] \qquad \text{(II-13)}$$

Thus equations (II-9) with (II-12) define the concentration of dissolved oxygen deficit in the upper layer and equations (II-10) with (II-13) in the lower layer. Conversion to dissolved oxygen values is made by subtracting the calculated deficit from the equilibrium saturation value specific to a given location for a given surface salinity and temperature regime.

The various transfer, kinetic and density coefficients were assigned on the basis of either direct measurement or values reported in the literature. These data are primarily derived from ongoing MESA research in the Bight, and supplemented by previous historical studies. A discussion of the coefficients employed in the analysis is contained in section VIII. The specific coefficients utilized in the vertical dissolved oxygen calculations are indicated in Figure II-1 and II-2 which present calculated and observed dissolved oxygen for a series of stations in the Bight for the summer conditions of 1974 and 1976.

III. HORIZONTAL ANALYSIS

The horizontal analysis applies to the region in the apex which is influenced by the fresh water discharge of the Hudson River. There are evident horizontal gradients of both salinity and dissolved oxygen in the vicinity of the Sandy Hook Transect. Because of the many factors which affect the dissolved oxygen, as described in the previous section, it is appropriate to look to the horizontal salinity distribution for evaluation of transport parameters. The approximations contained in a steady-state horizontal analysis of salinity are probably more crude than those in the vertical dissolved oxygen case. The procedure, however, does permit at least a quantification of the range of the horizontal dispersion and of the system sensitivity to this parameter.

During periods of high runoff in the spring the Hudson River plume is clearly defined, usually deflected, to some degree, to the west along the Jersey shore. Following a path of minimum salinity, which may be characterized by a maximum velocity and lateral mixing, the following flux equation may be written for the salinity deficit:

$$0 = E_y \frac{\partial^2 c}{\partial y^2} - U_x \frac{\partial c}{\partial x} \qquad \text{(III-1)}$$

The concentration, c, is defined as a reference ocean salinity, s_o, minus the observed concentration, s, along the characteristic. The solution for the above, with a boundary condition c_o at $x = 0$ and $c = 0$ at $x = \infty$, is:

$$\frac{c}{c_o} = \text{erf}\left[\frac{UB}{E_y x}\right]^{\frac{1}{2}} \qquad \text{(III-2)}$$

FIGURE II-1.
VERTICAL DISTRIBUTION OF DISSOLVED OXYGEN, 1974

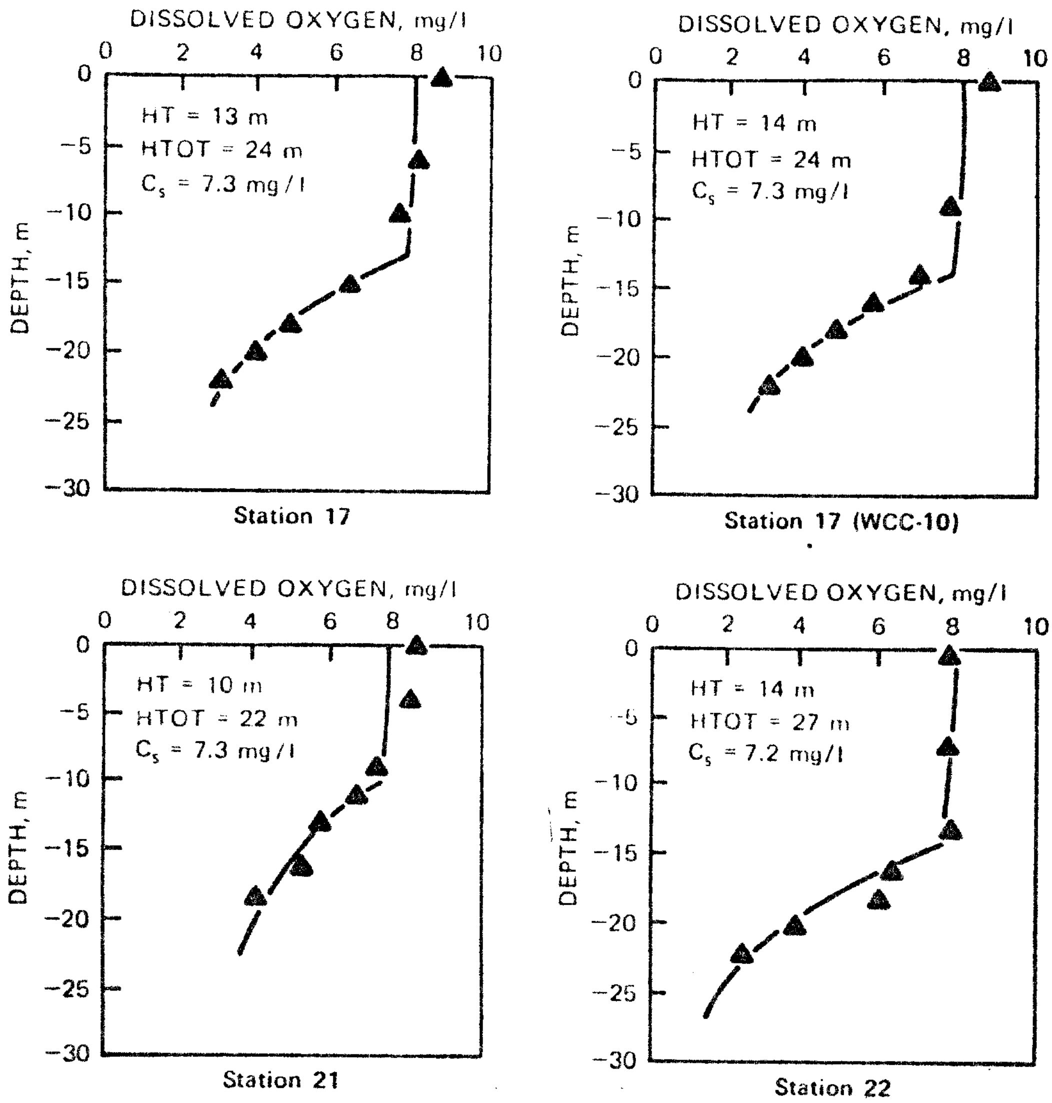

Parameters:

Vertical dispersion coefficient (top)	11.6 cm^2/sec
Oxygen production rate from photosynthesis	0.75 mg/l-day
Film transfer coefficient for dissolved oxygen	0.75 m/day
Bottom oxygen utilization rate	0.75 g/m^2-day
Water column utilization rate (respiration)	0.30–0.40 mg/l-day
Vertical dispersion coefficient (bottom)	0.6–1.0 cm^2/sec

FIGURE II-2.
VERTICAL DISTRIBUTION OF DISSOLVED OXYGEN, 1976

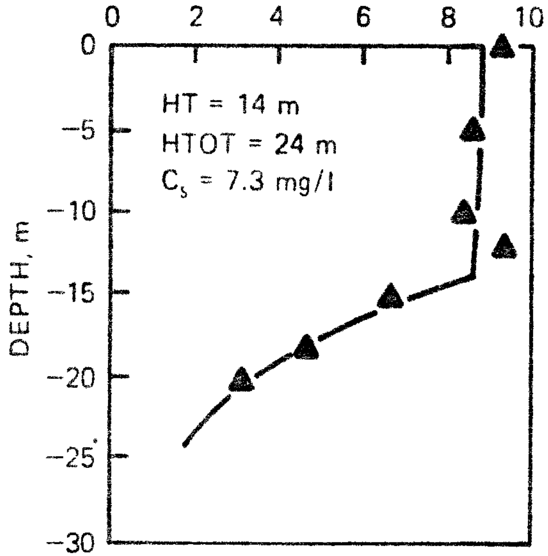

Station 21 (XWCC-10)

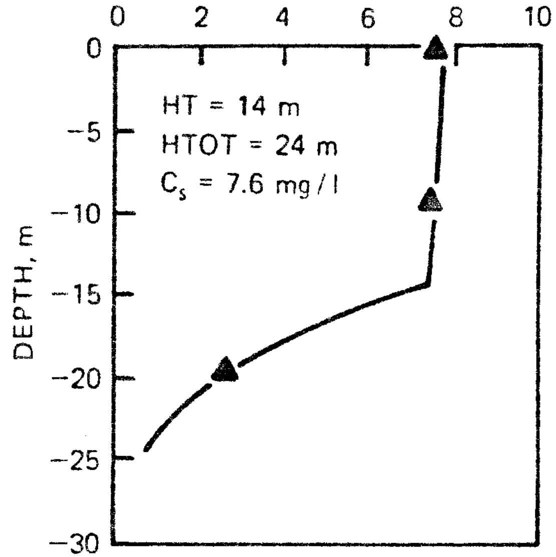

Station 21 (XWCC-11)

Parameters:

Vertical dispersion coefficient (top)	11.6 cm^2/sec
Oxygen production rate from photosynthesis	0.75 mg/l-day
Film transfer coefficient for dissolved oxygen	0.75 m/day
Bottom oxygen utilization rate	0.75 g/m^2-day
Water column utilization rate (respiration)	0.30–0.40 mg/l-day
Vertical dispersion coefficient (bottom)	0.46–1.0 cm^2/sec

in which

U = velocity

B = width at $x=o$

E_y = lateral dispersion

x = distance along the characteristic contour

The boundary condition, c_o, is that at the Sandy Hook transect and the velocity, U, is the freshwater discharge from the Hudson and Raritan drainage areas, divided by upper layer cross-sectional area. The value of the dispersion coefficient may be determined from the concentration distribution along the axis defined by the salinity deficit in accordance with the above expression. Application of this equation is shown in Figure III-1, which represents two Hudson River flow conditions, as shown. The value of 1 mi^2/day is assigned as the dispersion coefficient.

The vertical dissolved oxygen analysis of Section III and the horizontal chlorides analysis of this section are employed to define relatively narrow ranges for the vertical and horizontal dispersion coefficients respectively. These coefficients are employed in the three dimensional analysis to define a summer transport field for the Bight which follows.

IV. TRANSPORT EQUATION

Total transport is defined by the joint transport resulting from advective flow and dispersion;

$$\frac{\partial}{\partial x}(sU_x) + \frac{\partial}{\partial y}(sU_y) - \frac{\partial}{\partial z}(sU_z)$$

$$-[\frac{\partial}{\partial x}(E_x \frac{\partial}{\partial x}) + \frac{\partial}{\partial y}(E_y \frac{\partial}{\partial y}) + \frac{\partial}{\partial z}(E_z \frac{\partial}{\partial z})] = 0 \qquad \text{(IV-1)}$$

where x,y,z are the longitudinal, lateral and vertical axes respectively and

s = salinity concentration

U_x, U_y, U_z = Velocity in the direction of the specified axis.

E_x, E_y, E_z = Dispersion in the direction of the specified axis.

A numerical solution to equation IV-1 is obtained employing a finite difference approximation:

$$0 = \sum_{j=m}^{n} [-Q_{kj}(\alpha_{kj}S_k + \beta_{kj}S_j) + E'_{kj}(S_j - S_k)] \qquad \text{(IV-2)}$$

FIGURE III-1.
CALCULATED AND OBSERVED
ONE-DIMINSIONAL SALINITY

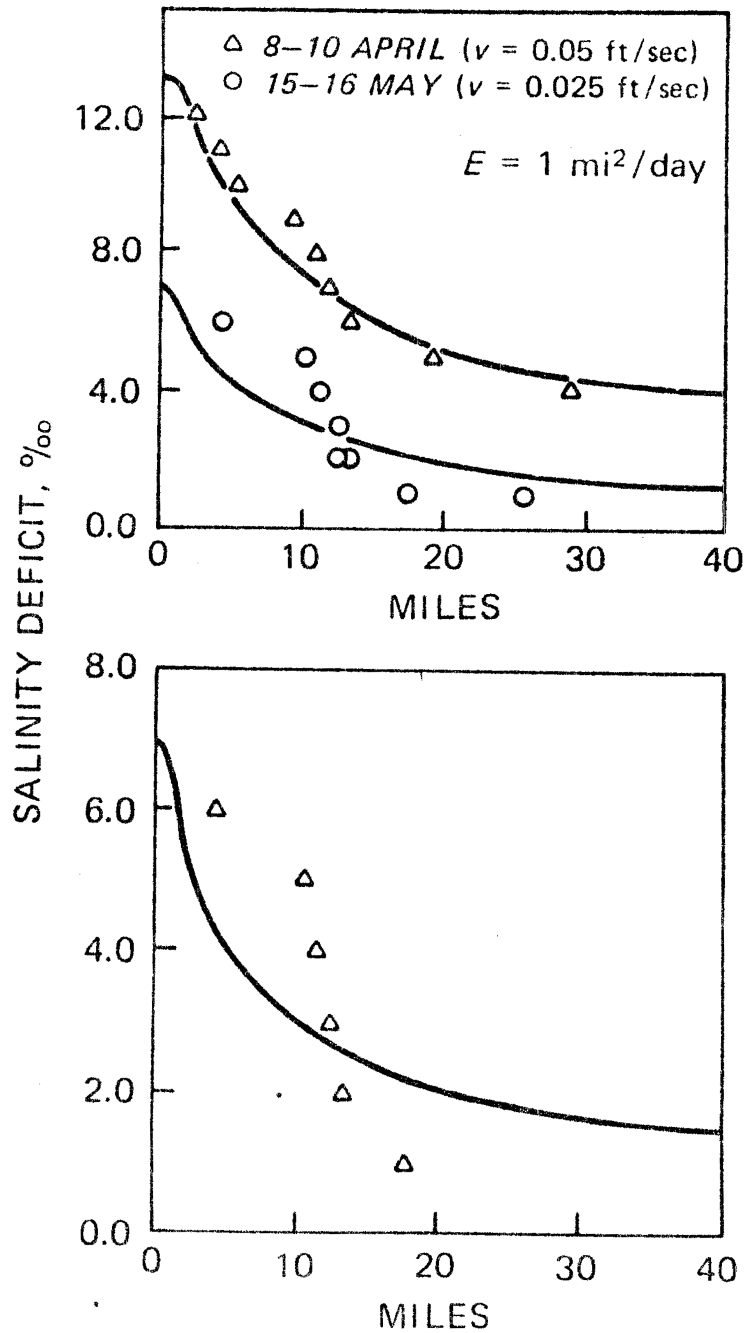

The x,y,z coordinate space is subdivided into spatial segments. A mass balance is taken around each segment (k) and summed over all adjacent segments (j). A more detailed discussion of the finite difference approach employed is presented in Appendix C. Transport is thus defined by an advective-dispersive field consisting of flows Q_{kj} and dispersion parameters E'_{kj} for each segment interface of the model. The dispersion parameter is equal to

$$E'_{kj} = \frac{E_{kj}A_{kj}}{\overline{L}_{kj}} \qquad \text{(IV-3)}$$

Q_{kj} = flow across segment interface kj
E'_{kj} = dispersion parameter across segment interface kj
E_{kj} = dispersion coefficient across segment interface kj
A_{kj} = area of segment interface kj
$\overline{L}_{kj}$ = average distance between the centers of segments k and j
α_{kj}, β_{kj} = concentration weight factors.

Examination of equations IV-2 and V-3 indicates that the transport field is defined by the advective flows "Q" and the dispersion coefficient "E". In addition the particular segmentation of the coordinate space x,y,z establishes the scale of the analysis and to an extent the values of the individual parameters "Q" and "E". Therefore the definition of a transport field for the New York Bight contains three interrelated factors. These are:

1. The segmentation of x,y,z coordinate space used in the analysis
2. The advective flow field appropriate for the spatial segmentation of the analysis.
3. The set of dispersion coefficients appropriate for the spatial segmentation of the analysis.

Subsequent sections of this report discuss each of these three components of the definition of the total transport field.

V. SYSTEM SEGMENTATION

The study area is segmented as illustrated on Figure V-1. The segmen-

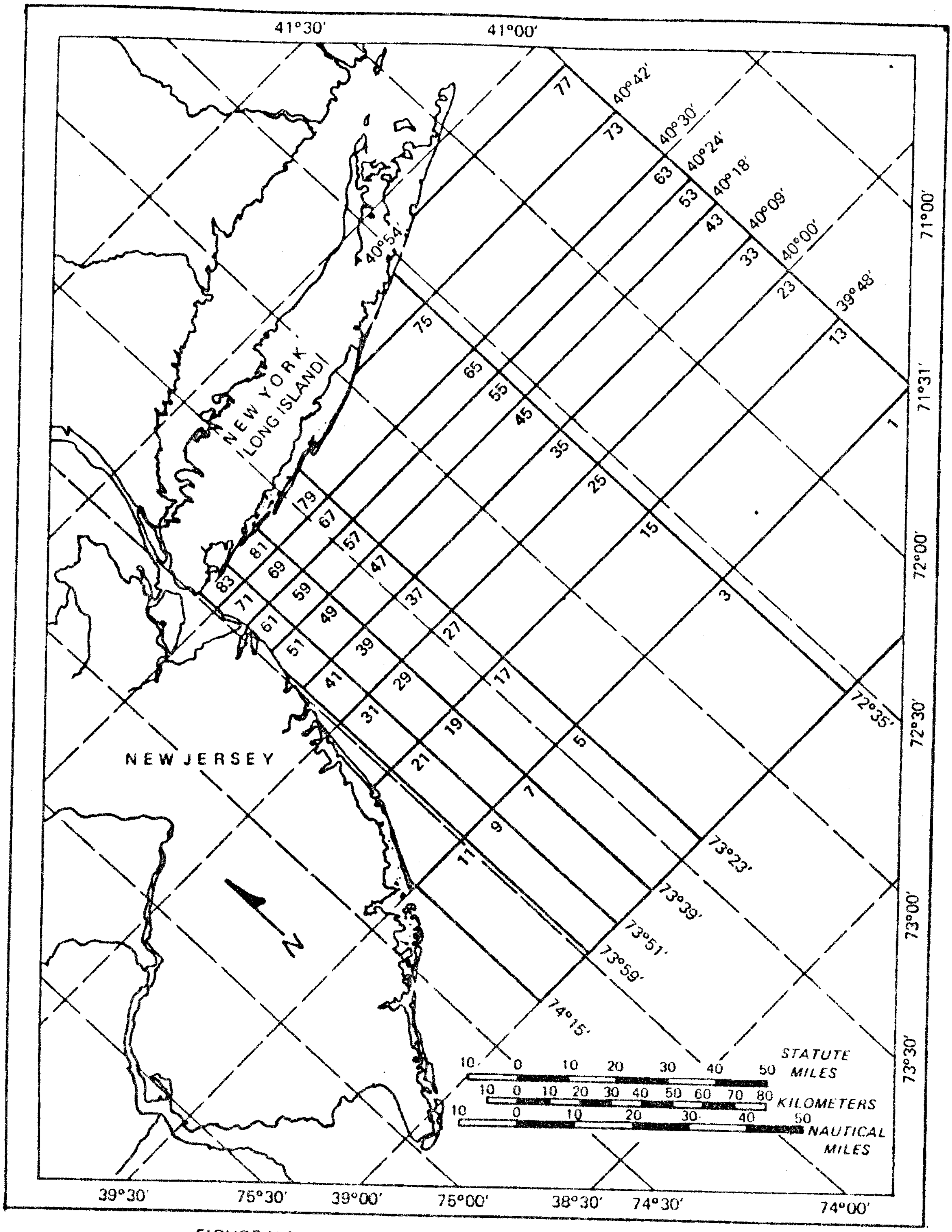

FIGURE V-1a. SURFACE SEGMENTATION – NEW YORK BIGHT

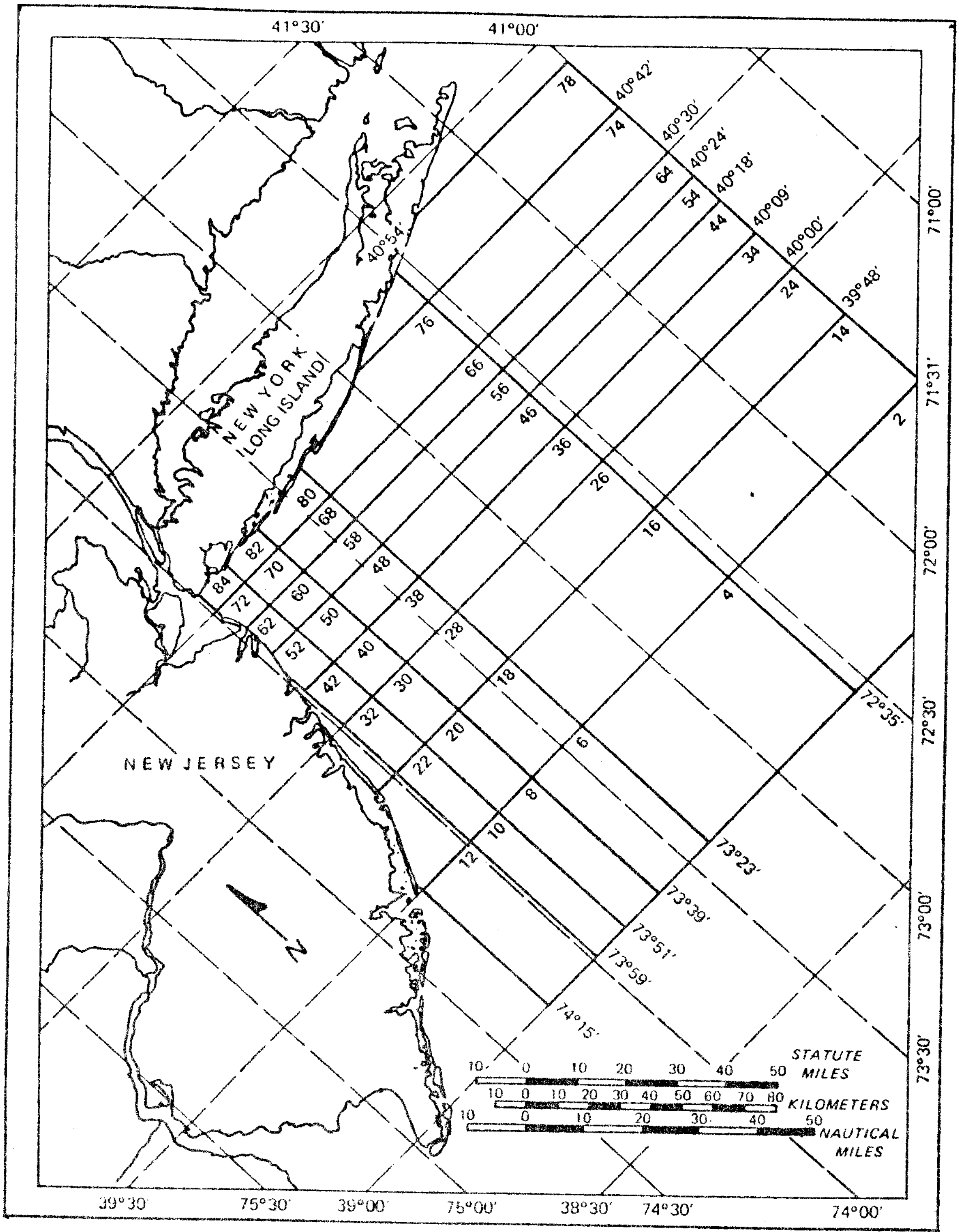

FIGURE V-1b. BOTTOM SEGMENTATION -- NEW YORK BIGHT tation indicated was employed in the steady state calculations of summer salinity and dissolved oxygen distributions. The area studied is bordered to the south by latitude 39°00'N, to the east by longitude 71°00'W, to the North by the Long Island coast, and to the west by the New Jersey coast. The system is divided into two vertical layers with a total of 86 segments. Even numbered segments represent the bottom waters of the study area while the odd numbered segments are employed to represent the surface waters of the Bight. As shown, the apex and the region adjacent to the New Jersey coast are defined by finer segmentation. These regions of the system, which have the largest gradients in water quality, are the locations in which depressed bottom dissolved oxygen levels have been observed. Details of the system segmentation used, were also controlled by format and geometry requirements of Brookhaven National Laboratories. The segmentation is consistent with the available data base and the degree of understanding of phenomena controlling water quality.

The location of the bottom of the pycnocline is defined from data presented by Starr and Steimle (1). This information was employed to define the boundary between top and bottom segments for both 1974 and 1976 conditions. The interface between top and bottom segments forms a surface which gently slopes seaward to a maximum depth of 35 meters in the region of the shelf break. Figure V-2, illustrates the vertical density structure observed at two stations during three surveys. The location of vertical interfaces are shown. The observed vertical structure varies between surveys. The depth of each segment is listed in Table D-2 of Appendix D. This appendix and Appendix A contain a discussion of the procedure employed to calculate volumes and cross-sectional areas for each segment with listings of the system geometry by segment and interface.

VI. Flow Balance

The information available on summer flow patterns in the New York Bight has been summarized by Hardy (2), Hansen (3), Bumpus (4)(5), Beardsley (6) and others. In general, average net velocities near the surface, in the summer, range between 5 and 20 cm/sec and are directed from the northeast towards the Southwest. Average summer net bottom velocities are weaker ranging between 0.2 and 3 cm/sec with an on-shore component in regions having depths less than 60 to 70 meters. In the deeper eastern portions of the Bight the

FIGURE V-2.
DENSITY vs. DEPTH AT TWO STATIONS

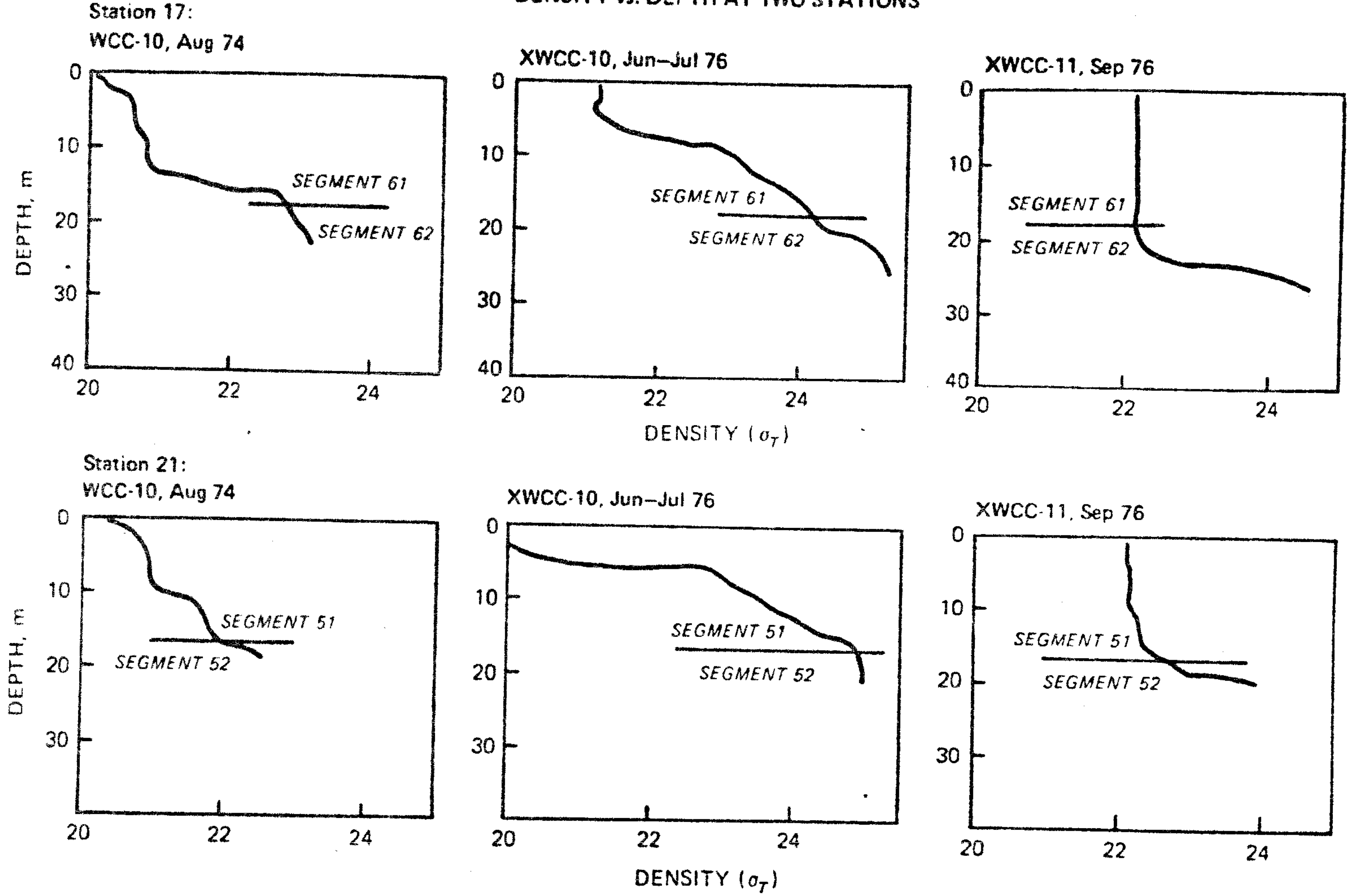

average summer net current direction in the bottom waters is from Northeast to Southwest.

The general descriptions of net current patterns in the Bight provides the bases for the definition of a flow field which is assumed to represent conditions in August 1974. There are 86 model segments with associated interfaces. Some interfacial velocities are specified either through measurements or from the available descriptions of the summer flow field in the New York Bight. For each segment, continuity requires that equation (V-1) be satisfied if evaporation is neglected.

$$\sum_{j=1}^{M} a_{ij} v_j = q_i \qquad i=1,2,\ldots,N \qquad \text{(V-1)}$$

where

a_{ij} = interfacial area between segments i and j

v_{ij} = velocity at interface

q_i = flow into segment i for specified flows.
q_i = 0 if all flows are unknown.

There are more unknown velocities than equations of continuity for each segment. An additional constraint is employed in the analysis: namely that the kinetic energy $1/2 \; \Sigma \; V_j^2$ be a minimum. The solution is obtained employing the method of Lagrange multipliers. The flow field is generated employing an alogarithm which imposed continuity and minimization of kinetic energy, as discussed in Appendix B.

The freshwater flow from the Hudson River for August 1974 is estimated at 16,300 cfs which includes upstream gaged inflows, waste discharges and estimated flows from ungaged tributary areas of New York Harbor. A typical estuarine circulation pattern exists in the Hudson estuary and New York Harbor (7)(8). From the work of Kao (8) it is estimated that the net shoreward flow through the bottom portion of a transect between Sand Hook and Rockaway Point was on the order of 52,000 cfs. This flow enters the Hudson estuary from the bottom model segments adjacent to New York Harbor (Segments 84 and 72) and is returned to the ocean through the comparable surface segments (Segments 83 and 71). The Hudson River flow also is introduced in these surface segments. Other freshwater flows and ground water inflow are not included in the analysis.

The flow field calculations used the cross-sectional area of each interface of the model, as listed in Appendix D. Bumpus' (4),(5), description of the summer flow field provided a basis for the definition of velocities for the bottom segments at the outer boundaries of the model and at the mouth of New York Harbor. Three near-shore segments adjacent to the New Jersey coast are left with unspecified velocities at the ocean boundaries. A program which implemented the alogarithm presented in Appendix B is then employed to calculate the velocities at each interface of the bottom segments of the model. The calculations include upwelling at the shoreline segments along the Long Island and New Jersey coasts. The velocity calculations for the surface layer proceed in a similar fashion. The calculated upwelling along the Long Island and New Jersey shorelines is inputted into the surface layer as equivalent velocities. This procedure insures overall system continuity. The velocities which are specified in the surface layer calculations include internal velocities. The results of the calculations are presented on Figure VI-1 for the surface and bottom layers of the system. The velocities which were specified at individual interfaces in the calculation procedure are shown in brackets.

A comparable calculation was made for 1976 summer conditions. The Hudson River freshwater flow was estimated at 29,250 cfs for August, 1976. In addition, current measurements in July and August of 1976 were available, from AOML (9), for four locations within the Bight. These data are employed to estimate specified velocities at the segment interfaces nearest the point of measurement. The calculated 1976 summer flow field used in this analysis is presented in figure VI-2. Bracketed velocities were specified as input in the calculation procedure.

The flows generated by the procedure discussed above should be considered as possible flow fields. The probability is remote that these flow patterns actually existed during the periods to which they have been assigned. Therefore from the standpoint of physical oceanography they provide no additional information.

These flow fields are, however, possible and further are consistent with the available data in terms of both the direction and magnitude of net velocities and flows. From the standpoint of the analysis of water quality they may be considered as a representative flow field which may be used to examine

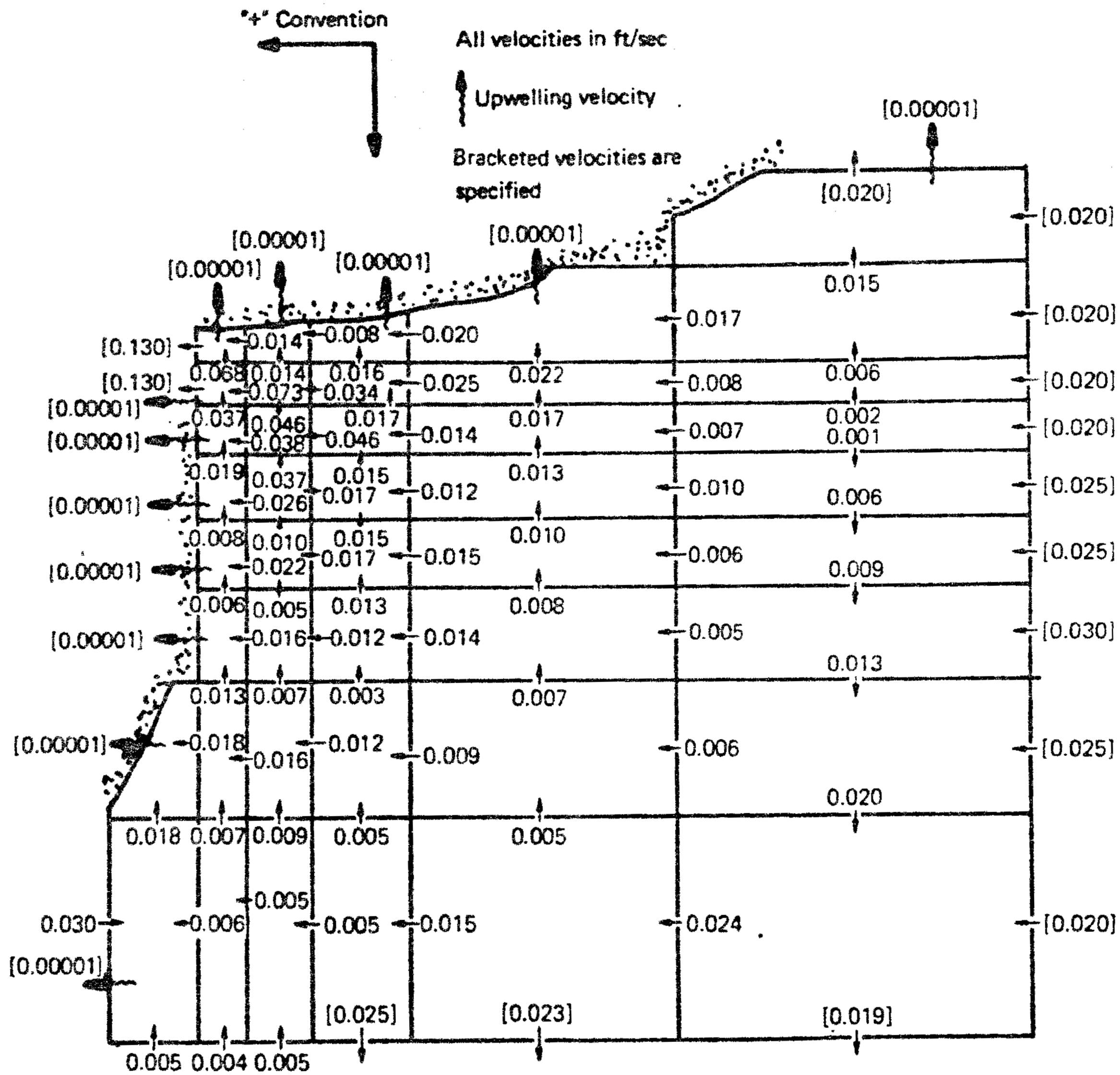

FIGURE VI-1a. LOWER LAYER VELOCITY FIELD FOR AUGUST 1974

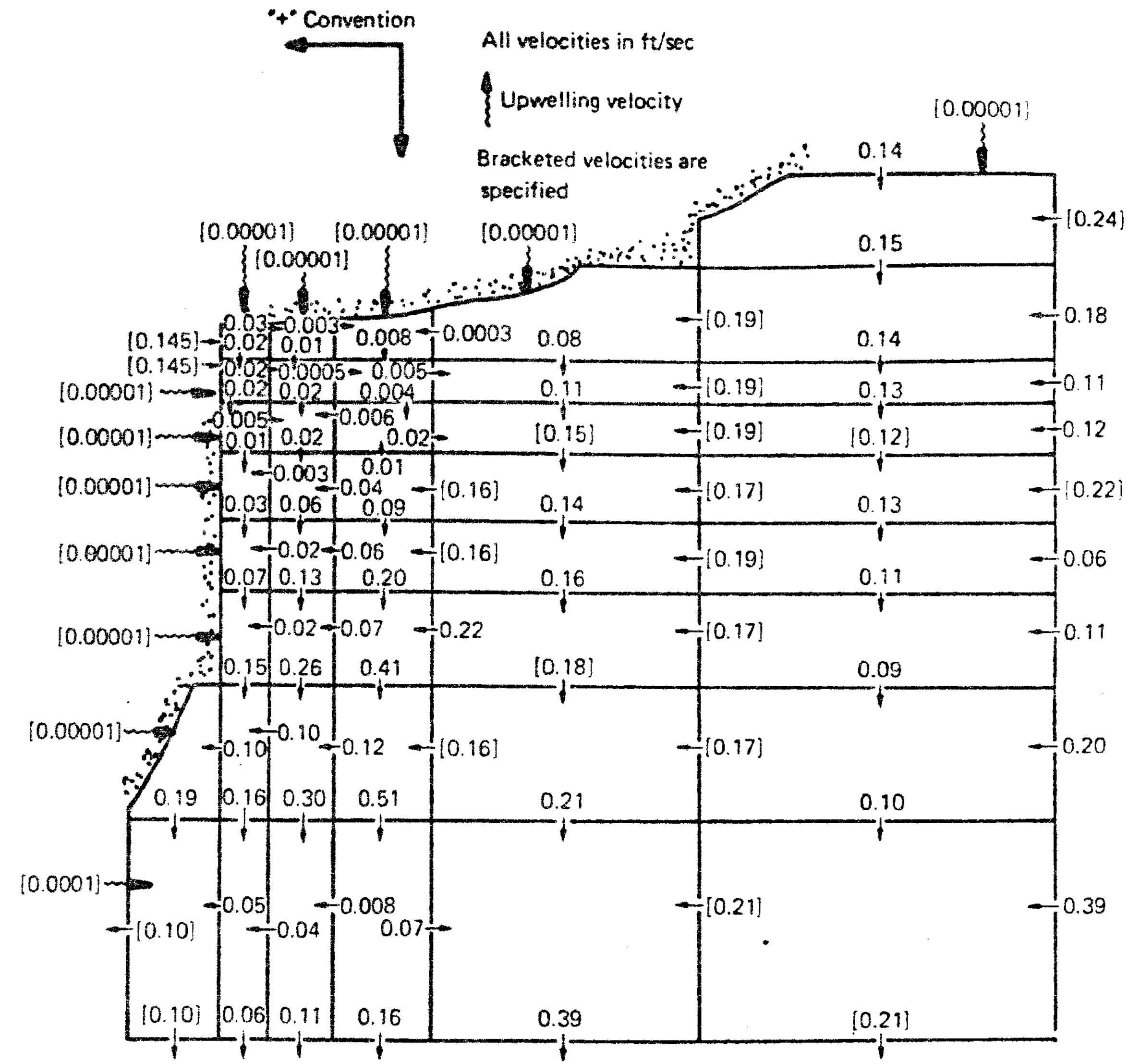

FIGURE VI-1b.UPPER LAYER VELOCITY FIELD FOR AUGUST 1974

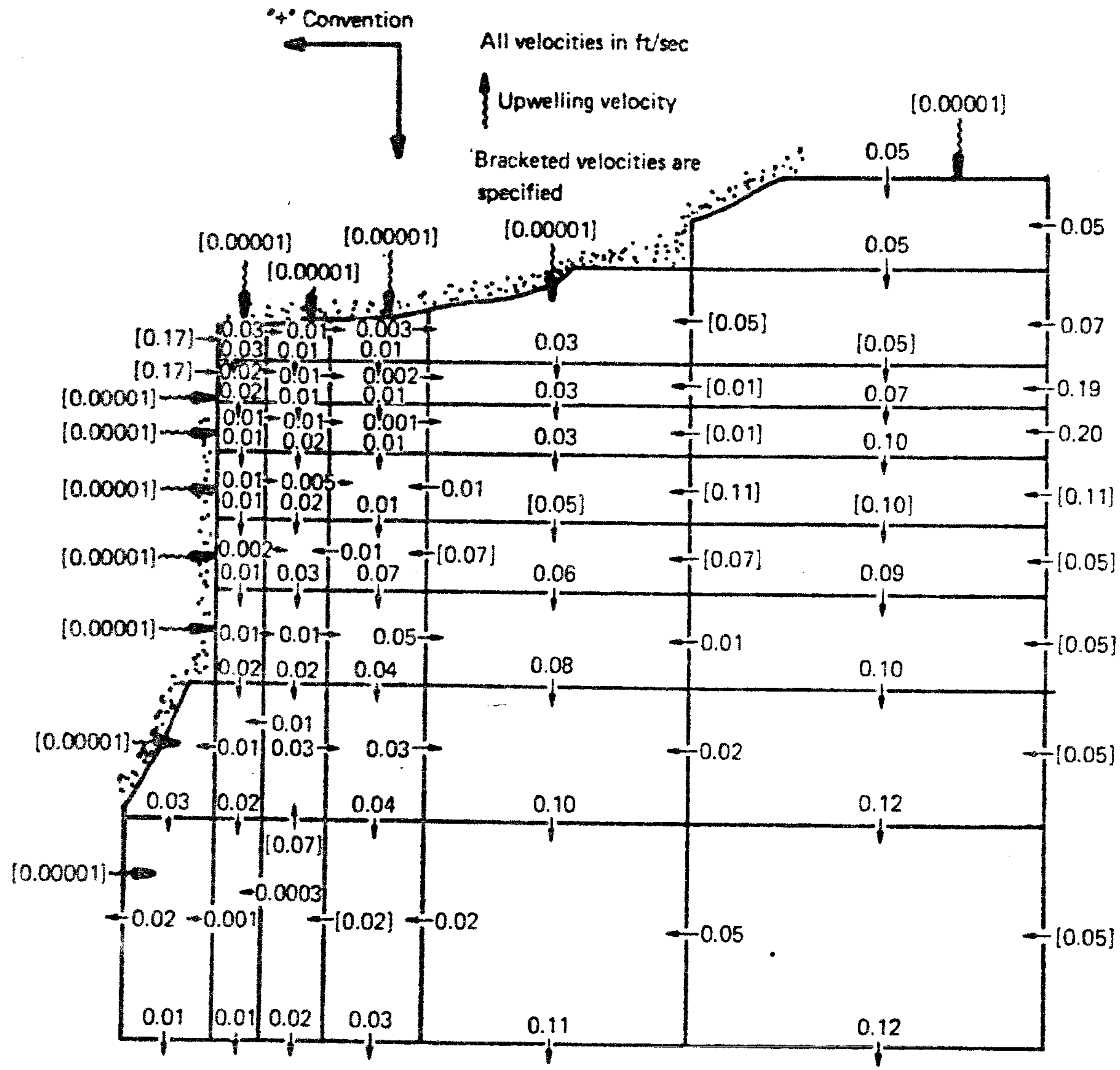

FIGURE VI-2a. UPPER LAYER VELOCITY FIELD FOR 1976

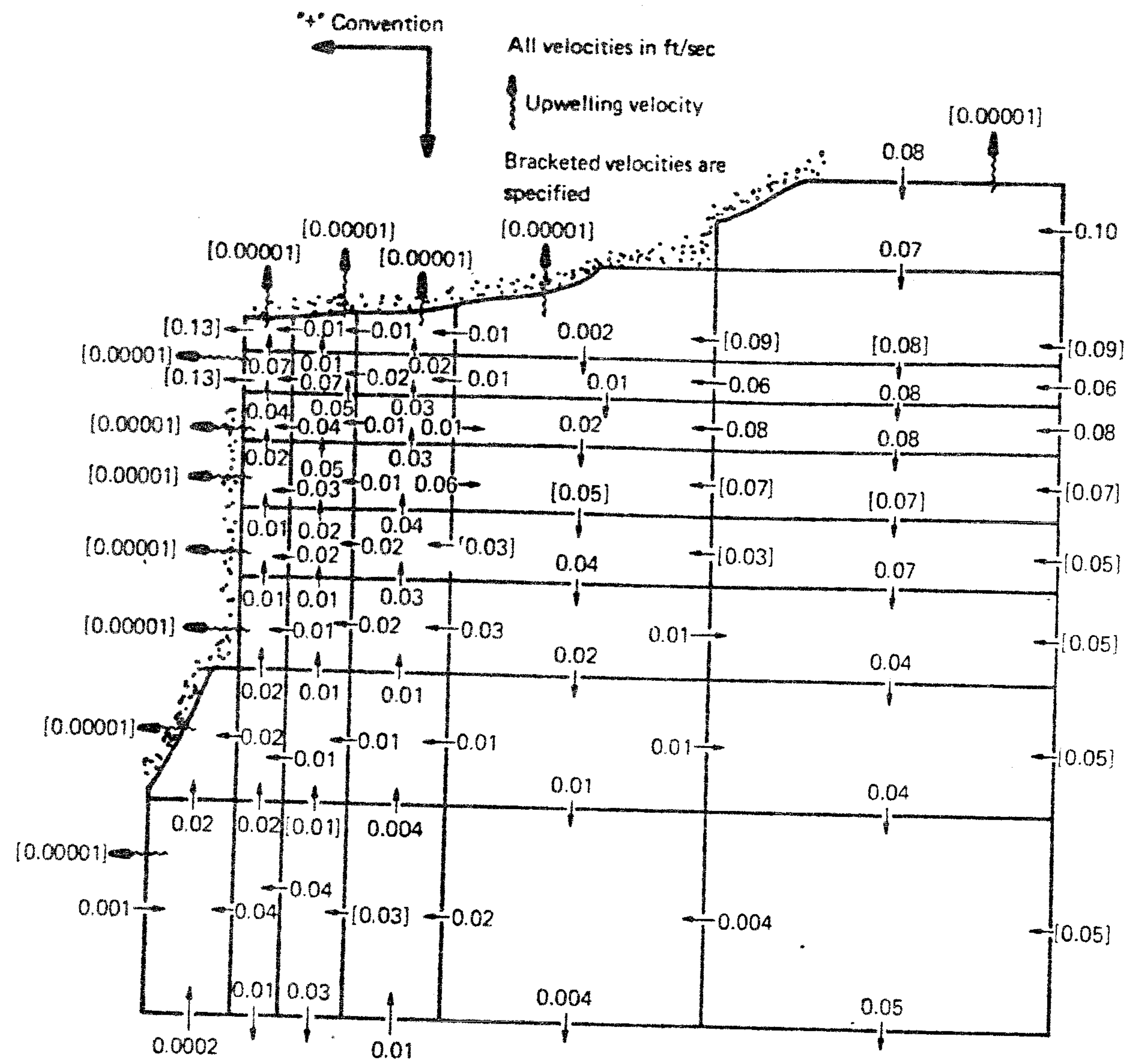

FIGURE VI-2b. LOWER LAYER VELOCITY FIELD FOR 1976 the system in the context of available information on water quality. It is with this perspective that the calculated flow field is employed in the following analysis.

VII. Transport Field

The transport field developed in this study was employed to calculate salinity profiles for summer periods. The flow portion of the transport fields are as defined in section VI. The 1974 flow field was defined using historical (4,5) data on general ocean currents and estimates of August 1974 freshwater inputs from New York Harbor. The 1976 flow field incorporated available current data at four sites and estimates of appropriate 1976 freshwater inputs from New York Harbor. The dispersion coefficients employed in the calculation of salinity were identical for each year. Figure VII-1 presents data relating the vertical dispersion coefficient to density gradient. The range of maximum density gradients observed in the Bight during the summer surveys in 1974 and 1976 are also shown on the figure. Calculations of vertical dissolved oxygen profiles presented in Section III indicate that the minimum vertical dispersion coefficient is in the range of 0.5 to 1.0 cm^2/sec. This range of the coefficient is consistent with the data presented on figure VII-1. Therefore data from the literature and the vertical dissolved oxygen analysis presented in section II suggest that an appropriate value for the minimum vertical dispersion coefficient is 1 cm^2/sec. This value of the coefficient was assigned to the interface between top and bottom segments in the three dimensional calculations for salinity and dissolved oxygen. The dispersion coefficients at the longitudinal and lateral interface in both surface and lower layer are assigned at a value of 2.6×10^6 m^2/day (1 mi^2/day) in the inner Bight and 1.3×10^6 m^2/day (0.5 mi^2/day) for the outer regions of the Bight as shown on Figure VII-2. The dispersion coefficients used in the analysis are derived from the horizontal analysis presented in section II and are consistent with those determined in large bays with weak tidal action and regular bottom topography (15). At the outer ocean boundaries the dispersion coefficient was assigned an arbitrary large value of 2.6×10^4 m^2/day (100 mi^2/day). This large value was chosen since no data beyond the boundary was available for any of the periods analyzed. The boundary salinity values were defined by observed data nearest the boundary. Figure VII-3

FIGURE VII-1.
VERTICAL DISPERSION COEFFICIENT AS A FUNCTION OF DENSITY GRADIENT

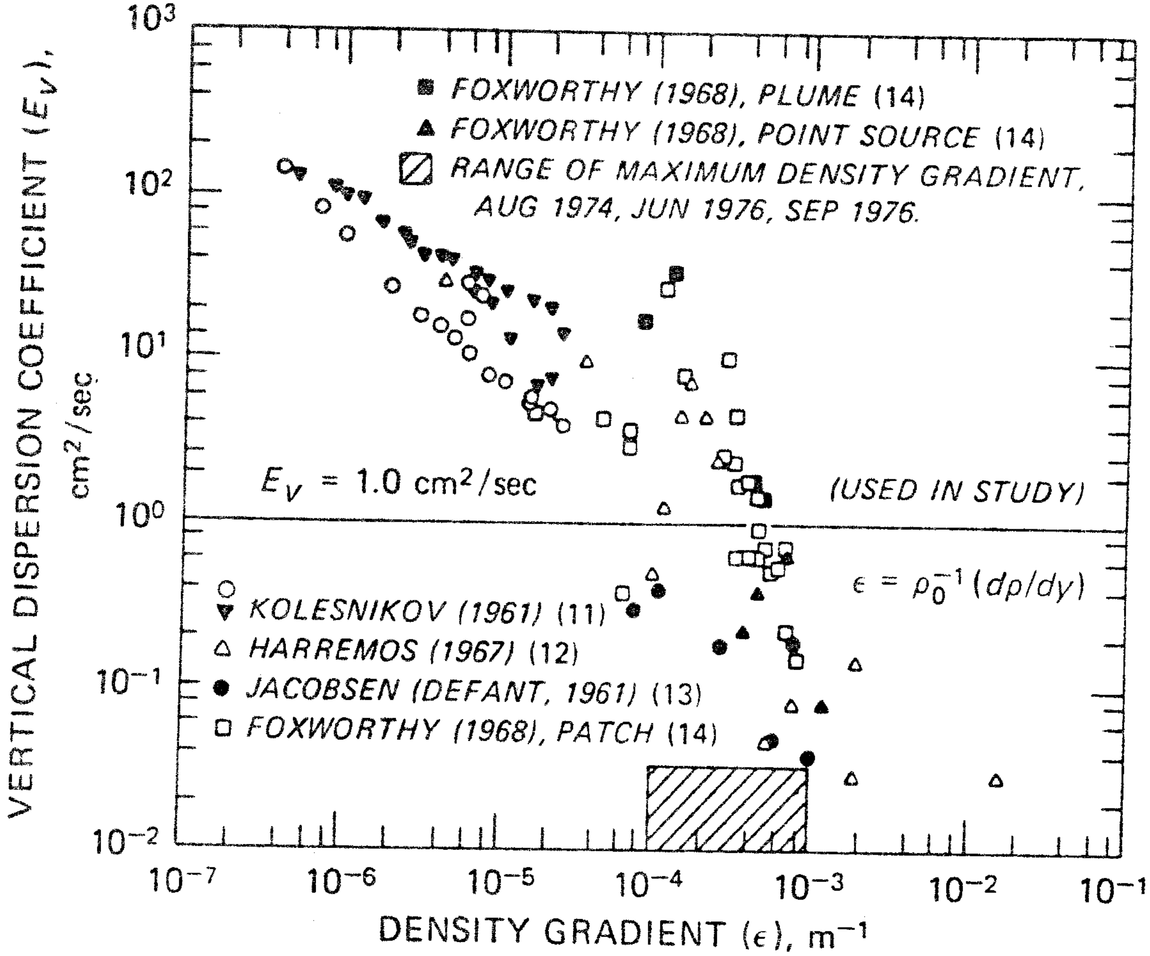

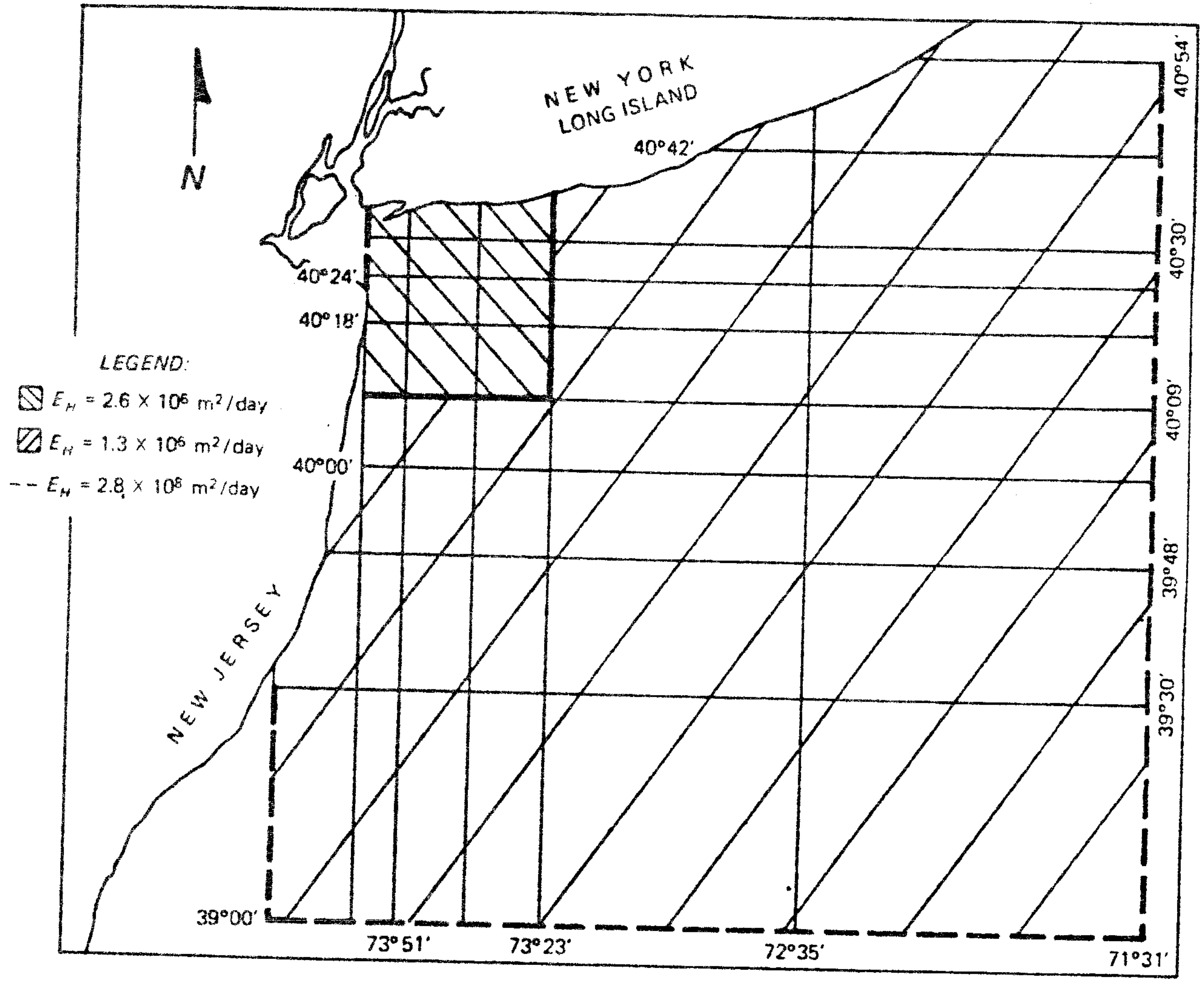

FIGURE VII-2. LATERAL AND LONGITUDINAL DISPERSION COEFFICIENTS and VII-4 present comparisons of observed salinities (shown by the iso-salinity contours) and calculated salinities (shown by the numerical values for each segment). These data are for August, 1974 (cruise WCC-10) and September, 1976 (cruise XWCC-11) respectively. The observed salinities of the inner Bight region associated with the bottom waters are comparable for both years. By contrast the surface salinities, for this region, in 1974 were on the order of a part per thousand lower than those observed during June 1976. The salinities calculated by the model employing the two transport fields agree reasonably with each year's data. The calculated salinities for 1974 are generally lower than the comparable calculated salinities for 1976.

A series of calculations were developed to determine the sensitivity of calculated salinities to variations in the transport field. Salinity distributions were calculated considering a factor of two change in the magnitude of the flow field and the horizontal dispersion coefficients. In general these computations indicated that the maximum salinity variations for an individual location was on the order of 0.5 parts per thousand. The average of the maximum variations in salinity was on the order of 0.3 parts per thousand. The calculated bottom salinities tended to be more sensitive to parameter changes than the comparable surface values.

Additional computations indicated that reduction of the vertical dispersion coefficient to 0.1 cm^2/sec (a ten fold change in parameter) resulted in increased salinity levels in the bottom waters at many locations on the order of 1 to 2 parts per thousand.

The transport system parameters used are presented in Appendix D. The transport fields provide a reasonable representation for a dissolved conservative constituent such as salinity. The observed and calculated salinity gradients were relatively small and therefore it would be prudent to consider the transport fields as possible transport fields which characterize the gross features of the system over a summer. Based on the sensitivity calculations it is concluded that comparison of calculated and observed salinity distributions provides one necessary aspect for defining adequate transport fields. This comparison is not sufficient to insure uniqueness of the field.

It is acknowledged that this transport field may not be unique. The sensitivity analysis provides further definition of the degree of uniqueness.

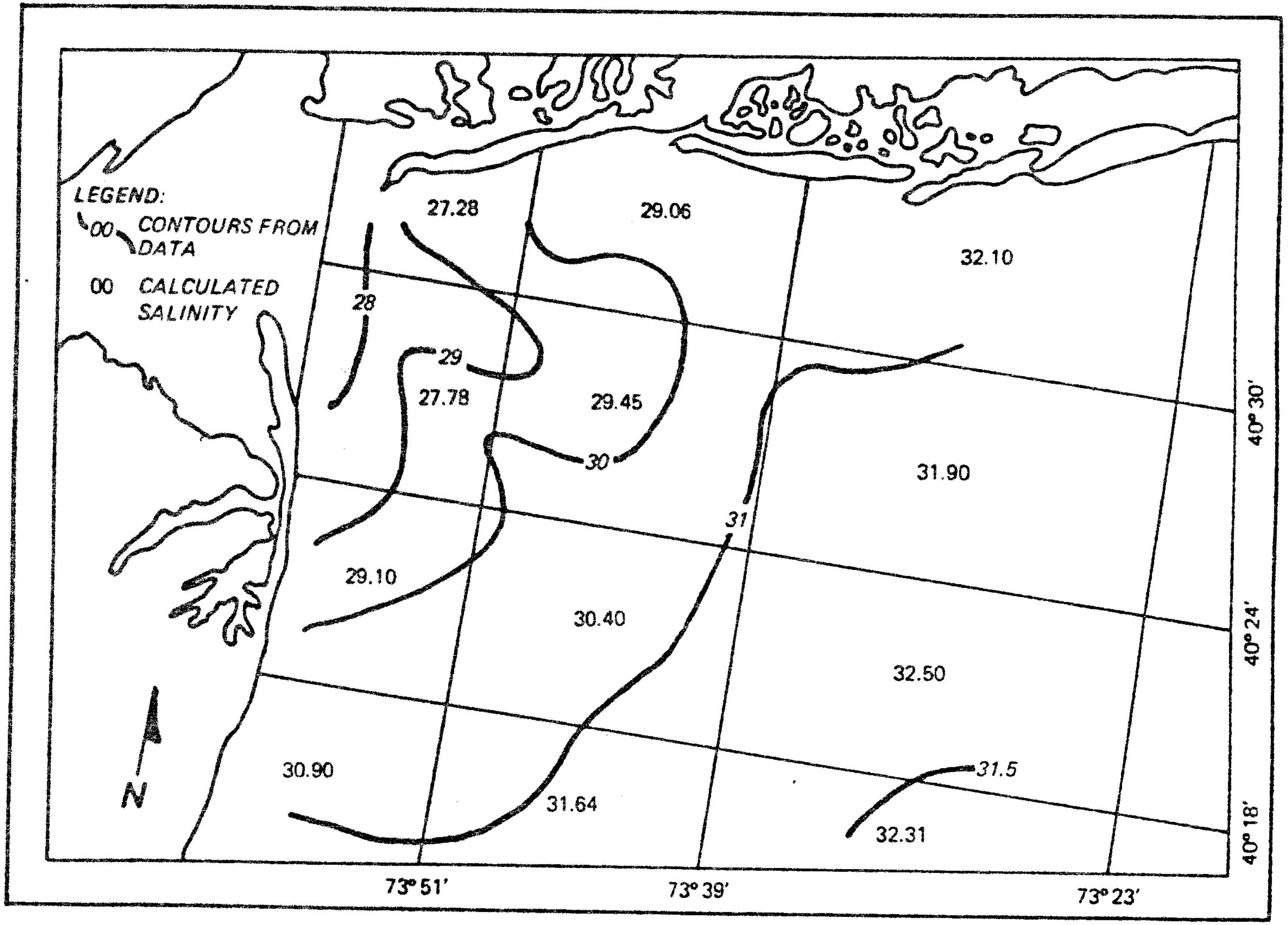

FIGURE VII-3a.
SURFACE SALINITY FIELD – OBSERVED AND CALCULATED – AUGUST 1974

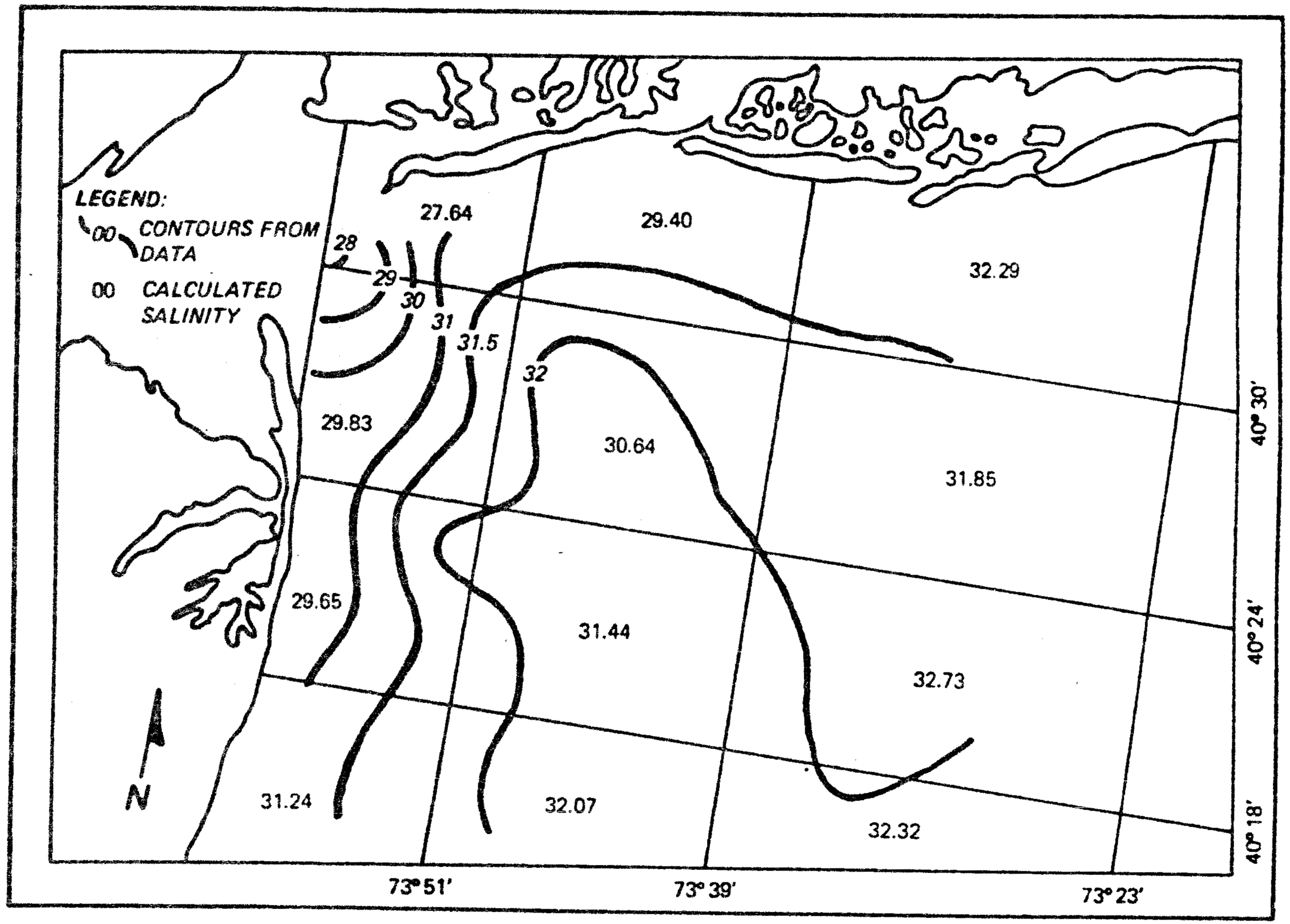

FIGURE VII-3b.
BOTTOM SALINITY FIELD – OBSERVED AND CALCULATED – AUGUST 1974

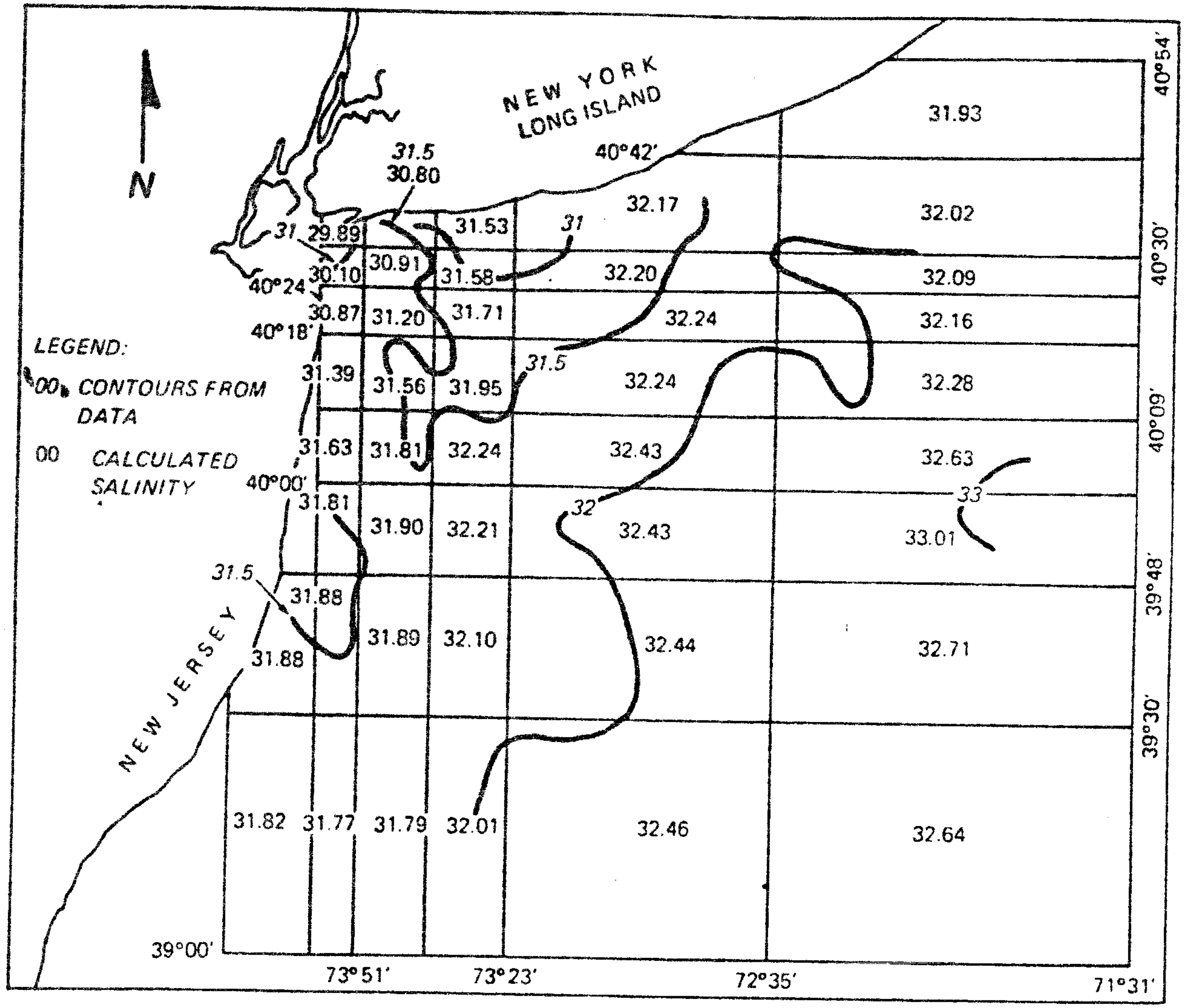

FIGURE VII-4a. SURFACE SALINITY FIELD, OBSERVED AND CALCULATED, JUNE 1976.

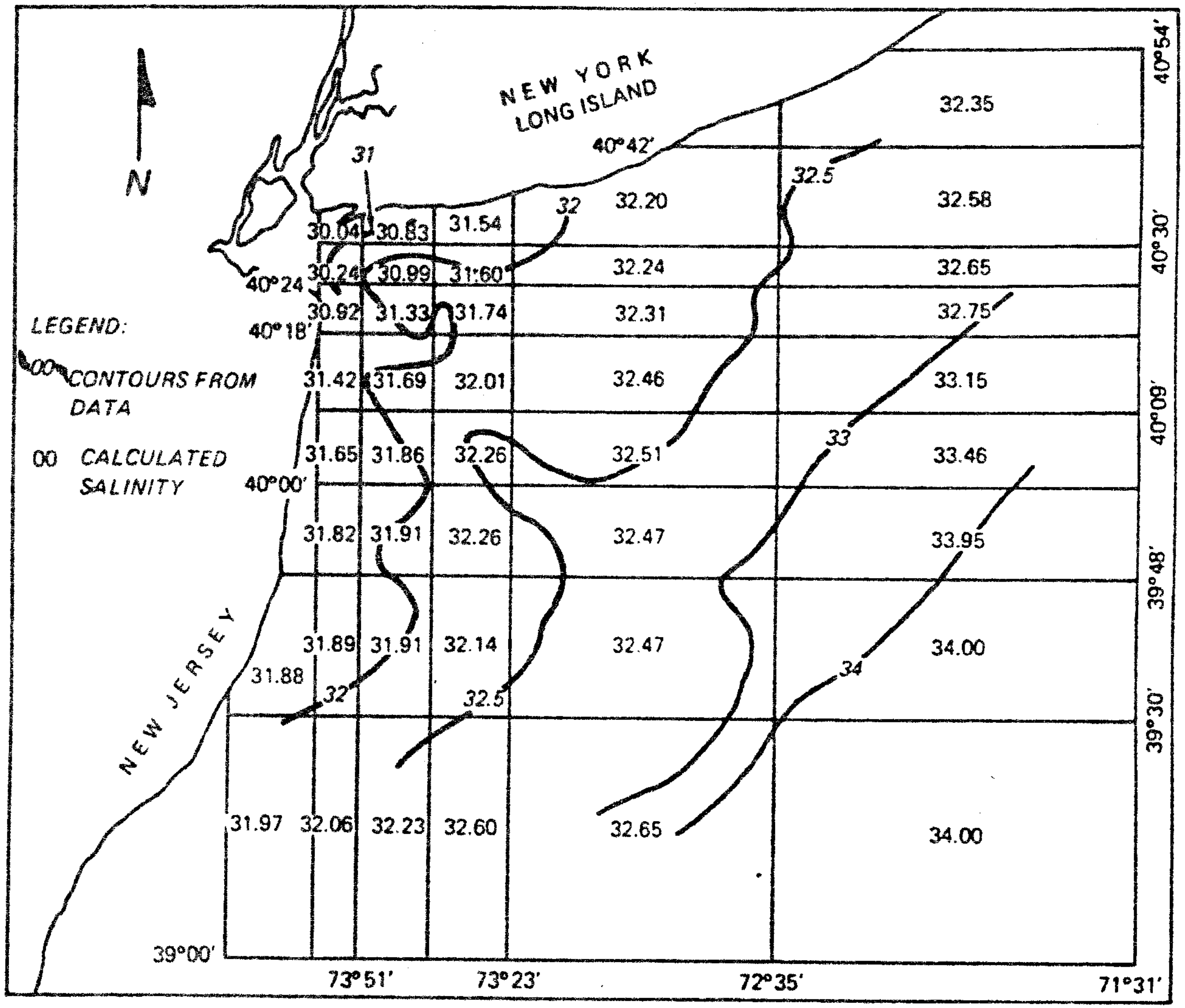

FIGURE VII-4b. BOTTOM SALINITY FIELD, OBSERVED AND CALCULATED, JUNE 1976

However, regardless of the model used, agreement between calculated and observed salinity distributions is a necessary condition for a valid transport analysis.

VIII. Dissolved Oxygen Analysis

The dissolved oxygen analysis employed the transport field discussed in section VII. Additional phenomena included in the analysis were the oxidation of organic carbon from New York Harbor sources, the oxygen produced by photosynthesis, the oxygen utilized by organic deposits on the sea bottom and the oxygen utilized by the respiration of phytoplankton. The latter sink of dissolved oxygen includes the oxidation of detritus carbon formed within the biological system of the Bight. The basic differential equation employed for the dissolved oxygen analysis is most conveniently written in terms of dissolved oxygen deficit which is defined by equation VIII-1.

$$D = C_s - C \qquad \text{(VIII-1)}$$

where: D = dissolved oxygen deficit at any location

C = dissolved oxygen at any location

C_s = saturation level of dissolved oxygen under the conditions of temperature and salinity at the surface

Replacing "s" in the transport equation IV-1 by deficit "D" and defining the resultant equation by "j" (D) the appropriate reaction and source-sink term may be added yielding:

$$V\frac{\partial D}{\partial t} = o = j(D) - P_{(x,y,z)} + K_d L_{(x,y,z)} + R_{(x,y,z)} \qquad \text{(VIII-2)}$$

with boundary conditions:

$$Z = o \qquad E_z \frac{dD}{dz} = k_L D_o$$

$$Z = H \qquad E_z \frac{dD}{dz} = S$$

Where: $j(D)$ = transport equation IV-1 with "s" replaced by "D"

D = dissolved oxygen deficit

k_L = liquid film coefficient

P = oxygen produced by photosynthesis

R = oxygen used by phytoplankton respiration

S = oxygen used by organic deposits on the sea bottom

L = BOD inputs to the system

k_d = oxidation rate of BOD

The above partial differential equation was solved with the finite difference approximations discussed in Appendix C. The reaeration term $k_a D$ is defined as a result of the finite difference approximation and is included in the diagonal terms of the resultant matrix while the remaining source and sink reaction terms including S are included in the forcing function as indicated in Appendix C.

Kinetic Coefficients and Boundary Conditions

The value of film transfer coefficient, K_L, was 1 m/day and is within the range of .3 to 5 m/day summarized[15] for values of this parameter. The film transfer coefficient divided by the depth of the surface segments yields the reaeration coefficient k_a for each surface segment of the model. Dissolved oxygen is transported into the bottom layers by vertical dispersion. All dispersion coefficients employed in the dissolved oxygen calculations were identical to those used in the salinity analysis.

Values of the bottom oxygen utilization rate reported by Thomas et al. (16) for August 1974 were used in the regions of the model where data were available. The bottom oxygen utilization rate varied spatially between 0.1 and 1.0 gms/m^2/-day. The region covered by the available data was generally associated with the inner Bight including the sludge dumping grounds. In the remainder of the system modeled, bottom oxygen utilization rates were set at .4 gm/m^{-2}-day which represent a relatively clean bottom without significant accumulations of oxidizable organics.

Oxygen utilization rates in the water column were reported[16] to range between 0.17 and 2.85 mg/ℓ-day. The average was 1.2 mg/ℓ-day which would yield an equivalent BOD_5 of approximately 4 mg/ℓ. This appears somewhat high for ocean water.

A classical problem has been encountered in developing organic carbon mass balances for all types of water bodies. The cause of this difficulty is associated with an increase in oxygen utilized by viable phytoplankton organisms resulting from the change in environment between the natural system and laboratory test conditions. The incubation period of the BOD test is usually five days and may extend to 20 or more days. During this period of incubation, in the dark, some portion of the original phytoplankton population may contribute to an increase in the quantity of oxygen used.

The respiration studies carried out with New York Bight water employed short incubation periods compared to BOD test conditions. This should tend to reduce the portion of the phytoplankton population which is adversely impacted by the changed environmental conditions. Oxygen utilization rates would tend to be increased due to the changed environment conditions of the testing procedure.

Approximate calculations employing chlorophyll a data by Malone(17,18) suggest that the sum of oxygen utilization attributable to phytoplankton respiration and oxidation of particulate organic carbon may be in the range of 0.20 mg/ℓ-day with some spatial variations. Oxidation of dissolved organic carbon and ammonia would increase total oxygen utilization rates. The calculations were developed employing the following equations:

$$R_p = P_a \cdot k \cdot a_{op} \cdot a_{oc} \qquad \text{VIII-3}$$

where:

R_p = oxygen used by phytoplankton respiration mg/ℓ-day
P_a = chlorophyll a concentration (μg/ℓ)
K = phytoplankton respiration rate (1/day)
a_{oc} = oxygen to carbon ratio (mgO_2/mgc)
a_{op} = carbon to chlorophyll ratio (mgc/μg Chℓ)

$$R_{poc} = (POC - P_a a_{op}) \cdot k_o \cdot a_{oc} \qquad \text{VIII-4}$$

where:

R_{poc} = oxygen used in oxidation of "POC" (mg/ℓ-day)
POC = particulate organic carbon (mg/ℓ-day)
k_o = oxidation rate (1/day)

The values used in the analysis are presented in table VIII-1.

$$R = R_p + R_{poc} \qquad \text{VIII-5}$$

Malone[17,18] measured chlorophyll a and total inorganic nitrogen concentrations in August 1974. These data were combined with secchi disc measurements and estimates of the depth to the pycnocline for the August 1974 period from cruise WWC-10. Based on these data calculations of the range of oxygen production rates in the apex of the New York Bight for August conditions were made.

The rate of dissolved oxygen production can be estimated by:

$$P = a_{op} \cdot G_p \cdot P_a \qquad \text{VIII-6}$$

where:

P = dissolved oxygen production rate (mg/ℓ-day)
a_{op} = oxygen to chlorophyll ratio (mgO_2/μg Chℓ)
G_p = depth averaged phytoplankton growth rate (1/day)
P_a = phytoplankton concentration (μg Chℓ/ℓ)

The growth rate is defined by:

$$G_p = k_1(T) \cdot r \cdot \frac{C_N}{k_{MN} + C_N} \qquad \text{VIII-7}$$

where the light correction, r, is:

$$r = \frac{ef}{k_e H} [\mathrm{Exp}(-\alpha_1) - \mathrm{Exp}(-\alpha_o)] \qquad \text{VIII-8}$$

and

$$\alpha_1 = \frac{I_a}{I_s} e^{-k_e H} \qquad \text{VIII-9}$$

$$\alpha_o = \frac{I_a}{I_s} \qquad \text{VIII-10}$$

where:

$k_1(T)$ = temperature dependent light saturated growth rate (1/day)
C_N = concentration of inorganic nitrogen (mg/ℓ)
k_{MN} = Michaelis concentration for nitrogen (mg/ℓ)
e = 2.71
f = photo period - fraction of day
H = depth of segment (M)

k_e = light extinction coefficient (1/m)

I_a = daily average solar radiation (Lys/day)

I_s = optimum light for growth (Lys/day)

Parameter values employed in the calculations are within the reported ranges [20] and are presented in table VIII-1.

TABLE VIII-1

Coefficients - Oxygen Production an Respiration Rates

OBSERVED CONCENTRATIONS & PARAMETERS	VALUE EMPLOYED	SOURCE
a_{cp} carbon to chlorophyll (mgc/mg Chℓ)	50 - 100	20
a_{op} oxygen to carbon (mgO_2/mgC)	2.66	20
a_{op} oxygen to chl. (mg/μg)	.133-.266	20
k_R respiration rate (1/day)	0.1	20
k_o POC oxidation rate (1/day)	.1 - .25	15
k_1(T)(1/day) max. growth rate	2.5 @ 20°C	20
f photo period	.5	Est. USWB
k_e light extinction (1/M)	.2 - .3	WCC-10
I_a daily solar radiation (Lys/day)	400	USWB
I_s saturation radiation (Lys/day)	300	20
k_{MN} Michaelis (μg/ℓ)	∿ 50	17,18
P_a chlorophyll (μg/ℓ)	2 - 10	17,18
POC particulate organic carbon	.5	15
H segment depth (M)	Variable	Model

The calculated oxygen production rates "P" ranges between 0.33 and 1.6 mg/ℓ-day for average chlorophyll a values of 2 to 10 μg/ℓ which are consistent with the available data for the period. These data suggest that a chlorophyll a gradient may exist with higher levels near the mouth of New York Harbor and levels decreasing towards the outer Bight. The oxygen production rate due to photosynthesis, less the oxygen used in respiration; (P-R) in equation VIII-2, in all the surface segments of the model was assigned at 0.4 mg/ℓ-day which is consistent with the range calculated from the August, 1974 chlorophyll a data.

The vertical segmentation is such that the ratio of depth of the bottom segment to the depth of the surface segment tends to increase seaward. This factor combined with the apparent chlorophyll a gradient suggest that the oxygen utilization rate associated with phytoplankton respiration would be lower in the outer Bight in contrast to those associated with the inner Bight areas. The oxygen utilization rate for the bottom waters of the Bight is assigned at 0.3 mg/ℓ-day for regions where the depth of the bottom waters is less than 20 meters and 0.05 mg/ℓ-day in regions with bottom water depths greater than 20 meters. In model segments 50,60,70 which appeared to have somewhat high chlorophyll a levels at the surface and low bottom dissolved oxygen levels the respiration rates are assigned at .65,.75, and .80 mg/ℓ-day respectively. It could be hypothesized that the higher rates are associated with the sludge dumping activities which could increase organic concentrations in the water column and yield nutrient releases from the resulting benthal deposits. Appendix D contains a tabulation of all system parameters by segment used in the dissolved oxygen analysis. Table VIII-2 summarizes the parameters used in the analysis.

Calculated dissolved oxygen distributions are compared to observed data (represented by contours) on Figure VIII-1 and 2 for the August 1974 period. The dissolved oxygen calculations presented on this figure employed the 1974 transport field discussed in Section VII.

The identical reactions and source-sink parameters were employed with the 1976 transport field to calculate dissolved oxygen levels. A comparison of observed June, 1976 and calculated distributions are shown on Figures VIII-3 and VIII-4. It is evident from the figures that for the 1976 conditions the calculated and observed dissolved oxygen data do not agree in the inner Bight. The calculated dissolved oxygen levels for the 1976 period are similar to those calculated and observed in 1974 while the data for this period shows substantially lower dissolved oxygen levels. Figures VIII-5a and 5b present calculated and observed dissolved oxygen deficits for 1976 on the Bightwide scale for the bottom waters.

TABLE VIII-2

Parameter values employed for the
1974 and 1976 Analysis

PARAMETER	REPORTED RANGE	VALUE USED Top	VALUE USED Bottom	REFERENCE[1]
1. Advective Flow	.2-20 cm/sec	5-20 cm/sec	.2-3 cm/sec	(4), (5)
2. Horizontal Dispersion[3]	1 to 5 x $10^6 m^2$/day	1.3 to 2.6 x $10^6 m^2$/day		(15)
3. Vertical Dispersion	4-40 m^2/day	8.6 m^2/day		(10),(11),(12),(13),(1
4. Oxygen Production	0.3-1.6 mg/ℓ-day		0.7 mg/ℓ-day	(17),(18),(19),(20)
5. Oxygen Utilization[2]	.2 - 2.85 mg/ℓ-day	.3 mg/ℓ-day		(16),(17, 18, 19)
6. Bottom Oxygen Demand	.1 - 1.0 gm/m^2-day		0.1-1.0 gm/m^2day	(16)
7. Oxygen Transfer Coefficient	.3 - 5 m/day		1m/day	(15)
8. BOD Oxidation rate	.05 - .4/day	.1/day		(15)

NOTES:

1. For Reported Range
2. Varied with depth & over sludge dumps
3. Varied at boundary of model.

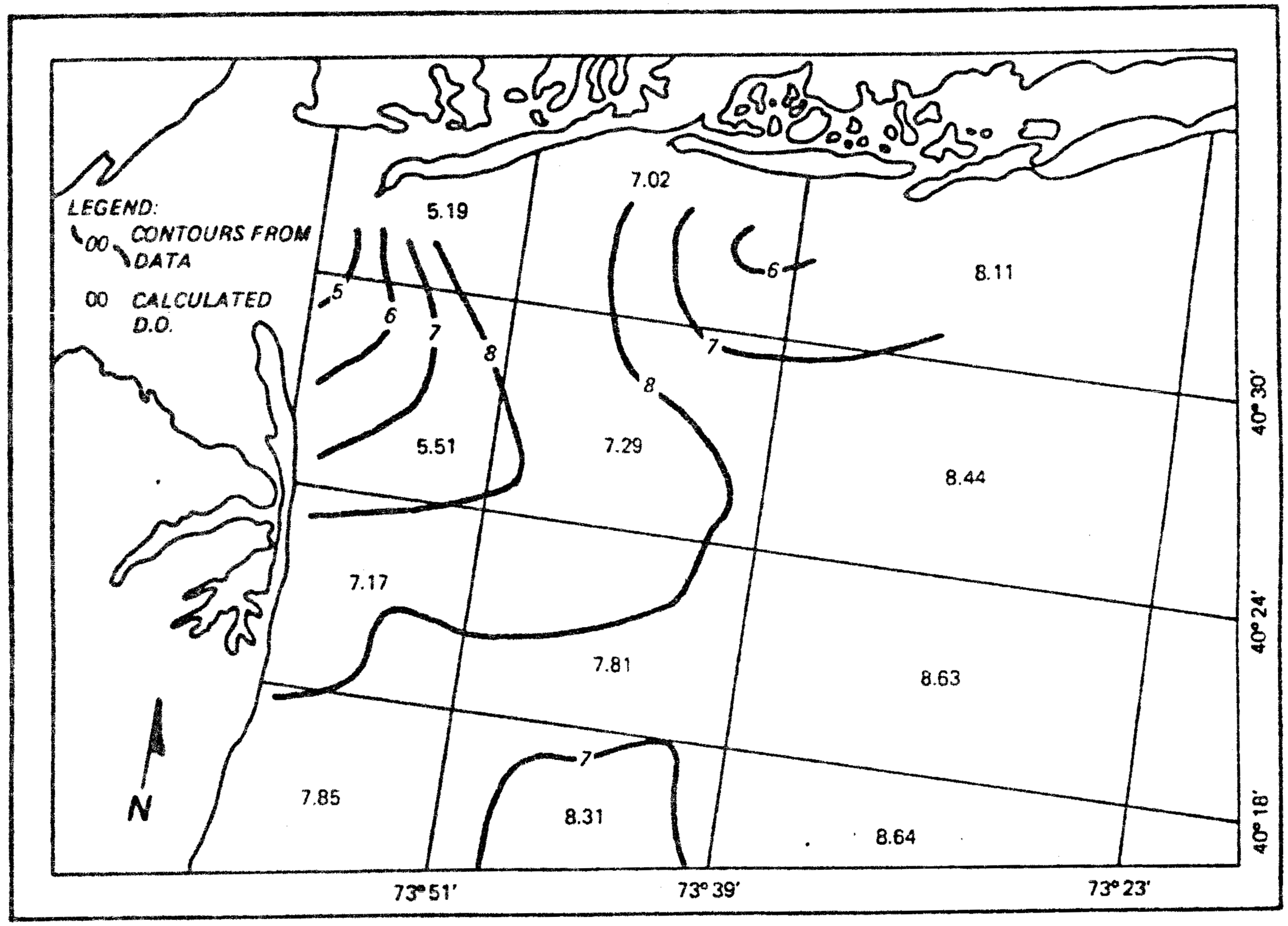

FIGURE VIII-1.
SURFACE DISSOLVED OXYGEN FIELD – OBSERVED AND CALCULATED – AUGUST 1974

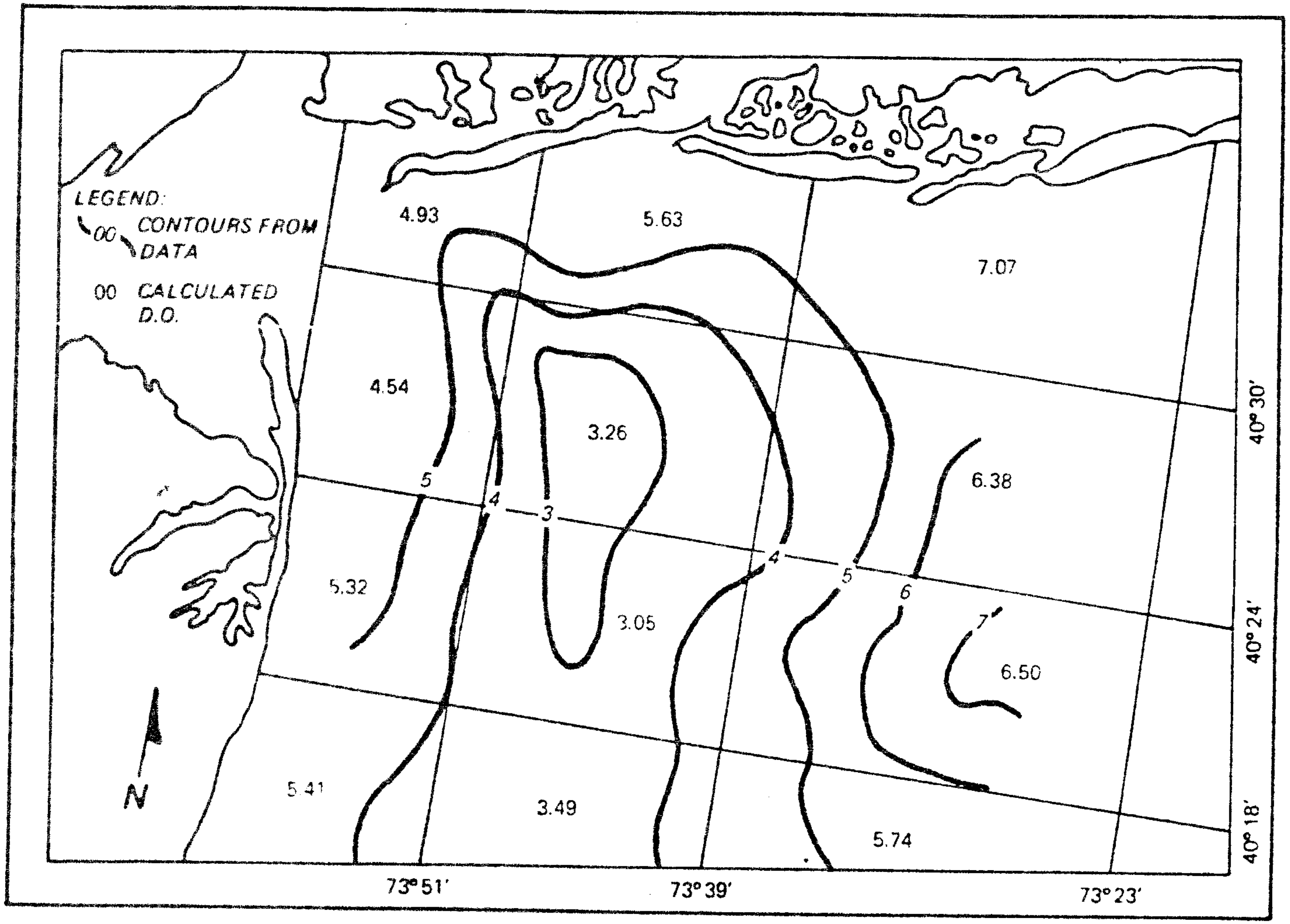

FIGURE VIII-2.
BOTTOM DISSOLVED OXYGEN FIELD – OBSERVED AND CALCULATED – AUGUST 1974

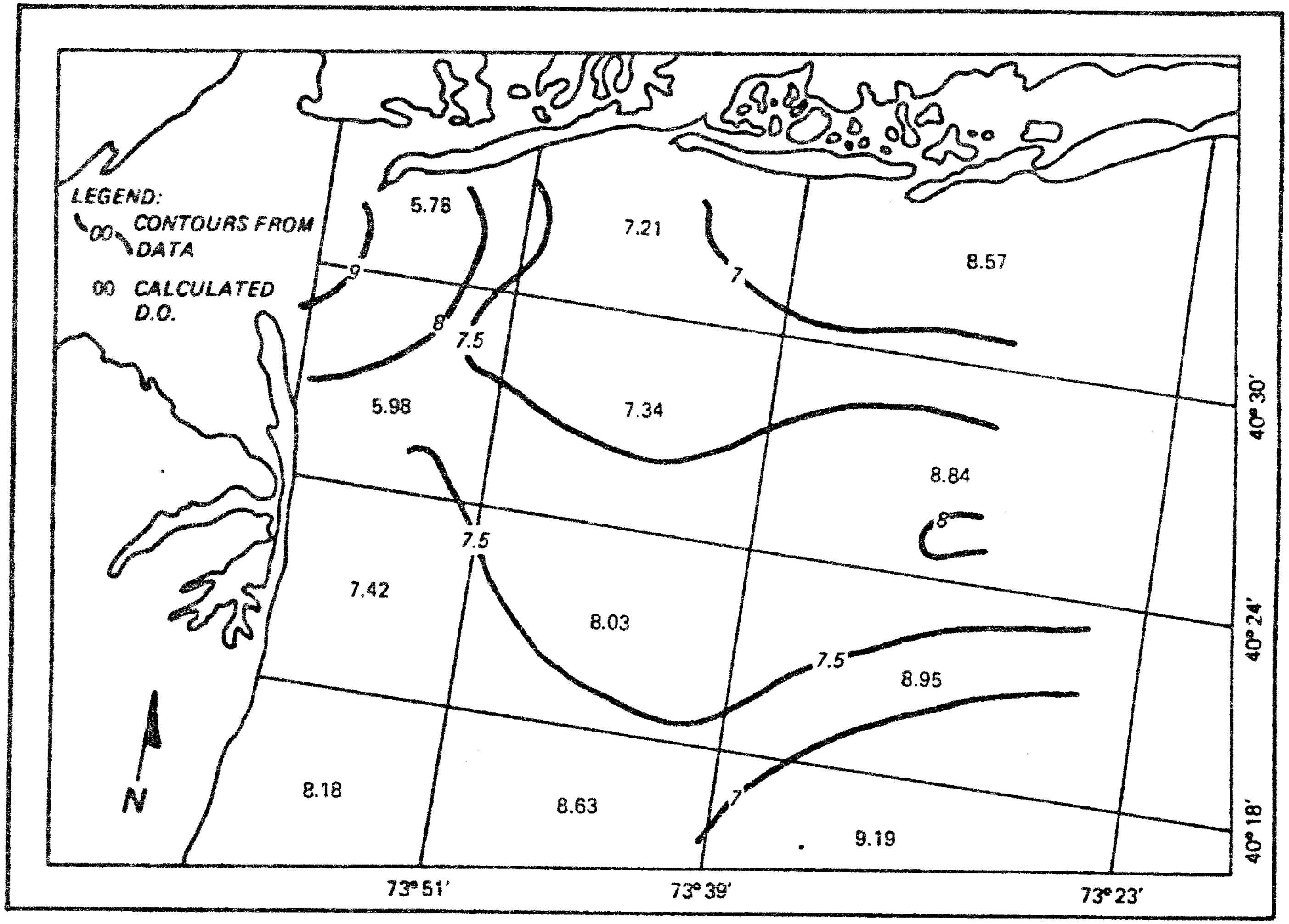

FIGURE VIII-3.
SURFACE DISSOLVED OXYGEN FIELD – OBSERVED AND CALCULATED – JUNE 1976

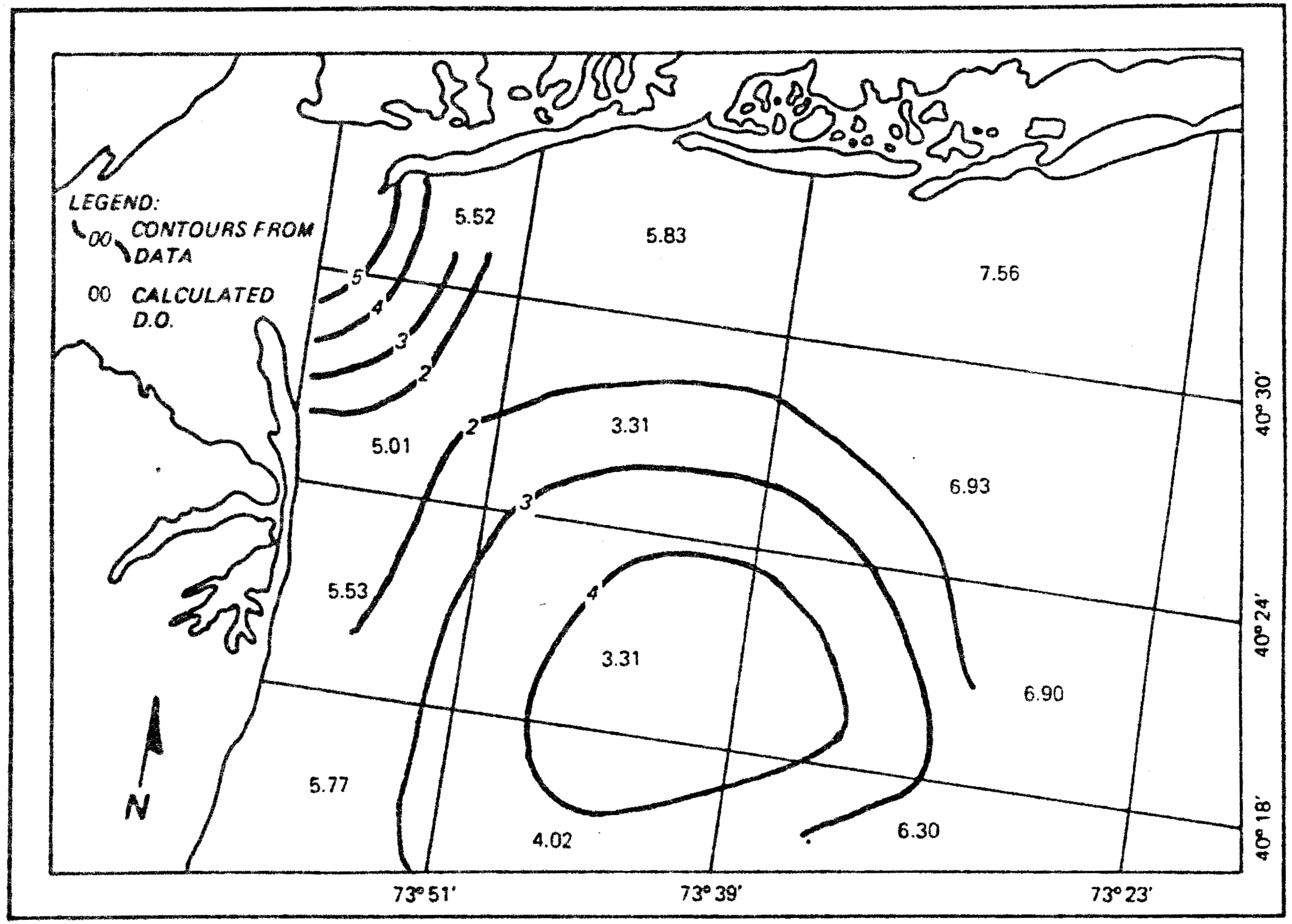

FIGURE VIII-4.
BOTTOM DISSOLVED OXYGEN FIELD – OBSERVED AND CALCULATED – JUNE 1976

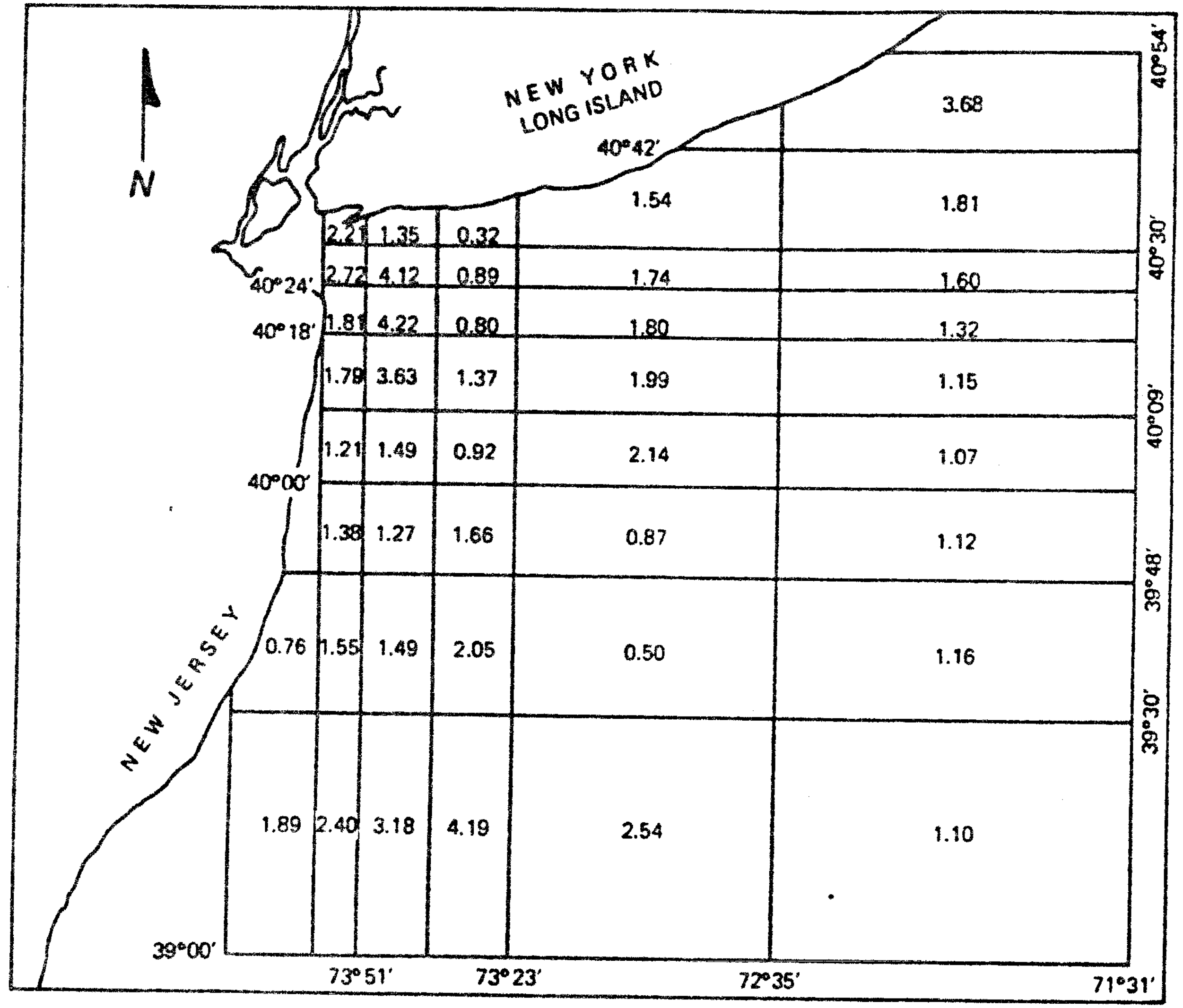

FIGURE VIII-5a. SYSTEM-WIDE CALCULATED BOTTOM DISSOLVED OXYGEN DEFICIT

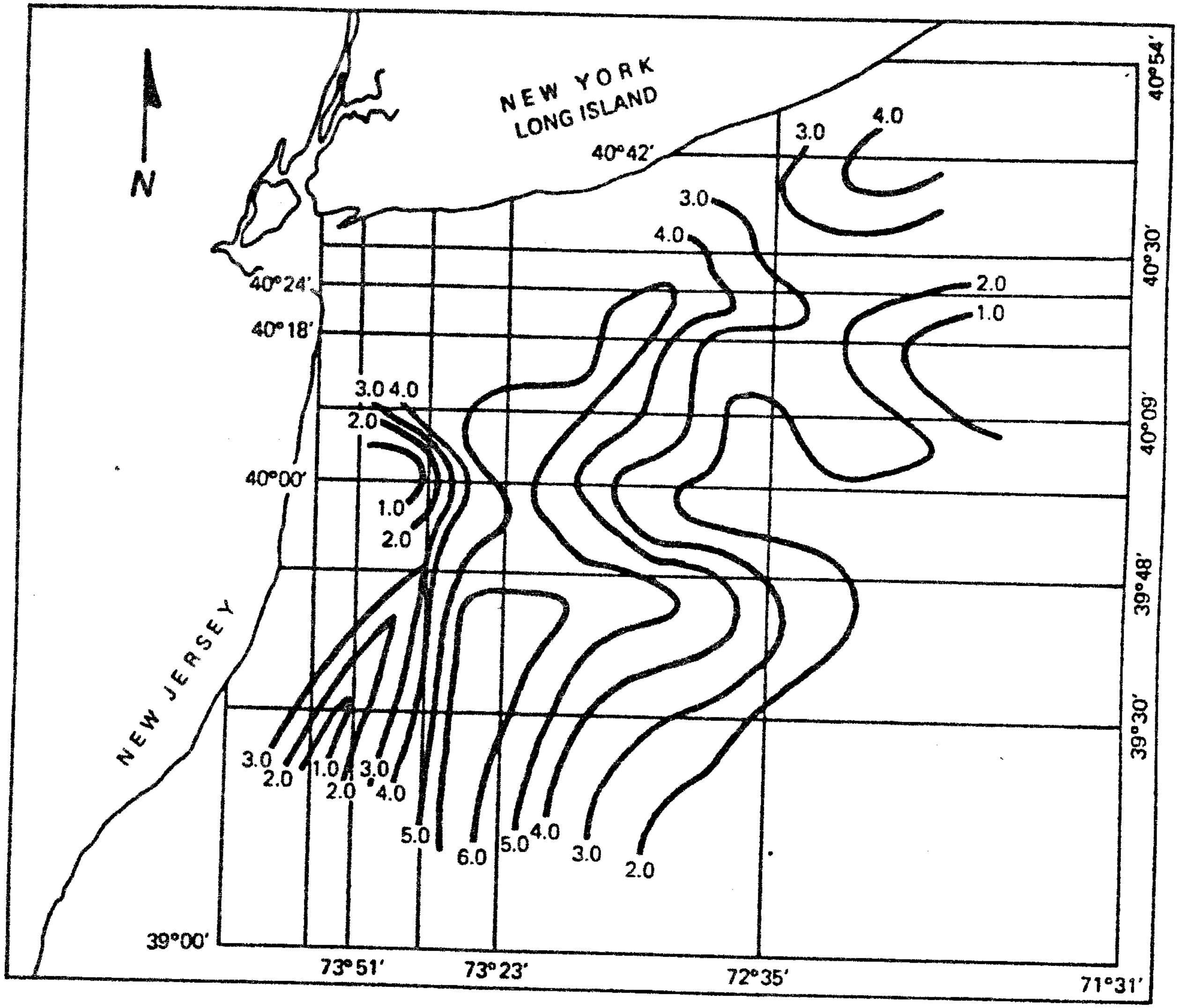

FIGURE VIII-5b. OBSERVED BOTTOM DISSOLVED OXYGEN DEFICIT – 1976 DATA

Examination of these figures suggests that, with the currently employed parameters, low dissolved oxygen levels at the southern ocean boundary are calculated to increase rapidly within the area. The observed data indicates that regions of depressed dissolved oxygen extend from this boundary northward into extensive portions of the New York Bight.

Dissolved oxygen levels were calculated for 1974 conditions with horizontal dispersion coefficients (surface and bottom segments of the Bight) set to zero. All other parameters were unchanged. This calculation (with $E_H = 0$) was compared to the 1974 calculated dissolved oxygen levels for the bottom waters of the system. It was found that calculated dissolved oxygen levels were essentially the same in the system for both values of the dispersion coefficient. The only exceptions were in segments immediately adjacent to the boundary where calculated dissolved oxygen increased on the order of 0.2 to 0.3 mg/ℓ.

Comparable calculations and comparisons were made for 1974 conditions considering the advective flow field. Figure VIII-6 presents the change in calculated bottom dissolved oxygen considering the 1974 flow field and a field with all flows set to zero. The influence of the advective flow field on the calculated steady state dissolved oxygen distributions is insignificant at the ocean boundaries and tends to increase somewhat in the inner regions of the Bight. The maximum difference calculated is on the order of 1 mg/ℓ. Figure VIII-7 illustrates the change in calculated bottom dissolved oxygen when the total horizontal transport field is set equal to zero. The major changes in calculated dissolved oxygen levels are associated with the segments adjacent to New York Harbor. This reflects the fact that residual effects from discharges to New York Harbor do not enter the Bight Model when there is no horizontal transport. Discounting these local New York Harbor effects it may be seen that the horizontal transport has an influence on calculated dissolved oxygen levels in the apex and at most of the system boundaries.

Figure VIII-8 presents the calculated differences in steady state dissolved oxygen values considering a ten fold reduction in the vertical dispersion coefficient. As shown on the figure major changes in calculated dissolved oxygen levels are associated with this change in the vertical dispersion coefficient. Decreases in dissolved oxygen along the shorelines

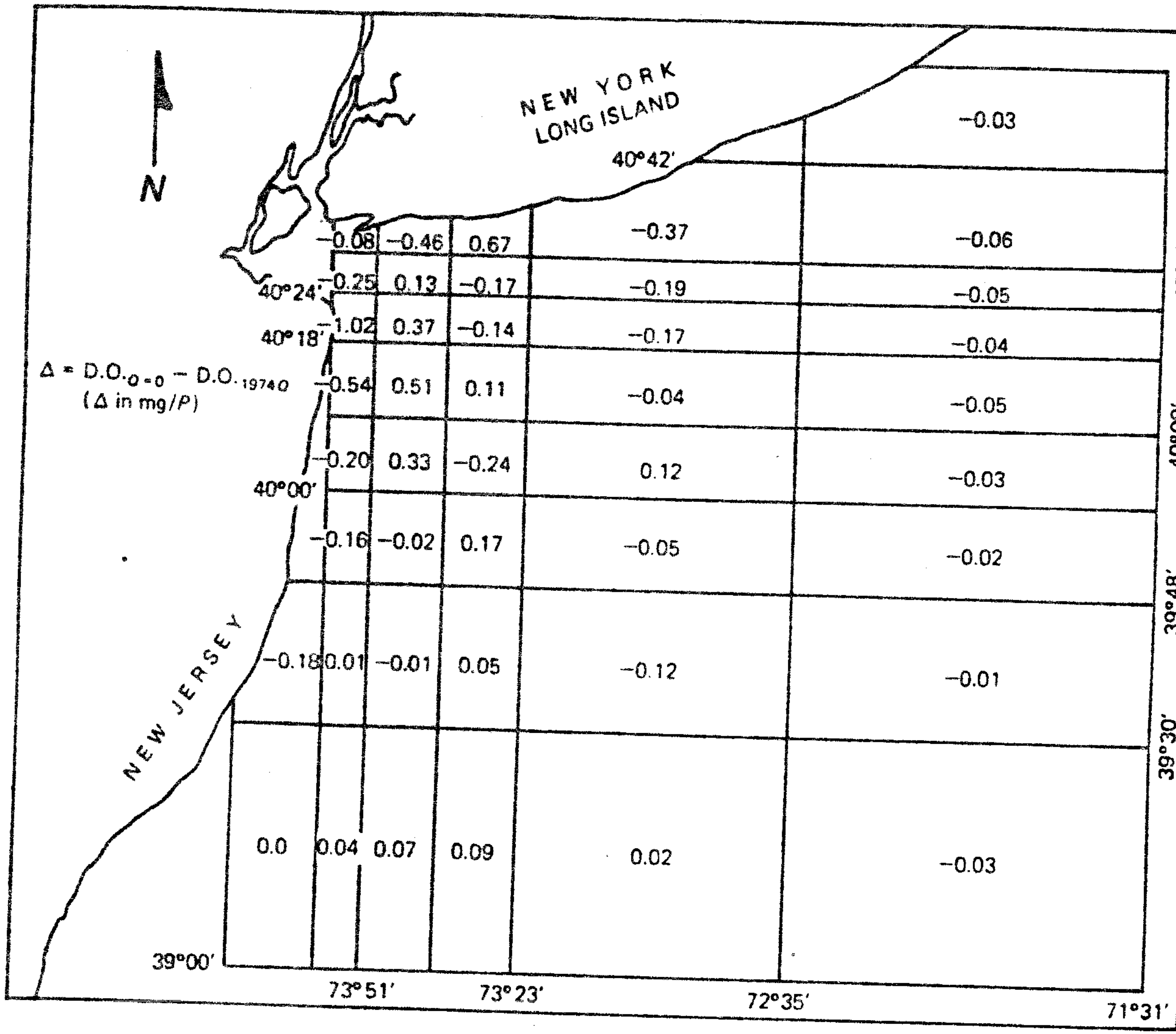

FIGURE VIII-6.
INFLUENCE OF CHANGES IN FLOW FIELD ON CALCULATED BOTTOM DISSOLVED OXYGEN CHANGE (Δ).

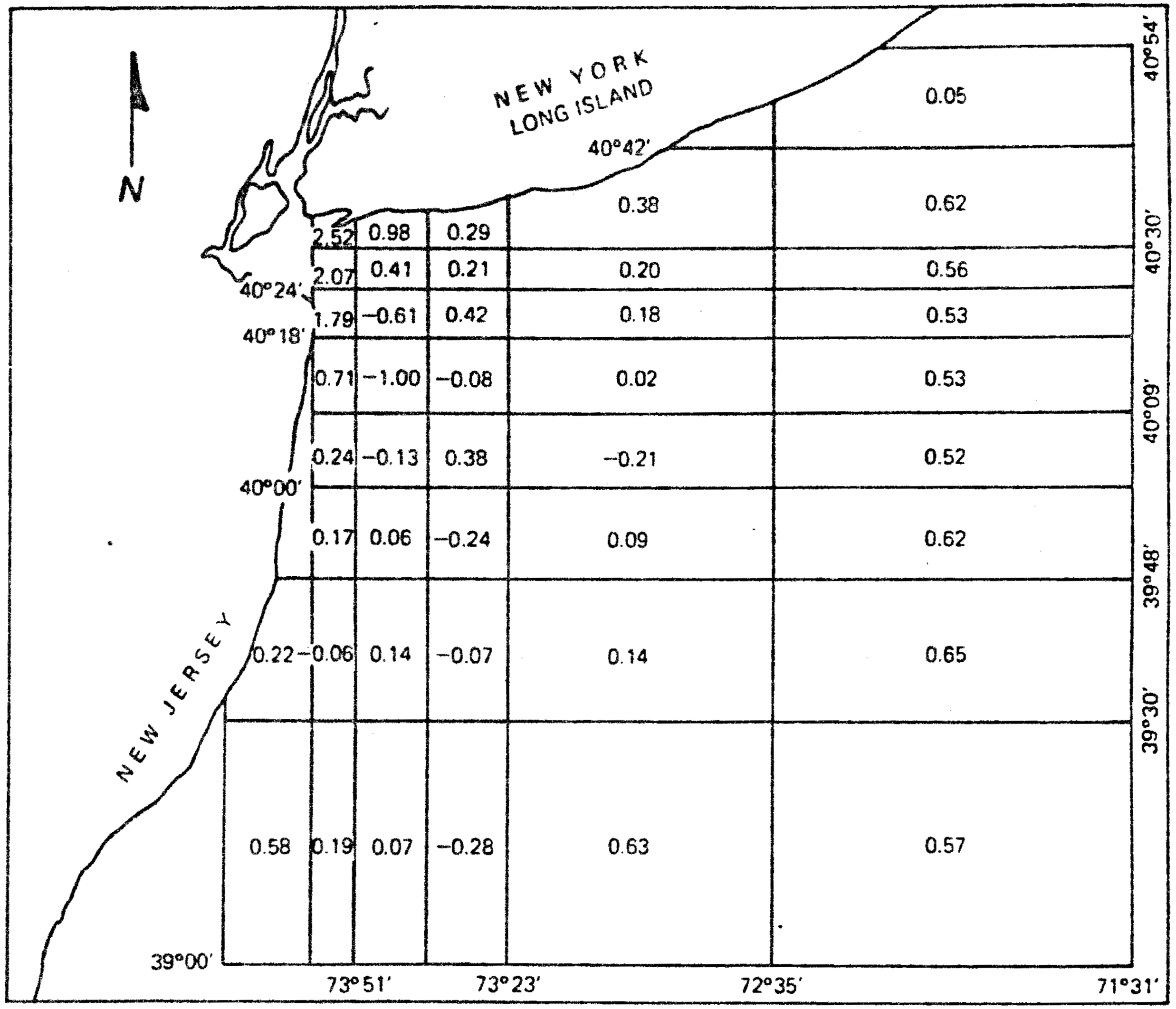

FIGURE VIII-7. CALCULATED DIFFERENCE IN BOTTOM D.O. USING 1974 TRANSPORT FIELD AND USING 1974 TRANSPORT FIELD AND NO HORIZONTAL TRANSPORT FIELD

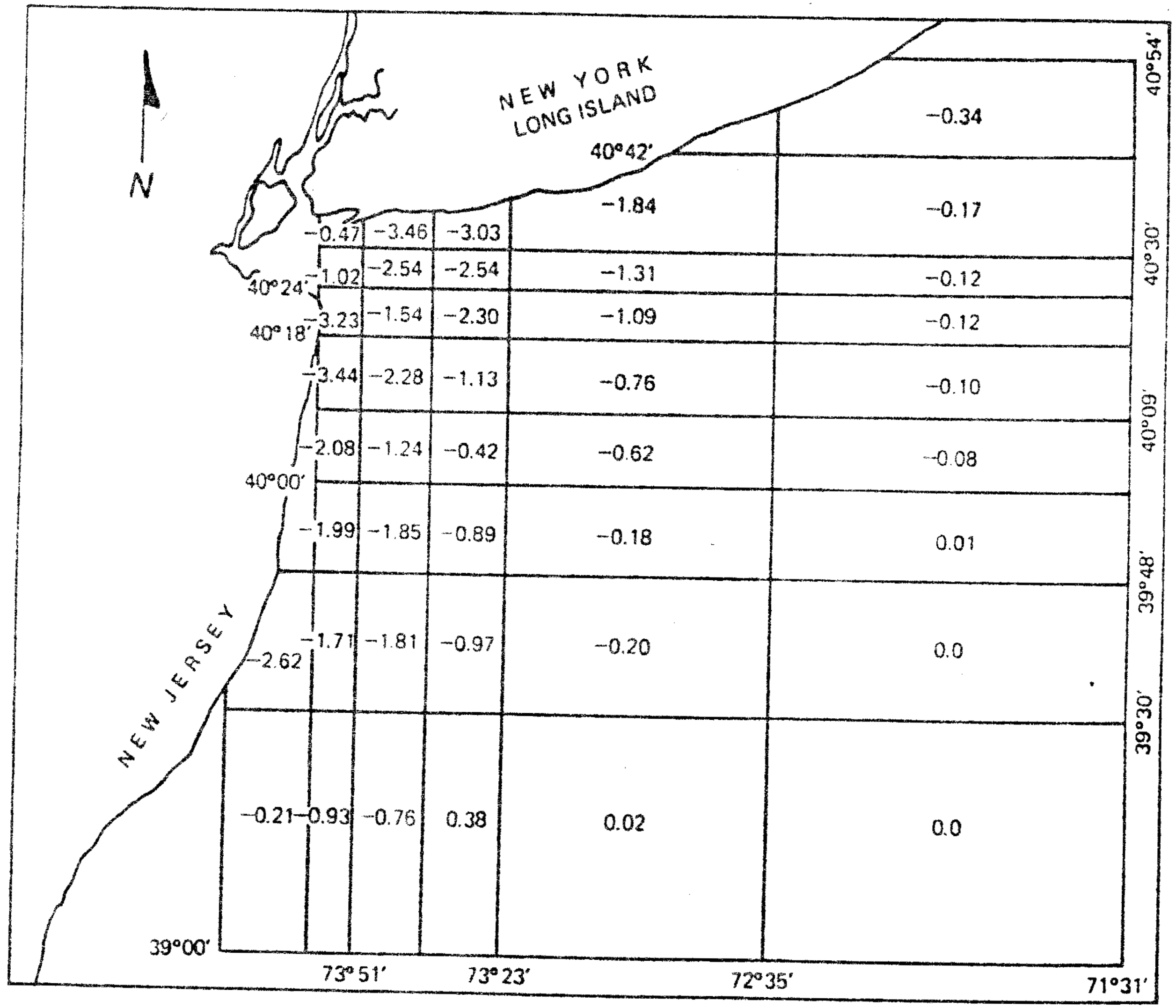

FIGURE VIII-8.
CALCULATED DIFFERENCE IN BOTTOM DISSOLVED OXYGEN FOR *EV* AT 10% OF 1974 VALUE

of New Jersey and Western Long Island range between 1.5 and 3.5 mg/ℓ. In addition the decreases in dissolved oxygen along the ocean boundary at the southern limit of the system off the New Jersey shore can be observed. The calculated dissolved oxygen levels are sensitive to vertical dispersion. Comparable calculation considering a fifty percent reduction in the reaeration coefficient indicated that bottom dissolved oxygens tended to increase on the order of a tenth of a mg/ℓ due to increased dissolved oxygen supersaturation in the surface layer.

Figure VIII-9 presents the change in calculated dissolved oxygen levels in the bottom due to a 50% increase in the oxygen utilization rate of the bottom waters. 1974 conditions were employed in these calculations. The increased bottom dissolved oxygen levels range between 0.1 and 2.0 mg/ℓ. Deeper sections of the system are not significantly impacted by changes in this parameter because the original value of oxygen utilization rate was low. The calculated dissolved oxygen levels are significantly influenced by changes in oxygen utilization rate as shown on Figure VIII-9. The influence of the oxygen utilized by bottom sediments is shown on Figure VIII-10 and can reach 1/2 mg/ℓ in the apex adjacent to sludge disposal area. Figure VIII-11 presents plots of the relative dissolved oxygen depression caused by waste discharges of ultimate oxygen demanding material from Long Island, New York Harbor, and the New Jersey shore. The influence of these loads on the scale of the Bight may be seen to be insignificant.

Based on the steady state calculations it is apparent that Bightwide dissolved oxygen levels are most sensitive to the vertical dispersion coefficient and the oxygen utilization of the bottom waters. This latter parameter is determined by phytoplankton growth, sinking, respiration and death. Light penetration relative to the location of the pycnocline may also be significant. The former parameter is essentially determined by the vertical density structure. The calculated dissolved oxygen levels are influenced to a lesser extent by the horizontal transport and bottom sediment oxygen utilization rates.

An examination of the density structure observed in 1974 and 1976 indicate that the vertical density gradients in the latter period tend to be somewhat higher and occur at slightly greater depths. This tendency is not uniformly observed nor well documented. The data bases which were examined

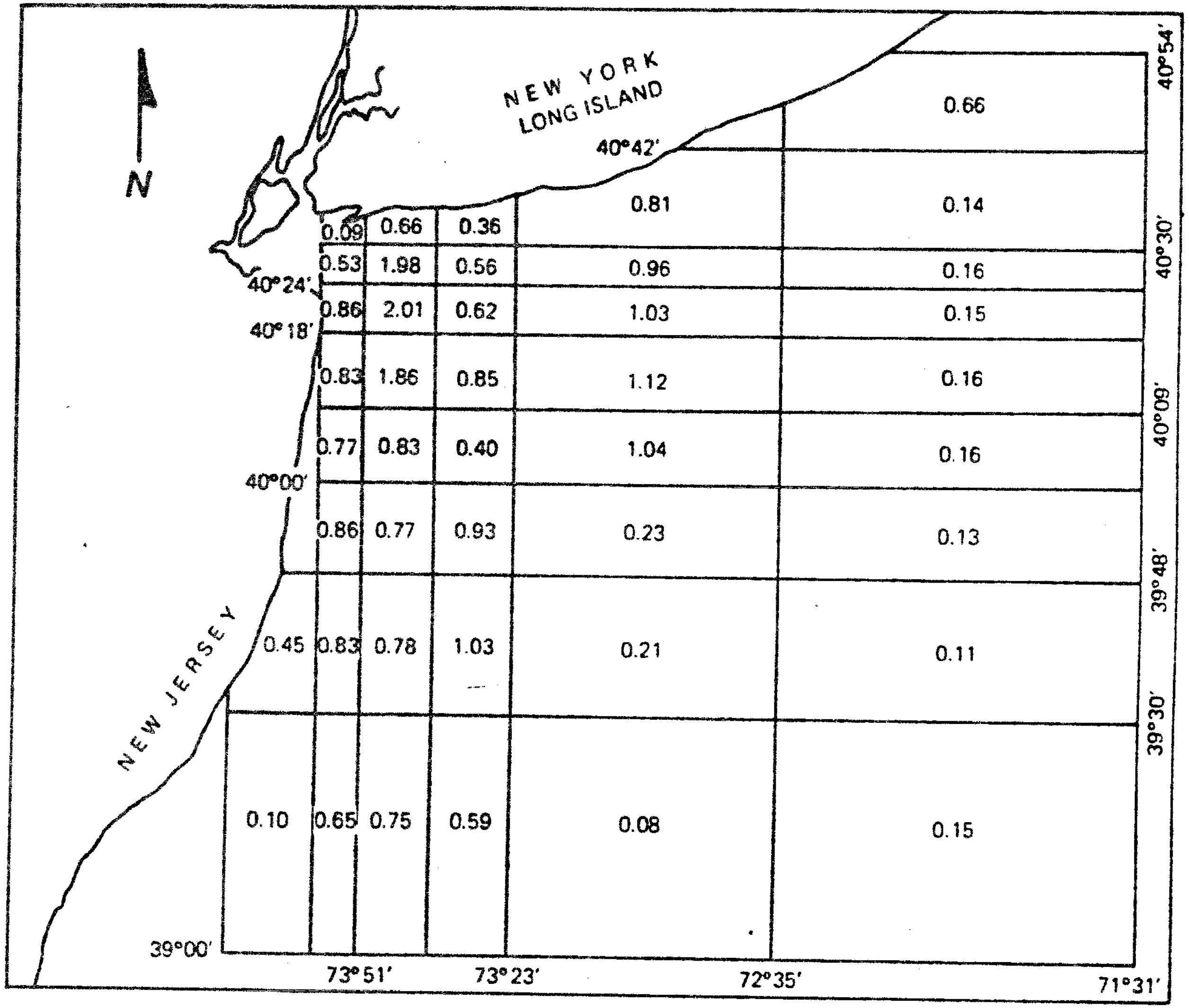

FIGURE VIII-9.
CALCULATED DIFFERENCE IN BOTTOM DISSOLVED OXYGEN FOR A 50% CHANGE IN RESPIRATION RATE

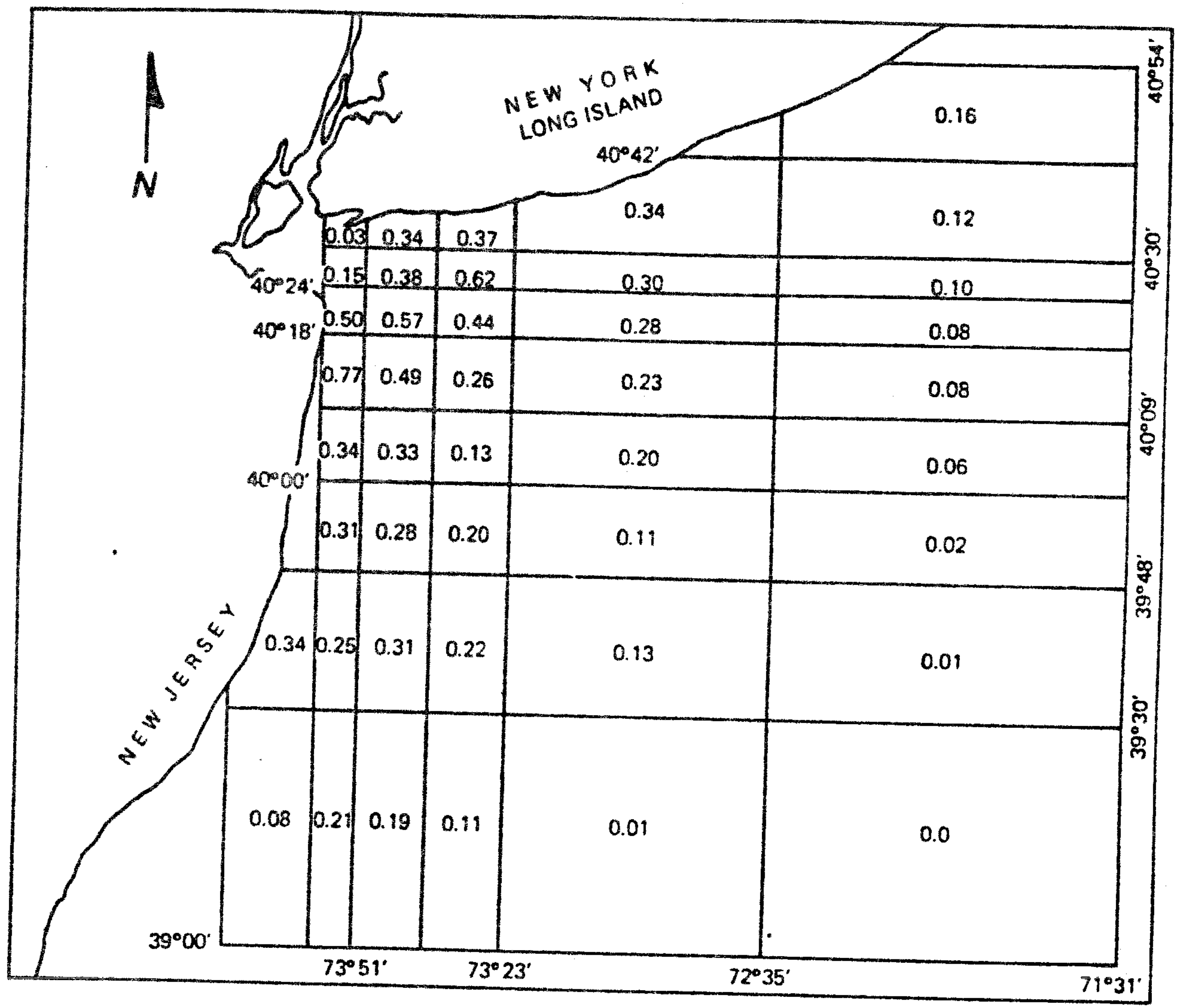

FIGURE VIII-10. DISSOLVED OXYGEN REDUCTION DUE TO BOTTOM OXYGEN DEMAND

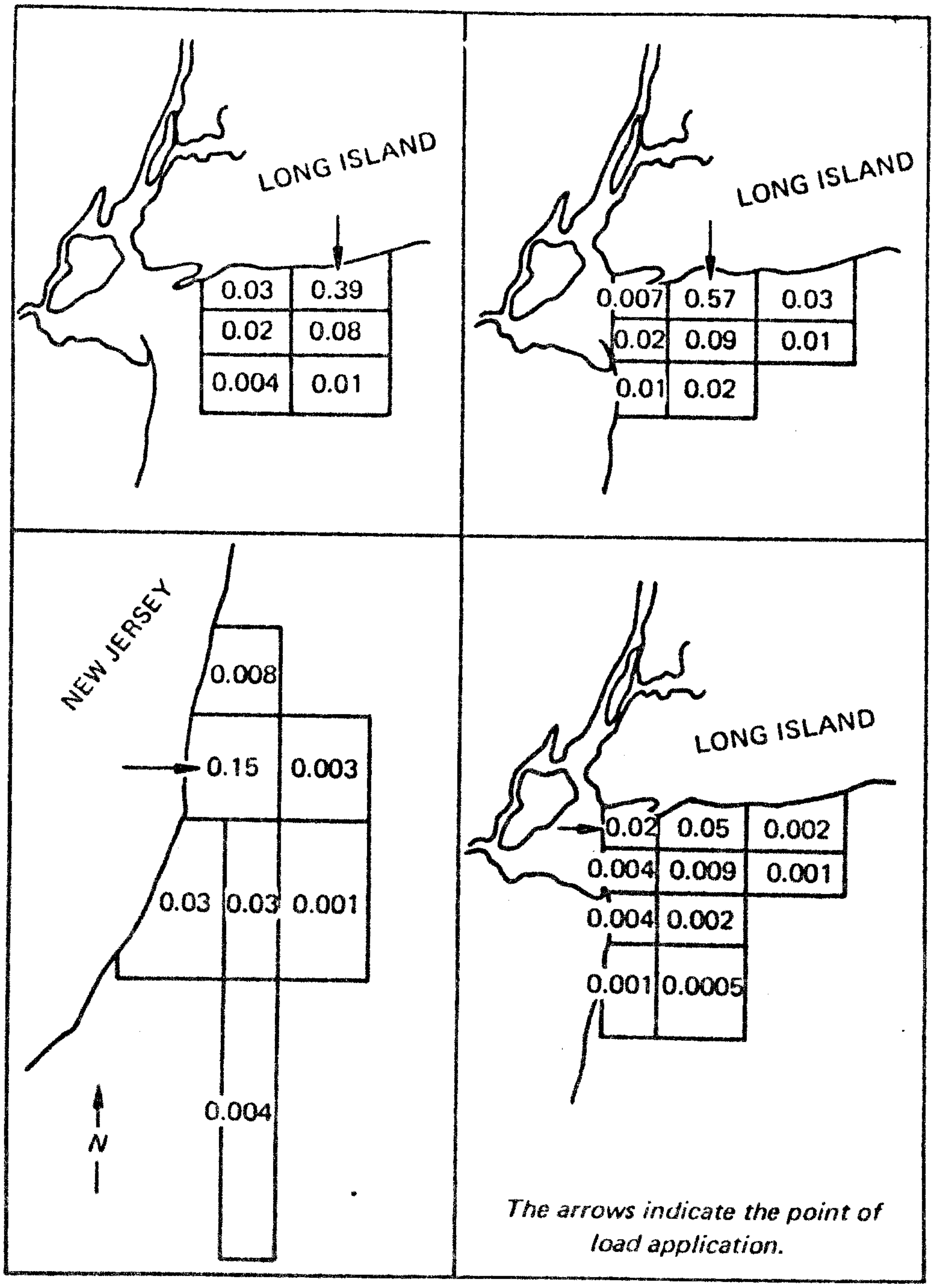

FIGURE VIII-11.
DISSOLVED OXYGEN DEFICIT RESPONSES (mg/l) TO A LOAD OF ONE MILLION POUNDS

were obtained at different periods of the year and comparable stations were not compared to any great degree. As the vertical density gradient increases, the vertical dispersion coefficient tends to decrease as seen in figure VII-1.

The low bottom dissolved oxygen levels observed in 1976 could be accounted for by either an increase in the oxygen utilization rate of bottom waters or a decrease in vertical dispersion. A combination of these two factors could also produce conditions observed in 1976. In any case the changes in these two parameters required to account for the 1976 conditions appear to be relatively small and within the range of values presented in Table VIII-1.

One method of better defining the relative impact of increases in the oxygen demand of bottom waters is to analyze the chemical and biological data currently being collected by MESA sponsored projects employing carbon-oxygen-nitrogen modeling with phytoplankton dynamics including settling. Steady-state seasonal calculations for spring-early summer periods as well as time variable calculations can be employed in the analysis. In addition, analysis in the vertical dimension using significant components of the phytoplankton models would provide additional insight. Thus future data analysis and modeling efforts should employ a combination of analysis frameworks similar to those utilized in the present study: a three dimensional analysis on a Bight-wide scale and a more detailed vertical analysis on a local scale. Three dimension models may be used to define Bight-wide phenomena while detailed vertical analysis assists in defining the influence of vertical dispersion in the context of other biological and physical phenomena.

Conclusions:

The steady-state analysis presented in this report provides a basis for assessment of dissolved oxygen in the New York Bight, particularly in the apex area. The analysis indicates that the discharge of carbonaceous and nitrogenous wastes does not materially affect the dissolved oxygen levels through bacterial oxidation. Furthermore, the discharge of solids (sludge disposal, dredge spoils and construction debris) do not influence these concentrations on a bight-wide scale. The localized sludge disposal area is evidently affected in this regard, but this area is restricted to a relatively limited extent. On the other hand, the depression of dissolved oxygen, particularly in the hypolimnetic waters, is affected by phytoplankton respirator and decay and the vertical transport structure. It is probable that the discharge of wastewater from the treatment plants and urban runoff has some effect on the growth of the phytoplankton and the subsequent decay through the inorganic nutrient route. The degree to which water quality conditions are affected by these inputs may be quantified by the development and validation of a model defining these kinetic interactions. The analysis, developed in this second phase, will be extended to incorporate the kinetic routes, relating the growth and decay of the phytoplankton to the nutrient concentrations resulting from these wastewater inputs. Thus, the effect of the discharges will be defined, providing a basis for areawide water quality planning, particularly with respect to the relative influence of the point sources from treatment plants and the distributed sources from urban runoff by contrast to the effects of other inputs such as the disposal practices and atmospheric inputs.

The present analysis is directed to the definition of a transport structure, in accordance with the original contract to provide the Brookhaven investigators with a reasonable transport field for summer conditions. The transport field developed in this work was calibrated and validated by the analysis of the salinity distribution for the years 1974 and 1976. Further confirmation of this transport field was provided by the dissolved oxygen analysis. The latter analysis was also employed as a basis for the conclusions expressed in the preceding paragraph.

The transport equations included advective and dispersive terms in a multi-segmented horizontal system with two vertical layers. The advective terms were developed by a minimum energy principle, which yielded the general observed flow patterns in the Bight. The overall transport field also included consistent values of the various dispersion coefficients. It is recognized that advective-dispersive models of this nature do not necessarily result in a unique solution for the transport. However, its validity to represent average summer conditions is demonstrated by its ability to reproduce the salinity distribution for the two years.

The analysis further indicates that the dissolved oxygen concentration in the hypolimnetic waters is particularly sensitive to the respiration and decay rates of the phytoplankton and the vertical dispersion coefficients. Relatively small changes of these parameters, within the range of measured values, causes significant changes in the dissolved oxygen levels.

Thus, from both a transport and kinetic viewpoint, the present analysis reasonably reproduces observed water quality conditions and permits assessment of the effect of wastewater inputs. In view of the potential significance of these discharges in dissolved oxygen and other water quality parameters this analysis had indicated the analytic direction on which to proceed and provided a valid basis for the more definitive time variable analysis.

REFERENCES

1. Starr, R.B., and Steimle, F.W. "Temporal Development of the Physical Characteristics of New York Bight Waters Related to the Anoxia Problem of 1976"; Draft Report MESA - New York Bight Project. 1977.

2. Hardy, C.D., Baylor, E.R., and Moskowitz, P. "Sea Surface Circulation in the Northwest Apex of the New York Bight"; NOAA Technical Memo. ERL MESA 13. 1977.

3. Hansen, D.V. "Circulation" MESA New York Bight Atlas Monograph 3. 1978.

4. Bumpus, D.F., and Lauzier, L.M. "Surface Circulation on the Continental Shelf off Eastern North America Between Newfoundland and Florida". Serial Atlas of the Marine Environment Folio 7, Amer. Geophys. Soc. 1965.

5. Bumpus, D.F. "A Description of Circulation on the Continental Shelf of the East Coast of the United States". Progress in Oceanography, Vol. 6, Pergamon Press; pp. 111-157. 1973.

6. Beardsley, R.C., Boicourt, W.C., and Hausen, D.V. "Physical Oceanography of the New York Bight". Amer. Soc. Limnol. and Oceanogr., Spec. Symp., Vol. 2, pp. 20-34, Allen Press. 1976.

7. O'Connor, D.J., St. John, J.P., and Leo, W.E. "New York City 208 - Task Report 314 - Season Steady State Model", Prepared by Hydroscience, Inc. 1978.

8. Koa, A. "A Study of the Current Structure in the Sandy Hook-Rockaway Point Transect". Unpubl. MS Res. Paper, Stony Brook, N.Y.: Marine Sci. Res. Ctr., State Univ. at New York. 1975.

9. 1976 Current Data Obtained by Atlantic Oceanographic and Meteoroligical Laboratories, NOAA, Miami, Fla., Unpubl.

10. Koh, R.Y., Fan, L.N. "Mathematical Model for the Prediction of Temperature Distributions Resulting from the Discharge of Heated Water into Large Bodies of Water". Report prepared by Tetra Tech, Inc. 1970.

11. Kolesnikov, A.G., Ivanova, Z.S., and Boguslavska, S.G. "The Effect of Stability on the Intensity of Vertical Transfer in the Atlantic Ocean". OK'eanologiya, Vol. 1, (4), English trans. 1961.

12. Harremos, P. "Diffuser Design for Discharge to a Stratified Water". The Danish Isotope Center, Copenhagen, Denmark, pp. 1-18. 1967.

13. Defant, A. Physical Oceanography, Vol. I; MacMillan Co., N.Y.C. 1961.

14. Foxworthy, J.E. "Eddy Diffusivity and the Four-Thirds Law in Nearshore (Coastal Waters)", Allan Hancock Foundation, Rept. 68-1, Univ. of So. Calif. 1968.

15. O'Connor, D.J., Thomann, R.V., DiToro, D.M. "Mathematical Modeling of Natural Systems". Manhattan College, Summer Instit. Notes. 1978.

16. Thomas, J.P., Phoel, W.C., Steimle, F.W., O'Reilly, J.E., and Evans, C.A. "Seabed Oxygen Consumption - New York Bight Apex". Amer. Soc. Limnol. and Oceanogr., Spec. Symp., Vol. 2, pp. 354-369, Allen Press. 1976.

17. Malone, T.C. "Phytoplankton Productivity in the Apex of the New York Bight: Environmental Regulation of Productivity/Chlorophyll-a". Amer. Soc. Limnol. and Oceanogr., Spec. Symp., Vol. 2, pp. 260-272, Allen Press. 1976.

18. Malone, T.C. "Phytoplankton Productivity in the Apex of the New York Bight: Sept., 1973-Aug. 1974". NOAA Tech. Memorandum ERL MESA-5, 1976.

19. DiToro, D.M., Thomann, R.V., O'Connor, D.J. and Mancini, J.L. "Estuarine Phytoplankton Biomass Model - Verification Analyses and Preliminary Applications". The Sea Vol. 6, Wiley-Interscience. 1977.

20. DiToro, D.M., O'Connor, D.J., Thomann, R.V. and Mancini, J.L. "Phytoplankton-Zooplankton - Nutrient Interaction Model for Western Lake Erie". System Analysis and Simulations in Ecology, Vol. III, Academic Press. 1975.

APPENDIX A

Methods Used to Develop System Segmentation and Define Segment Geometry

The segmentation employed in Phase I was developed through the mutual cooperation and agreement among Brookhaven National Laboratory, Manhattan College and the MESA project staff. The area is bordered to the South by latitude 39°00'N; to the East by longitude 71°31'W; to the North by the Long Island coast; and to the West by the New Jersey coast. New York Harbor is not included in the segmentation, since the boundary is set at longitude 73°59'W. However, the effect the Harbor has on conditions in the Bight is simulated by affixing appropriate boundary conditions.

The area of the Bight under study consists of a two layer network of 92, 46 upper and 46 lower, rectangular elements. Figure III-la and lb illustrates the segmentation and the numbering scheme utilized. The corresponding bottom layer segment numbers are discerned by adding one to their respective upper layer digits. Interfaces between top and bottom segments for the inner shelf areas form a surface which slopes gently seaward approximately at the bottom of the pycnocline as determined by Starr and Steimle(1) for September, 1976. This surface becomes less defined as the pycnocline thickens and weakens in the area of the continental shelf break. Due to this, a maximum depth of 35 meters, representative of the upper or middle portion of the pycnocline, was established, thus forcing the interface surface to flatten out.

The present water quality simulation software permits only one open boundary per segment. Therefore, any corner segment with two open boundaries must be equipped with a "dummy" segment. This provides an additional transport interface and allows advective transport across both open boundaries while not introducing any distortion into the calculations. Under these circumstances segments 87 through 92 were constructed to conform to the computer software.

Viewing Figure V-la and lb, it is evident that there are prisms of water situated between the boundaries of the segmentation network and the shoreline that were excluded from the network proper. These prisms were therefore annexed to the volumes of adjacent segments 31, 32, 41, 42, 51, 52, 75, and 76. The interfacial areas between segments, however, continue to conform to the segment grid as illustrated.

After the segmentation was established along specific latitude and longitude guidelines, it was necessary to determine the geomorphology of the area. In order to satisfy the computer program input format, the topography was studied to ascertain values for such features as depth, interface areas, segment volumes and characteristic lengths. For this purpose, the following National Ocean Survey charts were used - 12120, 12127, 12129, 12133, 12134, 12327, and 13051. The soundings, at mean low water, on the charts helped facilitate the drawing of a physical representation of the cross-sectional area between each segment. Through the application of geometry, the total area of each interface was determined. Following this, a line representing the pycnocline was placed on each cross-sectional area, thereby representing the line of demarcation between the top and the bottom segment. Since the pycnocline slopes gently seaward in a generally uniform manner, the area of the upper segment is easily obtained. The area of the bottom segment is computed by subtracting the area of the upper segment from the total cross-sectional area.

Utilizing the interface drawings, a total mean depth (incorporating both upper and lower layers) is generated. Multiplying the total mean depth by the surface area of the upper segment yields the total volume for top and bottom segments combined. By obtaining the mean depth for the upper layer, rather than for the irregularly shaped lower layer, its volume is also determined. Then, the bottom segment volume is arrived at by subtracting the top segment volume from the total volume.

TABLE A-I

Segment Geometry

SEGMENT #	FROM LONGITUDE WEST	TO LONGITUDE WEST	FROM LATITUDE NORTH	TO LATITUDE NORTH	VOLUME ($X10^6$ CUBIC METERS)
1	71°31'	72°35'	39°00'	39°30'	174,100
2	71°31'	72°35'	39°00'	39°30'	6,364,000
3	72°35'	73°23'	39°00'	39°30'	120,600
4	72°35'	73°23'	39°00'	39°30'	304,400
5	73°23'	73°39'	39°00'	39°30'	35,460
6	73°23'	73°39'	39°00'	39°30'	16,480
7	73°39'	73°51'	39°00'	39°30'	25,380
8	73°39'	73°51'	39°00'	39°30'	9,881
9	73°51'	73°59'	39°00'	39°30'	15,230
10	73°51'	73°59'	39°00'	39°30'	4,789
11	73°59'	74°15'	39°00'	39°30'	24,180
12	73°59'	74°15'	39°00'	39°30'	3,959
13	71°31'	72°35'	39°30'	39°48'	103,200
14	71°31'	72°35'	39°30'	39°48'	1,127,000
15	72°35'	73°23'	39°30'	39°48'	65,310
16	72°35'	73°23'	39°30'	39°48'	55,310
17	73°23'	73°39'	39°30'	39°48'	16,590
18	73°23'	73°39'	39°30'	39°48'	9,326
19	73°39'	73°51'	39°30'	39°48'	10,950
20	73°39'	73°51'	39°30'	39°48'	3,444
21	73°51'	73°59'	39°30'	39°48'	5,990
22	73°51'	73°59'	39°30'	39°48'	2,971
23	71°31'	72°35'	39°48'	40°00'	70,910
24	71°31'	72°35'	39°48'	40°00'	214,600
25	72°35'	73°23'	39°48'	40°00'	46,160
26	72°35'	73°23'	39°48'	40°00'	40,870
27	73°23'	73°39'	39°48'	40°00'	12,100
28	73°23'	73°39'	39°48'	40°00'	5,706
29	73°39'	73°51'	39°48'	40°00'	7,686
30	73°39'	73°51'	39°48'	40°00'	2,342
31	73°51'	73°59'	39°48'	40°00'	6,270
32	73°51'	73°59'	39°48'	40°00'	2,125
33	71°31'	72°35'	40°00'	40°09'	51,540
34	71°31'	72°35'	40°00'	40°09'	57,400
35	72°35'	73°23'	40°00'	40°09'	36,480
36	72°35'	73°23'	40°00'	40°09'	16,030
37	73°23'	73°39'	40°00'	40°09'	10,170
38	73°23'	73°39'	40°00'	40°09'	7,757
39	73°39'	73°51'	40°00'	40°09'	6,128
40	73°39'	73°51'	40°00'	40°09'	2,345
41	73°51'	73°59'	40°00'	40°09'	3,883
42	73°51'	73°59'	40°00'	40°09'	1,223
43	71°31'	72°35'	40°09'	40°18'	51,540
44	71°31'	72°35'	40°09'	40°18'	47,520
45	72°35'	73°23'	40°09'	40°18'	34,660
46	72°35'	73°23'	40°09'	40°18'	15,150
47	73°23'	73°39'	40°09'	40°18'	9,062
48	73°23'	73°39'	40°09'	40°18'	2,999

TABLE A-I (Continued)

SEGMENT #	FROM LONGITUDE WEST	TO LONGITUDE WEST	FROM LATITUDE NORTH	TO LATITUDE NORTH	VOLUME ($X10^6$ CUBIC METERS)
49	73°39'	73°51'	40°09'	40°18'	5,933
50	73°39'	73°51'	40°09'	40°18	3,364
51	73°51'	73°59'	40°09'	40°18'	2,971
52	73°51'	73°59'	40°09'	40°18'	695.3
53	71°31'	73°35'	40°18'	40°24'	35,480
54	71°31'	72°35'	40°18'	40°24'	29,650
55	72°35'	73°23'	40°18'	40°24'	22,250
56	72°35'	73°23'	40°18'	40°24'	7,173
57	73°23'	73°39'	40°18'	40°24'	5,231
58	73°23'	73°39'	40°18'	40°24'	767.5
59	73°39'	73°51'	40°18'	40°24'	3,871
60	73°39'	73°51'	40°18'	40°24'	1,628
61	73°51'	shoreline	40°18'	40°24'	1,769
62	73°51'	shoreline	40°18'	40°24'	196.5
63	71°31'	72°35'	40°24'	40°30'	35,480
64	71°31'	72°35'	40°24'	40°30'	26,880
65	72°35'	73°23'	40°24'	40°30'	20,670
66	72°35'	73°23'	40°24'	40°30'	6,213
67	73°23'	73°39'	40°24'	40°30'	4,531
68	73°23'	73°39'	40°24'	40°30'	866.6
69	73°39'	73°51'	40°24'	40°30'	3,243
70	73°39'	73°51'	40°24'	40°30'	1,617
71	73°51'	73°59'	40°24'	40°30'	1,433
72	73°51'	73°59'	40°24'	40°30'	471.2
73	71°31'	72°35'	40°30'	40°42'	67,010
74	71°31'	72°35'	40°30'	40°42'	39,650
75	72°35'	73°23'	40°30'	40°42'	31,410
76	72°35'	73°23'	40°30'	40°42'	7,658
77	71°31'	72°35'	40°42'	40°54'	53,040
78	71°31'	72°35'	40°42'	40°54'	23,900
79	73°23'	73°39'	40°30'	shoreline	2,807
80	73°23'	73°39'	40°30'	shoreline	495.3
81	73°39'	73°51'	40°30'	shoreline	1,648
82	73°39'	73°51'	40°30'	shoreline	412.1
83	73°51'	73°59'	40°30'	shoreline	524.2
84	73°51'	73°59'	40°30'	shoreline	58.25
85	73°59'	shoreline	39°30'	39°48'	6,842
86	73°59'	shoreline	39°30'	39°48'	1,711
87	DUMMY SEGMENT				2.832
88	DUMMY SEGMENT				2.832
89	DUMMY SEGMENT				2.832
90	DUMMY SEGMENT				2.832
91	DUMMY SEGMENT				2.832
92	DUMMY SEGMENT				2.832

Appendix B

Velocity Interpolation to Define Flow Field

I. Introduction

The problem of velocity interpolation consists in selecting a set of unknown velocities given a few known values and the laws of fluid mechanics. If only the law of fluid continuity is used and no dynamical effects are included, then the usual case is that there are infinite ways of specifying the velocities consistent with the known values and continuity. The reason is that continuity applies to a volume segment whereas the unknowns are at the interfaces bounding the volumes. The number of interfaces exceeds the number of segments for any two or three dimensional segmentation. Hence another principle is required to uniquely specify the velocities. In the present analysis the criteria of minimum kinetic energy was employed.

II. Method

Consider a segmented model with N segments and M interfaces at which the velocities are unknown. Some additional interfaces exist at which the velocities are known. The problem is to calculate the rest of the velocities such that fluid continuity is preserved. For each segment, continuity requires that

$$\sum_{j=1}^{M} a_{ij} v_j = q_i \qquad i = 1, \ldots, N \qquad \text{(b-1)}$$

where a_{ij} is the interfacial area if interface j bounds segment i, and $a_{ij} = 0$ otherwise; q_i is the flow into segment i if a known interfacial velocity bounds segment i; otherwise $q_i = 0$.

The suggested method can yield velocities with the property that the kinetic energy, $\frac{1}{2}\rho\Sigma\, v_j^{\,2}$, is minimum. For generality let the criteria to be minimized be

$$E = \frac{1}{2} \sum_{j=1}^{M} w_j v_j^{\,2} \qquad \text{(b-2)}$$

where v_j are the unknown interfacial velocities and w_j are arbitrary weights. For $w_j = \rho$ the criteria is that of minimum kinetic energy.

The solution is obtained using the method of Lagrange multipliers, the constraints are taken into account by increasing the number of unknowns from the M velocities to N + M where the additional N unknowns,

λ_i, are the Lagrange multiplier associated with the N fluid continuity equations. These constraining equations multiplied by the Lagrange multipliers added to the function being minimized

$$E = \frac{1}{2} \sum_{j=1}^{M} w_j v_j^2 - \sum_{i=1}^{N} \lambda_i \left(\sum_{j=1}^{M} a_{ij} v_j - q_i \right) \tag{b-3}$$

If the constraints are satisfied then the additional terms are zero and do not affect the value of E. The method of minimizing E can now proceed as though the problem were unconstrained. Thus the solution is obtained by setting $\partial E/\partial v_j = 0$ yielding

$$w_j v_j = \sum_{i=1}^{N} \lambda_i a_{ij} \qquad j = 1,\ldots,M \tag{b-4}$$

which is the solution for the v_j as functions of the λ_i, the Lagrange multipliers. To find the values of the multipliers, evaluate the constraint equation of continuity, $\Sigma a_{ij} v_j = q_i$, using the above solution for v_j:

$$\sum_{j=1}^{M} a_{ij} w_j^{-1} \sum_{\ell=1}^{N} \lambda_\ell a_{\ell j} = q_i \qquad i = 1,\ldots,N \tag{b-5}$$

or in standard form for simultaneous linear equations:

$$\sum_{\ell=1}^{N} r_{i\ell} \lambda_\ell = q_i \qquad i = 1,\ldots,N \tag{b-6}$$

where

$$r_{i\ell} = \sum_{j=1}^{M} w_j^{-1} a_{\ell j} a_{ij} \tag{b-7}$$

The above simultaneous equations (b-6) are solved for the λ's, and the velocities are evaluated using

$$v_j = w_j^{-1} \sum_{i=1}^{N} a_{ij} \lambda_i \qquad j = 1,\ldots,M \tag{b-8}$$

Thus the method is straightforward and requires the solution of only an N by N set of linear equations corresponding to the N segments at which continuity is required.

III. Relationship to Irrotational Flow

For the special case that all boundary and no internal velocities are specified, the minimum kinetic energy velocity field corresponds to the irrotational velocity field for that specification of the boundary velocities. This fact follows from a theorem by Lord Kelvin (Lamb, Hydrodynamics, p. 47): The irrotational motion of a liquid occupying a simply-connected region has less kinetic energy than any other motion consistent with the same normal motion at the boundary. The demonstration is direct. Let

$$T = \frac{1}{2}\rho \int_V (u^2 + v^2 + w^2)\, dV \qquad \text{(b-9)}$$

be the kinetic energy of the fluid in the volume V with the integral $\int_V dV = \iiint dx\, dy\, dz$ being the volume integral over V. For the irrotational velocity field u_i, v_i, w_i, let T_i be its kinetic energy. Consider a velocity field made up of the irrotational velocities and another velocity field u_o, v_o, w_o:

$$u = u_i + u_o = -\frac{\partial\phi}{\partial x} + u_o \qquad \text{(b-10a)}$$

$$v = v_i + v_o = -\frac{\partial\phi}{\partial y} + v_o \qquad \text{(b-10b)}$$

$$w = w_i + w_o = \frac{\partial\phi}{\partial z} + w_o \qquad \text{(b-10c)}$$

where ϕ is the potential that specifies the irrotational velocities. The additional velocities must satisfy continuity:

$$\frac{\partial u_o}{\partial x} + \frac{\partial v_o}{\partial y} + \frac{\partial w_o}{\partial z} = o \qquad \text{(b-11)}$$

and must be zero at the boundary since the irrotational field satisfies the specified boundary velocities exactly. The kinetic energy of the composite velocity field is computed directly from the definition:

$$T = \frac{1}{2}\rho \int_V (u_i^2 + v_i^2 + w_i^2)dV - \rho \int_V (u_o \frac{\partial\phi}{\partial x} + v_o \frac{\partial\phi}{\partial y} + w_o \frac{\partial\phi}{\partial z})dV$$

$$+ \frac{1}{2}\rho \int_V (u_o^2 + v_o^2 + w_o^2)dV$$

$$= T_i + T_o - \rho \int_V (u_o \frac{\partial\phi}{\partial x} + v_o \frac{\partial\phi}{\partial y} + w_o \frac{\partial\phi}{\partial z})dV \qquad \text{(b-12)}$$

where T_i and T_o are the kinetic energy of the irrotational flow and the additional flow field respectively. The integral is evaluated by noting that:

$$\int_V (u_o \frac{\partial\phi}{\partial x} + v_o \frac{\partial\phi}{\partial y} + w_o \frac{\partial\phi}{\partial z})dV = \int_V [\frac{\partial}{\partial x}(u_o\phi) + \frac{\partial}{\partial y}(v_o\phi) + \frac{\partial}{\partial z}(w_o\phi)]dV$$

$$- \int_V \phi(\frac{\partial u_o}{\partial x} + \frac{\partial v_o}{\partial y} + \frac{\partial w_o}{\partial z})dV \qquad \text{(b-13)}$$

The second integral is zero by the constraint that the velocity field u_o, v_o, w_o satisfy fluid continuity. The first integral is a divergence and can be converted to a surface integral via Green's theorem, where the surface is that bounding the volume, V. But u_o, v_o, w_o are zero at this surface and so the surface integral is zero. Hence the total kinetic energy is:

$$T = T_i + T_o \qquad \text{(b-14)}$$

which is minimum only if $T_o = 0$ (since T_o and T_i are necessarily positive). Hence the minimum kinetic energy velocity field is irrotational.

It should be noted that if internal velocities are specified, such as in regions of known upwellings, then the resulting velocity field, although of minimum energy, may not be irrotational.

IV. Relationship to the Theory of Solutions of Linear Equations

Consider a set of linear equations with N equations and M unknowns. For the common case that N = M, the equations have a unique solution if they are not singular. That is if the equations are $Ax = b$, then $x = A^{-1}b$.

Suppose, however, that $N > M$, i.e. there are more equations than unknowns. Then it is impossible to satisfy all the equations exactly and some error must be tolerated. Let $Ax-b = \varepsilon$ be the error vector. The method of least squares gives the solution for which $\Sigma\, \varepsilon_i^2$ is minimum. In matrix form the equation for at least mean square solution is:

$$x = (A^T A)^{-1} A^T b \tag{b-15}$$

Note that $A^T A$ has dimension M by M and can be inverted since it is square.

Consider, now, what happens if $M > N$, that is, there are more unknowns than equations. For this case it is possible to satisfy all the equations exactly with any of an infinity of solutions. What is required is a principle that selects some solution from all the rest. Consider, by analogy to the least mean square error criteria, the least mean square solution criteria. That is, select that solution which minimizes $\Sigma\, x_j^2$, subject to $\Sigma\, a_{ij} x_j = b_i$; $i=1,\ldots,N$. In a sense it is the smallest of all the available solutions. As shown in the previous section the result, if translated to matrix form, is

$$x = A^T (AA^T)^{-1} b \tag{b-16}$$

Note that AA^T has dimension N by N where N is the number of equations so that it is reasonable to expect that its inverse exists. Also note that only $N < M$ equations need be solved to obtain the M unknowns, x.

It is of interest to note that the matrices $(A^T A)^{-1} A^T$ and $A^T (AA^T)^{-1}$ solve the rectangular set of equations $Ax=b$ so it is reasonable to define a generalized inverse A^* which solves $Ax=b$ as $x = A^* b$. For square A, $A^* = A^{-1}$; For $N > M$: $A^* = (A^T A)^{-1} A^T$; for $M > N$: $A^* = A^T (AA^T)^{-1}$. Thus a method is available that solves linear equation whatever the number of equations and unknowns.

The method suggested for velocity interpolation is that the linear equations specifying velocity continuity be solved using a generalized inverse with the consequent property that its solution have a minimum squared solution.

Appendix C

Steady-State Water Quality Model

A steady-state mass balance around a segment k is formulated as follows (all flows from segment k to segment j):

$$V_k \frac{dC_k}{dt} = 0 = \sum_j \underbrace{[-Q_{kj}(\alpha_{kj}C_k + \beta_{kj}C_j)}_{(1)} + \underbrace{E'_{kj}(C_j - C_k)]}_{(2)} - \underbrace{V_k K_k C_k}_{(3)} + \underbrace{W_k}_{(4)} \qquad \text{(C-1)}$$

where:

C_k = concentration of water quality variable in segment k, (M/L^3)

V_k = volume of segment k, (L^3)

Q_{kj} = net flow from segment k to segment j (positive outward) (L^3/T)

α_{kj} = finite difference weight

β = $1 - \alpha$

E'_{kj} = dispersion parameter between segments k and j, (L^3/T) $E'_{kj} = E_{kj}A_{kj}/\overline{L}_{kj}$

K_k = first order reaction coefficient in segment k for water quality variable C $(1/T)$

E_{kj} = dispersion coefficient between segments k and j (L^2/T)

A_{kj} = cross-sectional area between segments k and j (L^2)

L_k = characteristic length of segment k (L) normal to interface jk

$\overline{L}_{kj}$ = average of characteristic lengths of segment k and j (L)

$$\overline{L}_{kj} = \frac{1}{2}(L_k + L_j)$$

W_k = source (or sink) of variable C in segment k (M/T) where M, L, T are the mass, length and time units.

The first term on the righthand side of Equation (C-1) represents the mass entering or leaving (depending on the sign of the flow, Q) segment k due to net currents. The second term represents the dispersive transport. The sum of the flow and dispersion transport extends over all segments j, horizontal and vertical, bordering on segment k. The first order decay (if any) of the variable is given by the third term, while the last term on the righthand side of Equation (C-1) incorporates all direct sources and sinks of the variable, C.

If all terms involving the dependent variable, C, are grouped on the lefthand side, Equation (C-2) is obtained:

$$a_{kk}C_k + \sum_j a_{kj}C_j = W_k \tag{C-2}$$

where:

$$a_{kk} = \sum_j (Q_{kj}\alpha_{kj} + E'_{kj}) + V_k K_k$$

$$a_{kj} = Q_{kj}\beta_{kj} - E'_{kj} \qquad k \neq j$$

Only the diagonal term contains the reaction rate. A similar procedure is followed for each of the 86 segments into which the New York Bight has been divided. A series of 86 equations can be written. Some special conditions apply at the water boundaries of the system. For a section k where the flow between the boundary and the section is designated by Q_{kk} and is leaving the section (positive), and the dispersion parameter is designated by E'_{kk}, then a_{kk} becomes:

$$a_{kk} = \sum_j (Q_{kj}\alpha_{kj} + E'_{kj}) + V_k K_k + Q_{kk}\alpha_{kk} + E'_{kk}$$

and the forcing function is:

$$W_k = W_k + (E'_{kk} - Q_{kk}\beta_{kk})\, C_B \tag{C-2a}$$

where C_B is the boundary concentration of the variable C and is presumed known. For the flow entering the system from a boundary (Q_{kk} negative) the appropriate terms are:

$$a_{kk} = \sum_j (Q_{kj}\alpha_{kj} + E'_{kj}) + V_k K_k + Q_{kk}\beta_{kk} + E'_{kk}$$

and

$$W_k = W_k + (E'_{kk} - Q_{kk}\alpha_{kk})\, C_B \qquad \text{(C-2b)}$$

The n equations with suitable incorporation of boundary conditions considered as incorporated in the W_k's and a_{kk}'s are given by:

$$\begin{aligned} a_{11}C_1 + a_{12}C_2 + \cdots\cdots + a_{1n}C_n &= W_1 \\ a_{21}C_1 + a_{22}C_2 + \cdots\cdots + a_{2n}C_n &= W_2 \\ &\cdots\cdots \\ &\cdots\cdots \\ a_{n1}C_1 + a_{n2}C_2 + \cdots\cdots + a_{nn}C_n &= W_n \end{aligned} \qquad \text{(C-3)}$$

All a_{ij} and W_i quantities are assumed known in Equation (C-3). The problem is to obtain the C_k values which represent the steady-state spatial distribution of the water quality variable being considered. In the form shown in Equation (C-3) it is assumed that all segments interact with all other segments. This, of course, is not the case for the New York Bight for which a large number of zeros can be expected in the terms of Equation (C-3).

There are a number of numerical procedures for solving a set of n simultaneous equations in n unknowns, such as given by Equation (C-3). These include the Gauss-Seidel relaxation method which is appropriate for this class of equations. The theoretical development may also be interpreted by writing the equations in matrix form. Thus, one can express the n equations as:

$$[A]\,(C) = (W) \qquad \text{(C-4)}$$

where [A] is an n x n matrix and (C) and (W) are n x 1 column vectors. The formal solution of Equation (C-4) is:

$$(C) = [A]^{-1}(W) \qquad \text{(C-5)}$$

Therefore, the problem of determining the spatial steady-state water quality response in a multi-dimensional system reduces to solving a set of n simultaneous equations or determining the inverse of the system parameter matrix.

The above development is suitable for "single system" variables, i.e., water quality variables that are not forced by outputs from other quality systems. Examples of single system variables are salinity (where the reaction coefficient, K is zero, representing a conservative variable), coliform bacteria and Biochemical Oxygen Demand, BOD. For coupled system variables, such as Dissolved Oxygen, (DO) one must recognize that the DO, in addition to responding to direct sources and sinks of DO (e.g. benthal demand), also responds to the utilization of oxygen to satisfy the biochemical oxygen demand.

The mass balance equation can be most conveniently written in terms of dissolved oxygen deficit D_k:

$$D_k = C_k - C_{ks}$$

$$V_k \frac{dD_k}{dt} = 0 = \sum_j \left[-Q_{kj}(\alpha_{kj} D_k + \beta_{kj} D_j) + E'_{kj}(D_j - D_k)\right] + V_k K_{ak}(D) - V_k K_{dk} L_k \pm W_k \tag{C-6}$$

where C_{ks} is the saturation value of DO at the surface - K_{ak} is the reaeration coefficient in segment k, K_{dk} is the deoxygenation coefficient, L_k is the biochemical oxygen demand, and $\pm W_k$ is now interpreted as sources and sinks of DO such as benthal demands and photosynthetic production or respiration.

A matrix formulation can be followed as before for the BOD and DO. Therefore, for BOD:

$$(L) = [A]^{-1}(W) \tag{C-7}$$

where [A] has the BOD decay coefficient on the main diagonal and (W) is the vector of waste load inputs. This is the same as Equation (C-5) where the variable is interpreted as the BOD. Following a similar procedure for DO gives:

$$(C) = [B]^{-1}(VK_dL + W_D) \qquad (C\text{-}8)$$

where (C) is the vector of DO decreases due to the BOD input vector given by (VK_dL and W_D) and bottom oxygen demand, phytoplankton oxygen production and respiration as determined from Equation (C-6) and where [B] has the reaeration coefficient on the main diagonal.

APPENDIX D

Transport System Parameters

Dissolved Oxygen System Parameters

TABLE D-I
Transport System Parameters

Seg. Interface Designation		Dispersion Coefficient	Interface Area	Characteristic Length		Velocity	Flow
				I	J		
I	J*	(CM^2/S)	(KM^2)	(KM)	(KM)	CM/S	M^3/S
1	2	1.0	4.97×10^{3}	3.51×10^{-2}	1.28 -	-	-
3	4	1.0	3.73×10^{3}	3.23×10^{-2}	8.17×10^{-2}	-	-
5	6	1.0	1.23×10^{3}	2.89×10^{-2}	1.34×10^{-2}	-	-
7	8	1.0	9.48×10^{2}	2.68×10^{-2}	1.04×10^{-2}	-	-
9	10	1.0	6.14×10^{2}	2.48×10^{-2}	7.80×10^{-3}	-	-
11	12	1.0	1.23×10^{3}	1.97×10^{-2}	3.23×10^{-3}	-3.05×10^{-4}	-3.74×10^{3}
13	14	1.0	2.94×10^{3}	3.51×10^{-2}	3.84×10^{-1}	-	-
15	16	1.0	2.21×10^{3}	2.95×10^{-2}	2.50×10^{-2}	-	-
17	18	1.0	7.26×10^{2}	2.28×10^{-2}	1.28×10^{-2}	-	-
19	20	1.0	5.62×10^{2}	1.95×10^{-2}	6.13×10^{-3}	-	-
21	22	1.0	3.64×10^{2}	1.65×10^{-2}	8.17×10^{-3}	-	-
23	24	1.0	2.03×10^{3}	3.51×10^{-2}	1.06×10^{-1}	-	-
25	26	1.0	1.51×10^{3}	3.04×10^{-2}	2.69×10^{-2}	-	-
27	28	1.0	4.99×10^{2}	2.42×10^{-2}	1.14×10^{-2}	-	-
29	30	1.0	3.86×10^{2}	1.99×10^{-2}	6.07×10^{-3}	-	-
31	32	1.0	2.50×10^{2}	1.58×10^{-2}	6.19×10^{-3}	-3.05×10^{-4}	-7.62×10^{2}
33	34	1.0	1.47×10^{3}	3.51×10^{-2}	3.90×10^{-2}	-	-
35	36	1.0	1.11×10^{3}	3.29×10^{-2}	1.46×10^{-2}	-	-
37	38	1.0	3.63×10^{2}	2.80×10^{-2}	2.14×10^{-2}	-	-
39	40	1.0	2.81×10^{2}	2.18×10^{-2}	8.35×10^{-3}	-	-
41	42	1.0	1.85×10^{2}	1.54×10^{-2}	5.21×10^{-3}	-3.05×10^{-4}	-5.64×10^{2}
43	44	1.0	1.47×10^{3}	3.51×10^{-2}	3.23×10^{-2}	-	-
45	46	1.0	1.11×10^{3}	3.14×10^{-2}	1.37×10^{-2}	-	-
47	48	1.0	3.63×10^{2}	2.50×10^{-2}	8.26×10^{-3}	-	-
49	50	1.0	2.77×10^{2}	2.14×10^{-2}	1.21×10^{-2}	-	-
51	52	1.0	1.77×10^{2}	1.50×10^{-2}	3.63×10^{-3}	-3.05×10^{-4}	-5.41×10^{2}
53	54	1.0	1.01×10^{3}	3.51×10^{-2}	2.93×10^{-2}	-	-
55	56	1.0	7.60×10^{2}	2.93×10^{-2}	9.45×10^{-3}	-	-
57	58	1.0	2.53×10^{2}	2.07×10^{-2}	3.05×10^{-3}	-	-
59	60	1.0	1.91×10^{2}	2.03×10^{-2}	8.53×10^{-3}	-	-
61	62	1.0	9.94×10^{1}	1.61×10^{-2}	5.49×10^{-4}	-3.05×10^{-4}	-3.03×10^{2}
63	64	1.0	1.01×10^{3}	3.51×10^{-2}	2.65×10^{-2}	-	-
65	66	1.0	7.60×10^{2}	2.72×10^{-2}	8.17×10^{-3}	-	-
67	68	1.0	2.53×10^{2}	1.80×10^{-2}	3.44×10^{-3}	-	-
69	70	1.0	1.91×10^{2}	1.70×10^{-2}	8.47×10^{-3}	-	-
71	72	1.0	9.66×10^{1}	1.14×10^{-2}	4.88×10^{-3}	-3.05×10^{-4}	-2.95×10^{2}
73	74	1.0	2.03×10^{3}	3.31×10^{-2}	1.96×10^{-2}	-	-
75	76	1.0	1.28×10^{3}	2.21×10^{-2}	5.55×10^{-3}	-3.05×10^{-4}	-3.90×10^{3}
77	78	1.0	1.88×10^{3}	2.80×10^{-2}	1.27×10^{-2}	-3.05×10^{-4}	-5.73×10^{3}
79	80	1.0	2.35×10^{2}	1.19×10^{-2}	2.10×10^{-3}	-3.05×10^{-4}	-7.18×10^{2}
81	82	1.0	1.25×10^{2}	1.06×10^{-2}	2.65×10^{-3}	-3.05×10^{-4}	-3.81×10^{2}
83	84	1.0	8.24×10^{1}	6.37×10^{-3}	7.01×10^{-4}	-3.05×10^{-4}	-2.51×10^{2}
85	86	1.0	5.42×10^{2}	1.26×10^{-2}	3.17×10^{-3}	-3.05×10^{-4}	-1.65×10^{3}
1	0	3.01×10^{7}	1.92 -	9.05×10^{1}	9.05×10^{1}	-1.19×10^{1}	-2.29×10^{5}
2	0	3.01×10^{7}	1.33×10^{2}	9.05×10^{1}	9.05×10^{1}	-6.10×10^{-1}	-8.10×10^{5}
3	0		2.38 -	5.49×10^{1}	5.49×10^{1}	1.18×10^{1}	2.82×10^{5}
4	0		1.61×10^{1}	5.49×10^{1}	5.49×10^{1}	7.01×10^{-1}	1.13×10^{5}

* I J
Convention - For Velocity and Flow, Positive is assumed from I to J.

TABLE D-1 (continued)

Seg. Interface Locations I	J	Dispersion Coefficients (CM^2/S)	Interface Areas (KM^2)	Characteristic Lengths I (KM)	J (KM)	Velocity CM/S	Flow M^3/S
5	0	3.01×10^{7}	7.83×10^{-1}	5.49×10^{1}	5.49×10^{1}	4.84 -	3.79×10^{4}
6	0	3.01×10^{7}	4.08×10^{-1}	5.49×10^{1}	5.49×10^{1}	7.62×10^{-1}	3.11×10^{3}
7	0	3.01×10^{7}	5.71×10^{-1}	5.49×10^{1}	5.49×10^{1}	3.44 -	1.97×10^{4}
8	0	3.01×10^{7}	1.16×10^{-1}	5.49×10^{1}	5.49×10^{1}	-1.62×10^{-1}	-1.88×10^{2}
9	0	3.01×10^{7}	3.47×10^{-1}	5.49×10^{1}	5.49×10^{1}	1.83 -	6.36×10^{3}
10	0	3.01×10^{7}	7.06×10^{-2}	5.49×10^{1}	5.49×10^{1}	-1.22×10^{-1}	-8.52×10^{1}
11	0	3.01×10^{7}	6.65×10^{-1}	2.23×10^{1}	2.23×10^{1}	3.05 -	2.03×10^{4}
12	0	3.01×10^{7}	3.90×10^{-1}	2.23×10^{1}	2.23×10^{1}	-9.02×10^{-1}	-3.51×10^{3}
13	0	3.01×10^{7}	1.14 -	9.05×10^{1}	9.05×10^{1}	-5.99 -	-6.82×10^{4}
14	0	3.01×10^{7}	4.92×10^{1}	9.05×10^{1}	9.05×10^{1}	-7.62×10^{-1}	-3.75×10^{5}
23	0	3.01×10^{7}	7.83×10^{-1}	9.05×10^{1}	9.05×10^{1}	-3.40 -	-2.66×10^{4}
24	0	3.01×10^{7}	6.71 -	9.05×10^{1}	9.05×10^{1}	-9.14×10^{-1}	-6.13×10^{4}
33	0	3.01×10^{7}	5.69×10^{-1}	9.05×10^{1}	9.05×10^{1}	-1.89 -	-1.08×10^{4}
34	0	3.01×10^{7}	9.08×10^{-1}	9.05×10^{1}	9.05×10^{1}	-7.62×10^{-1}	-6.92×10^{3}
43	0	3.01×10^{7}	5.69×10^{-1}	9.05×10^{1}	9.05×10^{1}	-6.71 -	-3.82×10^{4}
44	0	3.01×10^{7}	7.45×10^{-1}	9.05×10^{1}	9.05×10^{1}	-7.62×10^{-1}	-5.68×10^{3}
53	0	3.01×10^{7}	3.92×10^{-1}	9.05×10^{1}	9.05×10^{1}	-3.79 -	-1.49×10^{4}
54	0	3.01×10^{7}	4.97×10^{-1}	9.05×10^{1}	9.05×10^{1}	-6.10×10^{-1}	-3.03×10^{3}
63	0	3.01×10^{7}	3.92×10^{-1}	9.05×10^{1}	9.05×10^{1}	-3.31 -	-1.30×10^{4}
64	0	3.01×10^{7}	4.62×10^{-1}	9.05×10^{1}	9.05×10^{1}	-6.10×10^{-1}	-2.82×10^{3}
71	0	3.01×10^{7}	2.28×10^{-2}	1.14×10^{1}	1.14×10^{1}	-4.42 -	-1.01×10^{3}
72	0	3.01×10^{7}	1.93×10^{-2}	1.14×10^{1}	1.14×10^{1}	3.96 -	7.66×10^{2}
73	0	3.01×10^{7}	7.83×10^{-1}	9.05×10^{1}	9.05×10^{1}	-5.57 -	-4.36×10^{4}
74	0	3.01×10^{7}	7.58×10^{-1}	9.05×10^{1}	9.05×10^{1}	-6.10×10^{-1}	-4.62×10^{3}
77	0	3.01×10^{7}	7.83×10^{-1}	9.05×10^{1}	9.05×10^{1}	-7.32 -	-5.73×10^{4}
78	0	3.01×10^{7}	5.89×10^{-1}	9.05×10^{1}	9.05×10^{1}	-6.10×10^{-1}	-3.59×10^{3}
83	0	3.01×10^{7}	2.11×10^{-2}	1.14×10^{1}	1.14×10^{1}	-4.42 -	-9.32×10^{2}
84	0	3.01×10^{7}	1.79×10^{-2}	1.14×10^{1}	1.14×10^{1}	3.96 -	7.11×10^{2}
87	0	3.01×10^{7}	3.18 -	5.49×10^{1}	5.49×10^{1}	6.40 -	2.03×10^{5}
88	0	3.01×10^{7}	1.96×10^{2}	5.49×10^{1}	5.49×10^{1}	5.79×10^{-1}	1.14×10^{6}
89	0	3.01×10^{7}	6.59×10^{-1}	5.49×10^{1}	5.49×10^{1}	3.05	2.01×10^{4}
90	0	3.01×10^{7}	1.32×10^{-1}	5.49×10^{1}	5.49×10^{1}	-1.52×10^{-1}	-2.01×10^{2}
91	0	3.01×10^{7}	1.56 -	2.23×10^{1}	2.23×10^{1}	-4.30 -	-6.72×10^{4}
92	0	3.01×10^{7}	9.38×10^{-1}	9.38×10^{1}	2.23×10^{1}	6.10×10^{-1}	5.72×10^{3}
1	87	1.505×10^{5}	3.18 -	5.49×10^{1}	5.49×10^{1}	6.40	2.03×10^{5}
2	88	1.505×10^{5}	1.96×10^{2}	5.49×10^{1}	5.49×10^{1}	$5.79.10^{-1}$	1.14×10^{6}
11	89	1.505×10^{5}	6.59×10^{-1}	5.49×10^{1}	5.49×10^{1}	3.05	2.01×10^{4}
12	90	1.505×10^{5}	1.32×10^{-1}	5.49×10^{1}	5.49×10^{1}	-1.52×10^{-1}	-2.01×10^{4}
77	91	1.505×10^{5}	1.56 -	2.23×10^{1}	2.23×10^{1}	-4.30 -	-6.72×10^{4}
78	92	1.505×10^{5}	9.38×10^{-1}	2.23×10^{1}	2.23×10^{1}	6.10×10^{-1}	5.72×10^{3}
1	13	1.505×10^{5}	3.18 -	5.49×10^{1}	3.26×10^{1}	-3.08 -	-9.77×10^{4}
2	14	1.505×10^{5}	7.29×10^{1}	5.49×10^{1}	3.26×10^{1}	-6.10×10^{-1}	-4.45×10^{5}
3	15	1.505×10^{5}	1.97 -	5.49×10^{1}	3.26×10^{1}	-6.36 -	-1.25×10^{5}
4	16	1.505×10^{5}	1.87 -	5.49×10^{1}	3.26×10^{1}	1.55×10^{-1}	2.90×10^{3}
5	17	1.505×10^{5}	4.80×10^{-1}	5.49×10^{1}	3.26×10^{1}	1.56×10^{1}	-7.50×10^{4}
6	18	$1.505.10^{5}$	3.34×10^{-1}	5.49×10^{1}	3.26×10^{1}	1.49×10^{-1}	5.02×10^{2}
7	19	1.505×10^{5}	3.35×10^{-1}	5.49×10^{1}	3.26×10^{1}	-9122 -	-3.09×10^{4}

Seg. Interface Locations I	J	Dispersion Coefficients (CM^2/S)	Interface Areas (KM^2)	Characteristic Lengths I (KM)	J (KM)	Velocity CM/S	Flow M^3/S
8	20	$1.505x10^5$	$1.74x10^{-1}$	$5.49x10^1$	$3.26x10^1$	$2.68x10^{-1}$	$4.65x10^2$
9	21	$1.505x10^5$	$2.06x10^{-1}$	$5.49x10^1$	$3.26x10^1$	-4.80 -	$-9.90x10^3$
10	22	$1.505x10^5$	$7.20x10^{-2}$	$5.49x10^1$	$3.26x10^1$	$2.16x10^{-1}$	$1.55x10^2$
11	85	$1.505x10^5$	$3.15x10^{-1}$	$5.49x10^1$	$5.49x10^1$	-5.71 -	$-1.80x10^4$
12	86	$1.505x10^5$	$1.03x10^{-1}$	$5.49x10^1$	$5.49x10^1$	$5.36x10^{-1}$	$5.53x10^2$
13	23	$1.505x10^5$	3.18 -	$3.26x10^1$	$2.23x10^1$	-2.79 -	$-8.87x10^4$
14	24	$1.505x10^5$	$1.78x10^1$	$3.26x10^1$	$2.23x10^1$	$-4.05x10^{-1}$	$-7.24x10^4$
15	25	$1.505x10^5$	1.94 -	$3.26x10^1$	$2.23x10^1$	-5.49 -	$-1.07x10^5$
16	26	$1.505x10^5$	1.85 -	$3.26x10^1$	$2.23x10^1$	$2.29x10^{-1}$	$4.21x10^3$
17	27	$1.505x10^5$	$4.91x10^{-1}$	$3.26x10^1$	$2.23x10^1$	$-1.26x10^1$	$-6.20x10^4$
18	28	$1.505x10^5$	$2.75x10^{-1}$	$3.26x10^1$	$2.23x10^1$	$8.53x10^{-2}$	$2.34x10^2$
19	29	$1.505x10^5$	$2.93x10^{-1}$	$3.26x10^1$	$2.23x10^1$	-7.83 -	$-2.29x10^4$
20	30	$1.505x10^5$	$1.36x10^{-1}$	$3.26x10^1$	$2.23x10^1$	$2.10x10^{-1}$	$2.85x10^2$
21	31	$1.505x10^5$	$1.49x10^{-1}$	$3.26x10^1$	$2.23x10^1$	-4.54 -	$-6.74x10^3$
22	32	$1.505x10^5$	$8.83x10^{-2}$	$3.26x10^1$	$2.23x10^1$	$3.90x10^{-1}$	$3.44x10^2$
23	33	$1.505x10^5$	3.18 -	$2.23x10^1$	$1.62x10^1$	-3.23 -	$-1.03x10^5$
24	34	$1.505x10^5$	4.26 -	$2.23x10^1$	$1.62x10^1$	$-2.80x10^{-1}$	$-1.19x10^4$
25	35	$1.505x10^5$	2.14 -	$2.23x10^1$	$1.62x10^1$	-4.93 -	$-1.05x10^5$
26	36	$1.505x10^5$	1.41 -	$2.23x10^1$	$1.62x10^1$	$2.35x10^{-1}$	$3.29x10^3$
27	37	$1.505x10^5$	$5.55x10^{-1}$	$2.23x10^1$	$1.62x10^1$	-6.16 -	$-3.42x10^4$
28	38	$1.505x10^5$	$3.79x10^{-1}$	$2.23x10^1$	$1.62x10^1$	$3.87x10^{-1}$	$1.47x10^3$
29	39	$1.505x10^5$	$3.47x10^{-1}$	$2.23x10^1$	$1.62x10^1$	-3.86 -	$-1.34x10^4$
30	40	$1.505x10^5$	$1.90x10^{-1}$	$2.23x10^1$	$1.62x10^1$	$1.58x10^{-1}$	$2.98x10^2$
31	41	$1.505x10^5$	$1.91x10^{-1}$	$2.23x10^1$	$1.62x10^1$	-2.01 -	$-3.85x10^3$
32	42	$1.505x10^5$	$4.92x10^{-2}$	$2.23x10^1$	$1.62x10^1$	$1.71x10^{-1}$	$8.47x10^1$
33	43	$1.505x10^5$	3.18 -	$1.62x10^1$	$1.62x10^1$	-3.93 -	$-1.25x10^5$
34	44	$1.505x10^5$	3.36 -	$1.62x10^1$	$1.62x10^1$	$-1.71x10^{-1}$	$-5.73x10^3$
35	45	$1.505x10^5$	2.24 -	$1.62x10^1$	$1.62x10^1$	-4.40 -	$-9.85x10^4$
36	46	$1.505x10^5$	$9.57x10^{-1}$	$1.62x10^1$	$1.62x10^1$	$3.05x10^{-1}$	$2.91x10^3$
37	47	$3.01x10^5$	$6.13x10^{-1}$	$1.62x10^1$	$1.62x10^1$	-2.63 -	$-1.61x10^4$
38	48	$3.01x10^5$	$3.14x10^{-1}$	$1.62x10^1$	$1.62x10^1$	$4.63x10^{-1}$	$1.46x10^3$
39	49	$3.01x10^5$	$3.69x10^{-1}$	$1.62x10^1$	$1.62x10^1$	-1.91 -	$-7.03x10^3$
40	50	$3.01x10^5$	$2.73x10^{-1}$	$1.62x10^1$	$1.62x10^1$	$3.05x10^{-1}$	$8.28x10^2$
41	51	$3.01x10^5$	$1.56x10^{-1}$	$1.62x10^1$	$1.62x10^1$	-1.03 -	$-1.61x10^3$
42	52	$3.01x10^5$	$5.27x10^{-2}$	$1.62x10^1$	$1.62x10^1$	$2.29x10^{-1}$	$1.20x10^2$
43	53	$1.505x10^5$	3.18 -	$1.62x10^1$	$1.12x10^1$	-3.66 -	$-1.16x10^5$
44	54	$1.505x10^5$	2.73 -	$1.62x10^1$	$1.12x10^1$	$-4.57x10^{-2}$	$-1.21x10^3$
45	55	$1.505x10^5$	2.00 -	$1.62x10^1$	$1.12x10^1$	-4.57 -	$-9.13x10^4$
46	56	$1.505x10^5$	$9.09x10^{-1}$	$1.62x10^1$	$1.12x10^1$	$3.99x10^{-1}$	$3.63x10^3$
47	57	$3.01x10^5$	$4.70x10^{-1}$	$1.62x10^1$	$1.12x10^1$	$3.23x10^{-1}$	$1.52x10^3$
48	58	$3.01x10^5$	$1.27x10^{-1}$	$1.62x10^1$	$1.12x10^1$	$4.69x10^{-1}$	$5.96x10^2$
49	59	$3.01x10^5$	$3.99x10^{-1}$	$1.62x10^1$	$1.12x10^1$	$-6.68x10^{-1}$	$-2.66x10^3$
50	60	$3.01x10^5$	$1.35x10^{-1}$	$1.62x10^1$	$1.12x10^1$	1.13 -	$1.53x10^3$
51	61	$3.01x10^5$	$1.68x10^{-1}$	$1.62x10^1$	$1.12x10^1$	$-4.54x10^{-1}$	$-7.64x10^2$
52	62	$3.01x10^5$	$3.01x10^{-2}$	$1.62x10^1$	$1.12x10^1$	$5.85x10^{-1}$	$1.76x10^2$
53	63	$1.505x10^5$	3.18 -	$1.12x10^1$	$1.12x10^1$	-3.90 -	$-1.24x10^5$
54	64	$1.505x10^5$	2.57 -	$1.12x10^1$	$1.12x10^1$	$5.79x10^{-2}$	$1.52x10^3$

Seg. Interface Locations		Dispersion Coefficients	Interface Areas	Characteristic Lengths		Velocity	Flow
				I	J		
I	J	(CM^2/S)	(KM^2)	(KM)	(KM)	CM/S	M^3/S
55	65	1.505×10^{5}	1.94 -	1.12×10^{1}	1.12×10^{1}	-3.45 -	-6.70×10^{4}
56	66	1.505×10^{5}	7.10×10^{-1}	1.12×10^{1}	1.12×10^{1}	5.09×10^{-1}	3.62×10^{3}
57	67	3.01×10^{5}	4.49×10^{-1}	1.12×10^{1}	1.12×10^{1}	-1.13×10^{-1}	-5.05×10^{2}
58	68	3.01×10^{5}	1.06×10^{-1}	1.12×10^{1}	1.12×10^{1}	5.21×10^{-1}	5.51×10^{2}
59	69	3.01×10^{5}	3.84×10^{-1}	1.12×10^{1}	1.12×10^{1}	-4.94×10^{-1}	-1.90×10^{3}
60	70	3.01×10^{5}	9.10×10^{-2}	1.12×10^{1}	1.12×10^{1}	1.40 -	1.27×10^{3}
61	71	3.01×10^{5}	1.55×10^{-1}	1.12×10^{1}	1.12×10^{1}	-5.46×10^{-1}	-8.45×10^{2}
62	72	3.01×10^{5}	4.28×10^{-2}	1.12×10^{1}	1.12×10^{1}	1.12 -	4.81×10^{2}
63	73	1.505×10^{5}	3.18 -	1.12×10^{1}	2.23×10^{1}	-4.21	-1.34×10^{5}
64	74	1.505×10^{5}	2.25 -	1.12×10^{1}	2.23×10^{1}	1.80×10^{-1}	4.07×10^{3}
65	75	1.505×10^{5}	1.75 -	1.12×10^{1}	2.23×10^{1}	-2.51 -	-4.39×10^{4}
66	76	1.505×10^{5}	5.11×10^{-1}	1.12×10^{1}	2.23×10^{1}	6.55×10^{-1}	3.35×10^{3}
67	79	3.01×10^{5}	3.60×10^{-1}	1.12×10^{1}	1.04×10^{1}	-2.29×10^{-1}	-8.26×10^{2}
68	80	3.01×10^{5}	9.66×10^{-2}	1.12×10^{1}	1.04×10^{1}	4.97×10^{-1}	4.79×10^{2}
69	81	3.01×10^{5}	2.61×10^{-1}	1.12×10^{1}	9.24 -	-3.51×10^{-1}	-9.18×10^{2}
70	82	3.01×10^{5}	8.78×10^{-2}	1.12×10^{1}	9.24 -	4.21×10^{-1}	3.69×10^{2}
71	83	3.01×10^{5}	7.61×10^{-2}	1.12×10^{1}	5.94 -	-7.28×10^{-1}	-5.55×10^{2}
72	84	3.01×10^{5}	4.51×10^{-2}	1.12×10^{1}	5.94 -	2.08 -	9.37×10^{2}
73	77	1.505×10^{5}	2.85 -	2.23×10^{1}	2.23×10^{1}	-4.57 -	-1.30×10^{5}
74	78	1.505×10^{5}	1.67 -	2.23×10^{1}	2.23×10^{1}	4.69×10^{-1}	7.86×10^{3}
1	3	1.505×10^{5}	1.92 -	9.05×10^{1}	6.80×10^{1}	6.40 -	1.23×10^{5}
2	4	1.505×10^{5}	1.63×10^{1}	9.05×10^{1}	6.80×10^{1}	7.38×10^{-1}	1.20×10^{5}
13	15	1.505×10^{5}	1.14 -	9.05×10^{1}	6.80×10^{1}	5.18 -	5.92×10^{4}
14	16	1.505×10^{5}	1.25 -	9.05×10^{1}	6.80×10^{1}	1.71×10^{-1}	2.15×10^{3}
23	25	1.505×10^{5}	7.83×10^{-1}	9.05×10^{1}	6.80×10^{1}	5.18 -	4.06×10^{4}
24	26	1.505×10^{5}	5.43×10^{-1}	9.05×10^{1}	6.80×10^{1}	1.52×10^{-1}	8.33×10^{2}
33	35	1.505×10^{5}	5.69×10^{-1}	9.05×10^{1}	6.80×10^{1}	5.79 -	3.30×10^{4}
34	36	1.505×10^{5}	3.76×10^{-1}	9.05×10^{1}	6.80×10^{1}	1.92×10^{-1}	7.27×10^{2}
43	45	1.505×10^{5}	5.69×10^{-1}	9.05×10^{1}	6.80×10^{1}	5.18 -	2.95×10^{4}
44	46	1.505×10^{5}	3.62×10^{-1}	9.05×10^{1}	6.80×10^{1}	3.20×10^{-1}	1.16×10^{3}
53	55	1.505×10^{5}	3.92×10^{-1}	9.05×10^{1}	6.80×10^{1}	5.79 -	2.27×10^{4}
54	56	1.505×10^{5}	1.50×10^{-1}	9.05×10^{1}	6.80×10^{1}	2.01×10^{-1}	2.99×10^{2}
63	65	1.505×10^{5}	3.92×10^{-1}	9.05×10^{1}	6.80×10^{1}	5.79 -	2.27×10^{4}
64	66	1.505×10^{5}	1.15×10^{-1}	9.05×10^{1}	6.80×10^{1}	2.35×10^{-1}	2.70×10^{2}
73	75	1.505×10^{5}	6.91×10^{-1}	9.05×10^{1}	6.80×10^{1}	5.79 -	4.00×10^{4}
74	76	1.505×10^{5}	1.60×10^{-1}	9.05×10^{1}	6.80×10^{1}	5.18×10^{-1}	8.27×10^{2}
3	5	1.505×10^{5}	1.66 -	6.80×10^{1}	2.23×10^{1}	-2.00 -	-3.32×10^{4}
4	6	1.505×10^{5}	1.01 -	6.80×10^{1}	2.23×10^{1}	4.48×10^{-1}	4.53×10^{3}
15	17	1.505×10^{5}	8.30×10^{-1}	6.80×10^{1}	2.23×10^{1}	4.88 -	4.05×10^{4}
16	18	1.505×10^{5}	3.22×10^{-1}	6.80×10^{1}	2.23×10^{1}	2.59×10^{-1}	8.39×10^{2}
25	27	1.505×10^{5}	5.95×10^{-1}	6.80×10^{1}	2.23×10^{1}	6.62 -	3.94×10^{4}
26	28	1.505×10^{5}	4.20×10^{-1}	6.80×10^{1}	2.23×10^{1}	4.18×10^{-1}	1.75×10^{3}
35	37	1.505×10^{5}	5.35×10^{-1}	6.80×10^{1}	2.23×10^{1}	4.88 -	2.61×10^{4}
36	38	1.505×10^{5}	2.45×10^{-1}	6.80×10^{1}	2.23×10^{1}	4.54×10^{-1}	1.12×10^{3}
45	47	3.01×10^{5}	4.58×10^{-1}	6.80×10^{1}	2.23×10^{1}	4.88 -	2.23×10^{4}
46	48	3.01×10^{5}	1.20×10^{-1}	6.80×10^{1}	2.23×10^{1}	3.63×10^{-1}	4.33×10^{2}
55	57	3.01×10^{5}	2.69×10^{-1}	6.80×10^{1}	2.26×10^{1}	-6.13×10^{-1}	-1.65×10^{3}

TABLE D-I (continued)

Seg. Interface Locations I	J	Dispersion Coefficients (CM^2/S)	Interface Areas (KM^2)	Characteristic Lengths I (KM)	J (KM)	Velocity CM/S	Flow M^3/S
56	58	3.01×10^5	7.01×10^{-2}	6.80×10^1	2.26×10^1	4.39×10^{-1}	3.08×10^2
65	67	3.01×10^5	2.17×10^{-1}	6.80×10^1	2.26×10^1	-1.62×10^{-1}	-3.52×10^2
66	68	3.01×10^5	7.20×10^{-2}	6.80×10^1	2.26×10^1	7.53×10^{-1}	5.42×10^2
75	79	3.01×10^5	1.74×10^{-1}	6.80×10^1	2.26×10^1	9.14×10^{-3}	1.70×10^1
76	80	3.01×10^5	4.38×10^{-2}	6.80×10^1	2.26×10^1	6.28×10^{-1}	2.75×10^2
5	7	1.505×10^5	1.58 -	2.23×10^1	1.73×10^1	2.44×10^{-1}	3.85×10^3
6	8	1.505×10^5	6.55×10^{-1}	2.23×10^1	1.73×10^1	1.40×10^{-1}	9.22×10^2
17	19	1.505×10^5	7.30×10^{-1}	2.23×10^1	1.73×10^1	3.76 -	2.75×10^4
18	20	1.505×10^5	2.91×10^{-1}	2.23×10^1	1.73×10^1	3.81×10^{-1}	1.11×10^3
27	29	1.505×10^5	5.28×10^{-1}	2.23×10^1	1.73×10^1	2.20 -	1.16×10^4
28	30	1.505×10^5	1.42×10^{-1}	2.23×10^1	1.73×10^1	3.63×10^{-1}	5.15×10^2
37	39	1.505×10^5	4.38×10^{-1}	2.23×10^1	1.73×10^1	1.83 -	8.05×10^3
38	40	1.505×10^5	2.19×10^{-1}	2.23×10^1	1.73×10^1	5.15×10^{-1}	1.13×10^3
47	49	3.01×10^5	3.76×10^{-1}	2.23×10^1	1.71×10^1	1.24 -	4.68×10^3
48	50	3.01×10^5	2.55×10^{-1}	2.23×10^1	1.71×10^1	5.06×10^{-1}	1.29×10^3
57	59	3.01×10^5	2.01×10^{-1}	2.26×10^1	1.71×10^1	1.89×10^{-1}	3.81×10^2
58	60	3.01×10^5	7.25×10^{-2}	2.26×10^1	1.71×10^1	4.88×10^{-1}	3.53×10^2
67	69	3.01×10^5	1.84×10^{-1}	2.26×10^1	1.71×10^1	-1.52×10^{-2}	-3.09×10^1
68	70	3.01×10^5	5.98×10^{-2}	2.26×10^1	1.71×10^1	1.02 -	6.14×10^2
79	81	3.01×10^5	1.07×10^{-1}	2.26×10^1	1.71×10^1	-8.53×10^{-2}	-9.12×10^1
80	82	3.01×10^5	1.48×10^{-2}	2.26×10^1	1.71×10^1	2.47×10^{-1}	3.65×10^1
7	9	1.505×10^5	1.41 -	1.73×10^1	1.12×10^1	1.07 -	1.51×10^4
8	10	1.505×10^5	4.51×10^{-1}	1.73×10^1	1.12×10^1	1.43×10^{-1}	6.45×10^2
19	21	1.505×10^5	6.26×10^{-1}	1.73×10^1	1.12×10^1	3.11 -	1.95×10^4
20	22	1.505×10^5	2.69×10^{-1}	1.73×10^1	1.12×10^1	4.79×10^{-1}	1.29×10^3
29	31	1.505×10^5	4.22×10^{-1}	1.73×10^1	1.12×10^1	5.06×10^{-1}	2.13×10^3
30	32	1.505×10^5	1.04×10^{-1}	1.73×10^1	1.12×10^1	4.82×10^{-1}	5.02×10^2
39	41	1.505×10^5	3.07×10^{-1}	1.73×10^1	1.14×10^1	5.46×10^{-1}	1.68×10^3
40	42	1.505×10^5	9.06×10^{-2}	1.73×10^1	1.14×10^1	6.61×10^{-1}	5.99×10^2
49	51	3.01×10^5	3.07×10^{-1}	1.71×10^1	1.14×10^1	1.01×10^{-1}	3.09×10^2
50	52	3.01×10^5	7.52×10^{-2}	1.71×10^1	1.14×10^1	7.92×10^{-1}	5.97×10^2
59	61	3.01×10^5	2.34×10^{-1}	1.71×10^1	1.04×10^1	-1.65×10^{-1}	-3.85×10^2
60	62	3.01×10^5	5.30×10^{-2}	1.71×10^1	1.04×10^1	1.15 -	6.07×10^2
69	71	3.01×10^5	1.86×10^{-1}	1.71×10^1	1.14×10^1	-5.43×10^{-1}	-1.01×10^3
70	72	3.01×10^5	6.84×10^{-2}	1.71×10^1	1.14×10^1	2.22 -	1.52×10^3
81	83	3.01×10^5	7.51×10^{-2}	1.71×10^1	1.14×10^1	-8.38×10^{-1}	-6.29×10^2
82	84	3.01×10^5	5.85×10^{-3}	1.71×10^1	1.14×10^1	4.33×10^{-1}	2.52×10^1
9	11	1.505×10^5	1.31 -	1.12×10^1	2.23×10^1	1.42 -	1.86×10^4
10	12	1.505×10^5	3.10×10^{-1}	1.12×10^1	2.23×10^1	1.86×10^{-1}	5.75×10^2
21	85	1.505×10^5	5.12×10^{-1}	1.12×10^1	1.58×10^1	3.19 -	1.63×10^4
22	86	1.505×10^5	1.98×10^{-1}	1.12×10^1	1.58×10^1	5.55×10^{-1}	1.10×10^3

TABLE D-II
Dissolved Oxygen System Parameters

SEGMENT NUMBER	DEPTH (meters)	P-R mg/ℓ-day	K_r 1/day	K_a 1/m
1	35.1	0.250	0.10	.0285
2	1280.2	-0.050	0.10	0
3	32.3	0.250	0.10	.0310
4	81.7	-0.050	0.10	0
5	29.0	0.250	0.10	.0345
6	13.4	-0.300	0.10	0
7	26.8	0.250	0.10	.0373
8	10.4	-0.300	0.10	0
9	24.7	0.250	0.10	.0405
10	7.9	-0.300	0.10	0
11	19.8	0.250	0.10	.0505
12	3.4	-0.300	0.10	0
13	35.1	0.250	0.10	.0285
14	382.5	-0.050	0.10	0
15	29.6	0.250	0.10	.0338
16	25.0	-0.050	0.10	0
17	22.9	0.250	0.10	.0437
18	12.8	-0.300	0.10	0
19	19.5	0.250	0.10	.0513
20	6.1	-0.300	0.10	0
21	16.5	0.250	0.10	.0606
22	8.2	-0.300	0.10	0
23	35.1	0.250	0.10	.0285
24	106.0	-0.050	0.10	0
25	30.5	0.250	0.10	.0328
26	26.8	-0.050	0.10	0
27	24.4	0.250	0.10	.0410
28	11.6	-0.300	0.10	0
29	19.8	0.250	0.10	.0505
30	6.1	-0.300	0.10	0
31	25.0	0.250	0.10	.0400
32	8.5	-0.300	0.10	0
33	35.1	0.250	0.10	.0285
34	39.0	-0.050	0.10	0
35	33.0	0.250	0.10	.0303
36	14.6	-0.300	0.10	0
37	28.0	0.250	0.10	.0357
38	21.3	-0.050	0.10	0
39	22.0	0.250	0.10	.0455
40	8.2	-0.300	0.10	0
41	21.0	0.250	0.10	.0475
42	6.7	-0.300	0.10	0
43	35.1	0.250	0.10	.0285
44	32.3	-0.050	0.10	0
45	31.4	0.250	0.10	.0319
46	13.7	-0.300	0.10	0
47	25.0	0.250	0.10	.0400
48	8.2	-0.300	0.10	0
49	21.3	0.250	0.10	.0470
50	12.2	-0.650	0.10	0

TABLE D-II (continued)

51	16.8	0.250	0.10	.0595
52	3.7	-0.300	0.10	0
53	35.1	0.250	0.10	.0285
54	29.3	-0.050	0.10	0
55	29.3	0.250	0.10	.0341
56	9.5	-0.300	0.10	0
57	20.7	0.250	0.10	.0483
58	3.0	-0.300	0.10	0
59	20.1	0.250	0.10	.0498
60	8.5	-0.750	0.10	0
61	17.7	0.250	0.10	.0565
62	1.8	-0.300	0.10	0
63	35.1	0.250	0.10	.0285
64	26.5	-0.050	0.10	0
65	27.1	0.250	0.10	.0369
66	8.2	-0.300	0.10	0
67	18.0	0.250	0.10	.0556
68	3.4	-0.300	0.10	0
69	16.8	0.250	0.10	.0595
70	8.5	-0.800	0.10	0
71	15.0	0.250	0.10	.0667
72	4.9	-0.300	0.10	0
73	32.9	0.250	0.10	.0304
74	19.5	-0.050	0.10	0
75	24.4	0.250	0.10	.0410
76	6.1	-0.300	0.10	0
77	28.3	0.250	0.10	.0353
78	12.8	-0.300	0.10	0
79	11.9	0.250	0.10	.0840
80	2.1	-0.300	0.10	0
81	13.1	0.250	0.10	.0763
82	3.1	-0.300	0.10	0
83	6.1	0.250	0.10	.1639
84	6.8	-0.300	0.10	0
85	12.8	0.250	0.10	.0781
86	3.1	-0.300	0.10	0